8-2016

# Nanocomposite Adhesive of English ivy (*Hedera helix*): Bioproduction, Nanoparticle Isolation, and Molecular Analysis

Jason Neil Burris
*University of Tennessee, Knoxville*, jburris1@utk.edu

To the Graduate Council:

I am submitting herewith a dissertation written by Jason Neil Burris entitled "Nanocomposite Adhesive of English ivy (*Hedera helix*): Bioproduction, Nanoparticle Isolation, and Molecular Analysis." I have examined the final electronic copy of this dissertation for form and content and recommend that it be accepted in partial fulfillment of the requirements for the degree of Doctor of Philosophy, with a major in Plants, Soils, and Insects.

C. Neal Stewart, Major Professor

We have read this dissertation and recommend its acceptance:

Scott C. Lenaghan, Juan-Luis Jurat-Fuentes, Terek Hewezi

Accepted for the Council:

Carolyn R. Hodges

Vice Provost and Dean of the Graduate School

(Original signatures are on file with official student records.)

# Nanocomposite Adhesive of English ivy (*Hedera helix*): Bioproduction, Nanoparticle Isolation, and Molecular Analysis

**A Dissertation Presented for the**
**Doctor of Philosophy**
**Degree**
**The University of Tennessee, Knoxville**

**Jason Neil Burris**
**August 2016**

# Dedication

This dissertation is dedicated to my father,

Nelson Burris, who inspired me to finish sooner rather than later.

## Acknowledgements

I would like to offer my sincere thanks and appreciation to Dr. Neal Stewart, my major professor, who provided me the opportunity to obtain this Ph.D. I would also like to thank Dr. Scott Lenaghan, Dr. Juan Luis Jurat-Fuentes and Dr. Tarek Hewezi, who served as committee members and provided valuable suggestions on my research and writing. I express my greatest appreciation to Dr. Scott Lenaghan, who without his guidance, advice and support, I would have never successfully completed this project.

I would like to especially thank my wife, friend and colleague, Dr. Kellie Burris, who with her love and support has enabled me to obtain this degree. Also, I would like to thank my parents, Nelson and Patti Burris, for their support and encouragement to complete my educational goals.

And a special thanks to my fellow colleagues in the Stewart laboratory for their assistance and advice.

## Abstract

English ivy naturally produces organic nanoparticles from its adventitious root hairs, and possesses characteristics that may allow them to replace metal-based nanoparticles in common applications, such as sunscreen. At the onset of the research, it was hypothesized that a physical mechanism of attachment, similar to the gecko footpad, was used to generate the adhesive force for attachment; however, through the results obtained from recent work, it is clear that a biochemical mechanism is involved in the generation of the strength of adhesion. Therefore, the goal of this research was to provide a better understanding of the genetic basis of nanoparticle biosynthesis and identify the putative gene(s) and encoded proteins that are involved in the formation or biosynthesis of the nanoparticle.

It was first necessary to develop a biofabrication system that produced large quantities of adventitious roots. This enhanced system was achieved by modifying GA7 Magenta boxes and identifying the optimal concentration of the auxin indole-3 butyric acid (IBA) for adventitious root growth. Maximum adventitious root production was achieved by a 4 h application of 1 mg/ml IBA to juvenile English ivy shoot segments cultured in custom vessels. This method produced 90 mg of dry weight nanoparticles, confirmed by atomic force microscopy, from 12 g adventitious roots after 2 wk.

Following bulk production, I utilized a proteomic- and transcriptomic-based approach to identify and analyze the specific proteins involved in the formation of the nanoparticle adhesive complex from adventitious root samples. A 10 mM dithiothreitol (DTT)-based extraction buffer allowed the separation of a single high molecular weight band (> 460 kDa) from nanoparticles into 9

bands ranging in molecular weight from 25-130 kD, with no effects on the size or stability of the nanoparticles. The results of the omics analysis identified 11 protein candidates from the English ivy adventitious root transcriptome, and 9 candidates from the UniProt (all plant) database for a combined total of 20 individual putative proteins that comprise ivy nanoparticles. These studies provide a reasonable starting point in the identification of those proteins involved in nanoparticle formation and function.

## Table of Contents

## List of Tables

## List of Figures

# Chapter 1. Introduction

Nanobiotechnology is one of the fastest growing research fields, and concerns over the safety of semiconductor-based nanomaterials has led to considerable effort to develop "green" chemistry approaches for their production. Many of these green approaches use the reducing capabilities of plants or their extracts to reduce metallic salts (silver nitrate $AgNO_3$, chloroauric acid $HAuCl_4$, etc.) into metal nanoparticles with distinct functional properties. Sundews, which are carnivorous perennial herbaceous plants having adhesive properties on their leaves that function to capture insects, also produce natural nanoparticles (Zhang et al. 2010). In 2008, it was first discovered that English ivy has the ability to secrete an adhesive matrix composed of highly uniform nanoparticles (Zhang et al. 2008). While several climbing vines are known to release adhesive materials (Endress and Thomson, 1976; Groot et al., 2003), English and Boston ivy are the only ones recognized to release nanoparticles naturally, without the addition of metallic salts.

English ivy (*Hedera helix* L.; Araliaceae family), is an evergreen flowering vine native to most of Europe and western Asia, and is considered to be an invasive species in North America. English ivy is well recognized for its climbing ability, which enables it to reach over 30 m from ground level (Metcalfe 2005). It also can grow laterally in shade to produce a thick ground cover. Its uncanny capacity to adhere to a variety of natural and artificial surfaces (wood, rocks, brick, mortar) with high tensile strength and independent of weather makes English ivy a natural source of inspiration for the development of bio-based adhesives (Melzer et al. 2010, 2011; Zhang et al. 2008).

Recently, the attachment process of English ivy has drawn significant interest leading to several studies focused on characterization of this process (Melzer et al. 2010; Melzer et al. 2011;

Lenaghan and Zhang 2012). The attachment of English ivy to natural and artificial substrates has been hypothesized to occur in a four-step process: initial physical contact with the substrate, closure formation of the root with the substrate, chemical adhesion, and changes to root hair shape to form closure with the substrate (Melzer et al. 2010). Ultimately, it was determined that structural changes at the subcellular level were partly responsible for adherence of English ivy adventitious roots to various substrates (Melzer et al. 2010). A follow-up study further characterized the attachment of English ivy to various substrates, including semi-artificial cork, tree bark and mortar, and determined that attachment at the interface did not fail on any of the substrates tested (Melzer et al. 2011). Further, it was concluded that English ivy was successfully adaptive to a variety of substrates (Melzer et al. 2011). However, English ivy has a limited ability to effectively attach to smooth surfaces, such as glass and aluminum (Melzer et al. 2009). Using real-time video microscopy, it was observed that prior to attachment the roots elongate with the tips orienting in multiple directions (Lenaghan and Zhang 2012). It was concluded that the root tip of English ivy provides the primary signal for attachment, acting as the "pressure sensor" for root attachment and adventitious root production (Lenaghan and Zhang 2012). The attachment strength of several climbing plants, including the attachment of roots from English ivy to bark, was quantified with its maximum force at failure determined to be 7.07 N and the mean value of maximum force at failure to be $3.81 \pm 2.41$ N, with decreases in force at each root field failure (Steinbrecher et al. 2011).

In 2008, it was first discovered that English ivy has the ability to secrete an adhesive matrix composed of highly uniform nanoparticles (Zhang et al. 2008). While several climbing vines are known to release adhesive materials (Endress and Thomson, 1976; Groot et al., 2003), English

and Boston ivy are the only plants recognized to naturally secrete nanoparticles. Sundews (*Drosera* spp.), which are carnivorous perennial herbaceous plants, produce adhesives containing nanoparticles on their leaves that function to capture insects (Zhang et al. 2010).

The nanoparticles produced by English ivy are 50-80 nm spheres, and were found to be produced by root hairs present on adventitious roots (Lenaghan and Zhang 2012; Xia et al. 2010a,b). Compared to algal adhesives, the nanocomposite adhesive from English ivy was found to have much greater adhesion strength (Xia et al. 2010a). Further, using a contact fracture mechanics model, it was demonstrated that van der Waals forces between the nanoparticles alone were not strong enough to produce the attachment strength observed experimentally (Wu et al. 2010). This observation led to the hypothesis that biochemical interactions between the nanoparticles and the polymer matrix generate the strength of adhesion, not a physical interaction between the nanoparticles and the surface. These types of interactions have been observed for other bioadhesives, such as those from marine mussels and barnacles, where an interaction of divalent cations with the adhesive proteins and polysaccharides occurs, generating a stable underwater adhesive (Coombs and Keller 1981).

While studies have extensively examined the physiochemical properties of nanoparticles from English ivy, limited data exist on the potential applications of these naturally produced nanocomposite adhesives. Naturally occurring nanoparticles from English ivy have been examined for their use as an alternative to metal-based nanoparticles for ultraviolet (UV) protection (Xia et al. 2010b). It was observed that ivy nanoparticles were more efficient at blocking UV light, less toxic to mammalian cells, easily degradable, and had limited permeation

through skin when compared to titanium dioxide (Xia et al. 2010b). At a concentration of 4.92 µg/ml the nanoparticles had much greater UV extinction compared to titanium dioxide ($TiO_2$)at the same concentration. Additionally, ivy nanoparticles had no toxic effect when examined using HeLa cells while $TiO_2$ had apoptosis rates that were significantly higher than controls. In order to determine the feasibility of utilizing ivy nanoparticles in cosmetic applications, such as sunscreens, their stability at extremes of temperature and pH was analyzed (Huang et al. 2013). It was found that the ivy nanoparticles were highly stable at temperatures between -20 to 40 °C; however, at 100 °C disruption of the nanoparticle structure was observed (Huang et al. 2013). Similarly, ivy nanoparticles were found to be more stable in neutral and alkaline conditions (pH 7.4, pH 8, pH 9 and pH 10) than acidic conditions (pH 4, pH 5 and pH 6) (Huang et al. 2013).

My PhD research goals were two-fold. First, I sought to develop a system to produce large quantities of adventitious roots from English ivy for harvesting of bulk nanoparticles, Second, I wished to identify the ivy gene(s) and encoded proteins that compose the nanoparticles using biochemical and molecular approaches. These outcomes are required to develop a system in ivy or a heterologous system for bulk production of ivy nanoparticles for commercial application.

This dissertation is organized into 6 chapters. This introduction provides a short background on the properties and sources of nanoparticles from English ivy and their potential in biomedical and cosmetic applications. Chapter 2 is a literature review on the morphological and biochemical adaptations of climbing plants. Chapters 3-6 encompass the breadth of the research and also exist as either published articles or submitted manuscripts for the peer-reviewed literature. Specifically, chapters are separated as follows: initial studies of English ivy nanoparticle

biofabrication (Chapter 3); isolation and chemical analysis of nanoparticles from English ivy (*Hedera helix* L.) (Chapter 4); and isolation and identification of the compounds contributing to nanoparticle formation in English ivy (Chapter 5). Finally, conclusions and future research directions are discussed in Chapter 6.

## References

Bowling A, and Vaughn K. Structural and immunocytochemical characterization of the adhesive tendril of Virginia creeper (*Parthenocissus quinquefolia* [L.] Planch.). Protoplasma. 2008; 232(3-4):153-163.

Coombs TL, Keller PJ. *Mytilus byssal* threads as an environmental marker for metals. Aquat Toxicol. 1981; 1(5-6):291-300.

Dashek WV. Methods for the cytochemical/histochemical localization of plant cell/tissue chemicals. In Methods in Plant Electron Microscopy and Cytochemistry. (ed. Dashek WV), Humana Press, 2000; 27-35.

Steinbrecher T, Beuchle G, Melzer B, Speck T, Kraft O, and Schwaiger R. Structural development and morphology of the attachment system of *Parthenocissus tricuspidata* Int J Plant Sci. 2011; 172(9):1120-1129.

Groot E, Sweeney E, and Rost T. Development of the adhesive pad on the climbing fig (*Ficus pumila*) stems from cluster. Plant Soil. 2003; 248:85-96.

Huang Y, Lenaghan S, Xia L, Burris J, Stewart CN Jr, Zhang M. Characterization of physicochemical properties of ivy nanoparticles for cosmetic application. J Nanobiotechnol. 2013; 11(1):3.

Li Q, Xi L, Zhang M, and Zhang Z. Ultraviolet extinction and visible transparency by ivy nanoparticles. Nanoscale Res Letters. 2010; 5:1487-1491.

Lenaghan SC, Zhang M. Real-time observation of the secretion of a nanocomposite adhesive from English ivy (*Hedera helix*). Plant Sci. 2012; 183(0):206-11.

Melzer B, Steinbrecher T, Seidel R, Kraft O, Schwaiger R and Speck T. The attachment strategy of English ivy: a complex mechanism acting on several hierarchical levels. J R Soc Interface. 2010; 7:1383-1389.

Melzer B, Seidel R, Steinbrecher T, and Speck T. Structure, attachment properties, and ecological importance of the attachment system of English ivy (*Hedera helix*) J. Exp. Bot. 2012; 63 (1): 191-201.

Melzer B, Steinbrecher T, Seidel R, Kraft O, Schwaiger R, Speck T. Mechanics and structure of the attachment system of English ivy (*Hedera helix* L.). In Proc. 6th Plant Biomechanics Conf., Cayenne, French Guyana, 16–21 November 2009 (ed. Thibaut B.), pp. 205–210. Cayenne: ECOFOG

Wu Y, Zhao X, Zhang M. Adhesion mechanics of ivy nanoparticles. J Colloid Interf Sci. 2010; 344(2):533-40.

Xia L, Lenaghan S, Zhang M, Wu Y, Zhao X, Burris J, et al. Characterization of English ivy

(*Hedera helix*) adhesion force and imaging using atomic force microscopy. J Nanopart Res. 2010a; 13:1029-37.

Xia L, Lenaghan S, Zhang M, Zhang Z, Li Q. Naturally occurring nanoparticles from English ivy: an alternative to metal-based nanoparticles for UV protection. J Nanobiotechnol. 2010b; 8(1):12.

Zhang M, Liu M, Prest H, Fischer S. Nanoparticles secreted from ivy rootlets for surface climbing. Nano Lett. 2008; 8(5):1277-80.

Zhang M, Lenaghan S C, Xia L, Dong L, He W, Henson W R, and Fan X. Nanofibers and nanoparticles from the insect-capturing adhesive of the Sundew (*Droser*a) for cell attachment J Nanobiotechnol. 2010; 8: 20.

# Chapter 2. Morphological and biochemical adaptations of climbing plants

Adapted from:

Jason N. Burris, Scott C. Lenaghan, and C. Neal Stewart, Jr. Morphological and Biochemical Adaptations of Climbing Plants. Submitted to Journal of the Royal Society B.

I partially conceived the idea for the review topic and wrote the manuscript.

## 2.1 Abstract

Although plants are generally considered sessile organisms, movement and vertical growth are an essential means by which plants gain a competitive advantage over surrounding species. The stems of climbing plants have little to no ability to bear weight, but they possess high tensile strength and flexibility, which allows them to utilize natural and manmade structures for support and growth. The climbing strategies of plants have intrigued scientists for centuries, yet practical translation of these strategies for engineering purposes has not been realized. In this review, the ecological approaches to various climbing strategies of plants will be discussed in light of their mechanisms. In addition, translation of these strategies into applications will be discussed, along with future perspectives regarding the continued research into climbing plants.

## 2.2 Introduction

For centuries, the specialized adaptations and strategies employed by climbing plants that enable them to compete for sunlight has fascinated researchers. Charles Darwin first categorized climbing plants into five distinct classes based on their modes of attachment: twining [1-4], hook,

leaf-angle [5, 6], tendril-bearer [1, 7-11], and root climbers [5, 10, 12-16] (**Figure 2-1**). Measurements of the adhesive strength of several such climbers, including *Hedera helix* (English ivy) [5, 12, 13, 17, 18], *Ficus pumila* (climbing fig) [15], *Parthenocisus tricuspidata* (Boston ivy) [10, 18], and *Parthenocissus quinquefolia* (Virginia creeper) [7] have been reported (**Table 2-1**). Despite the prolonged fascination with climbing plants, we know surprisingly little about the biology, ecology and biochemistry of attachment and climbing in plants. By way of contrast, we know much more about the mechanisms certain animals use to adhere to surfaces. While the permanent attachment of marine invertebrates [2-4, 19, 20] and the reversible attachment of insects, geckos, tree frogs and spiders [21-25], have received significant attention in recent years, especially with the advent of nanotechnology, less focus has been placed on analyzing attachment systems in plants. Considering the current trend in bioinspired engineering, and recent successes in the translation of fundamental principles gained from the study of animal attachment and climbing to robotics and adhesion [26-31], it makes sense to explore the various strategies and adaptations used by climbing plants. As such, in this review we will describe each of the five modes of attachment identified by Darwin, highlight their structural and mechanical differences, and provide specific examples addressing the ecological and evolutionary significance of their support-finding behavior. Specific attention will be focused on adhesives secreted by plants that enable climbing and how engineering might be inspired by the biology of these fascinating plants.

## 2.3 Evolution and taxonomic distribution of climbing plants

The ability to climb represents a competitive advantage of many plants pertaining to acquire space, light, and nutrients [18-20, 23]. One extreme example is *Convolvulus chilensis*

(correhuela), which has evolved an elegant strategy in plant defense by climbing onto cacti and thorny shrubs to deter mammalian grazers [21, 32]. Another, more common example is *Ipomoea purpurea* (common morning glory), which induces twining as a response to snail herbivory and drought conditions [22]. More generally, outstanding evolutionary success, as measured by the proliferation of species, often requires a key innovation, which allows a clade to exploit a previously under-utilized resource [20]. In the case of vines, a literature survey of 45 families of flowering plants found that 38 taxa with climbers were more diverse than their non-climbing sister groups, which suggests that climbing was a key innovation to success [33]. Additionally, 171 families were found to contain at least one climbing plant species. These families were distributed among ferns (9), gymnosperms (2), basal angiosperms (3), magnoliids (8), monocots (22) and eudicots (127) [34]. Greater than one-third of all seed plant families and three-quarters of all dicots contain climbing plant species [34], indicating that the climbing habit has evolved many more times than originally hypothesized [34]. Considering the fitness benefits imparted by climbing, it is not surprising that climbing has evolved independently in numerous taxa with physiological constraints dictating the biomechanical mode of attachment and climbing [35]. Genetic differentiation is greater in climbing plants and is unlikely due to phylogenetic bias [34]. For example, climbers such as the liana *Berberidopsis carallina* and the non-climber tree *Aextoxicon punctatum* belong to sister families Berberidopsidaceae and Aextoxicaceae within Berberidopsidales [36] and climber liana *Luzuriaga radicans* and the perennial non-climber *Alstroemeria aurea* belong to sister families Luzuriagaceae and Alstroemeriaceae within Liliales [36].

## 2.4 Ecological adaptations by climbing type

### 2.4.1 Twining climbers

Twining plants utilize helical stems to grab support structures and generate a “squeezing” force that prevents slippage down the support structure (**Figure 2-A**) [37]. The change in stem geometry can be predicted based upon the diameter of the supporting structure, with instability occurring as the radius of the support approaches the radius of curvature of the helix [38, 39]. When searching for a substrate, the stem of twining plants increases in length and generates a helical form dictated by the flexible apical region. This apical region can undergo broad bending movements, turning either clockwise or counterclockwise, with early hypotheses suggesting that external stimuli (humidity, light and heat) affect the symmetry of helices [38]. However, recent research has found that the vast majority of twining plants (92%) form right-handed helices, regardless of the hemisphere, latitude, and thigmotrophic responses [40]. After initial contact, the stem continues to expand from the apex, and a uniform helix is formed [38, 39]. In order to strongly adhere to the surface, the helix is tightened around the substrate by twisting, bending, or stretching, with the dominant mechanism remaining unknown. Despite the similarity in overall strategy, twining plants have developed numerous strategies and structures for placing the stem under tension and generating the squeezing force necessary to climb substrates.

These varying approaches to climbing behavior in twining plants can be based upon a variety of ecological factors including, climate, host tree attributes (the size (diameter) of the support), support features (tree bark roughness or smoothness) and other environmental conditions [23]. It was recently found that a greater proportion of twining plants occurred in subtropical regions with warmer climates than temperate climates [41]. In a global analysis of trait variation and

evolutionary study in climbing plants, twining was identified as the most common climbing mechanism and represented 42-75% of all species [42]. There is evidence of genetic variation with regards to differences in winding and morphological adaptability between vines of related origins *Convolvulus* spp., *Ipomoea* spp., [21] and *Lonicera* spp. [43] tested in a common environment.

Mechanistically, one example of a twining climber is the air potato and its relatives, which generate the squeezing force necessary for climbing by the expansion of rigid, flange-like stipules that extend from the base of petioles [44]. Despite a relatively sparse distribution along the stem, the expansion of these structures places the rigid basal portion of the stem under tension, and serves as the points-of-contact between the stem and substrate [44]. While the discovery of the contribution of stipules to climbing in the air potato was novel, a survey of twining plants revealed that monocot and dicot twiners have similar structures (e.g., stipules in *Humulus lupulus*, a curved petiole base in *Phasolus vulgaris*, and the pulvinate petiole in twining Menispermaceae) indicating that this is a conserved mechanism [45]. Despite the commonality of these structures, in the early stages of twining, the dominant force is frictional contact between the flexible apical region and substrate, not the squeezing force that provides stability later in climbing. Generation of a frictional contact force by the flexible apical region has been implicated in the generation of the initial climbing force in many twining plants, such as the common morning glory [33]. In this example, the frictional forces generated were related to the diameter of the substrate, with thicker substrates requiring a larger twining force than slender substrates, owing to its ability to form more gyres per unit length in the slender substrate compared to the thicker one [33]. A similar trend was observed for the invasive vine *Mikania*

*micrantha* (bitter vine), where increasing of the substrate diameter reduced climbing efficiency due to the requirement of a higher squeezing force [46]. Unlike the air potato, however, when the morning glory was removed from its support, its helical stem formed a coil of smaller radius, smaller wavelength, and larger torsion [47], indicating lignification of the basal stem structure for the morning glory. The difference in rigidity between the stem helices, may be a result of the secondary squeezing force provided by the stipules in the air potato that is not generated in the morning glory.

### 2.4.2 Hook and leaf-angle climbers

While the stem plays a key role in twining, hook and leaf-angle climbers employ a strategy in which specialized structures are used as the point of attachment. In the case of hook climbers, recurved spines, hooks, or thorns, are used to passively assist the plant in climbing. These hooks are present on the plant during all stages of growth, and allow the plants to lean on surrounding vegetation without firmly attaching to a support [39]. In opposition to this strategy are leaf-angle climbers, which utilize touch-responsive attachment structures (irritable organs) that undergo morphological changes after contacting a substrate to strongly adhere [35]. Additionally, both hook and leaf-angle climbers are less prone to extreme mechanical stress and cannot be dislodged from a support by movement or mechanical failure, as can be observed in twining plants [48]. The best studied example of hook-climbers are the climbing palms (Calamoideae and *Desmoncus*), which utilize modified leaf apices (cirri) or inflorescences (flagella) that have recurved spines or hooks to grab surrounding host plants and supporting structures (**Figure 2-1C**) [45, 46]. The size of the spines and hooks is dependent on the body size of the plant, with smaller understory climbers developing small sharp hooks and larger canopy climbers

developing large hooks capable of grabbing twigs and branches [48, 49]. Hooks and spines are typically oriented in the direction of least resistance and are capable of disengagement and reengagement as the climber becomes dislodged from its host [48]. In this way, the climbing palms have developed a reversible form of attachment and climbing that is suitable for upward growth and fixed hook position. While this mechanism of attachment provides superior mechanical strength [49], long-term attachment in these species is limited by the senescence of leaves and flagella, which leaves few points of contact with surrounding substrates [50]. This causes these hook-climbers to constantly slip down from the canopy as old growth senesces, forcing newer leaves at the apices to "catch" the plant. This strategy results in an endless cycle of stem growth, cirrus/flagellum production, attachment, senescence, and slippage [50]. The proportion of species utilizing the spine and hook climbing mechanism was found to be greatest around the 5°-10° latitudinal bands, tropical regions [42].

Unlike hook-climbers, leaf-angle climbers utilize modified leaves to cling to surrounding support structures. One example of such a modification can be found in *Galium aparine* (cleavers or catchweed bedstraw), where small hooks, modified trichomes, are present on both the abaxial and adaxial surfaces of the leaves (**Figure 2-1D**) [51, 52]. On the abaxial surface, the hooks are curved towards the leaf base, are situated along the midrib and leaf margins, and are a continuously lignified hollow structure [52, 53]. On the adaxial surface, the hooks are smaller, oriented towards the leaf tip, and evenly distributed across the leaf surface [52, 53]. The difference in orientation of the hooks between the abaxial and adaxial surface allows the abaxial surface to "grab" surrounding leaves and substrates through frictional forces, while the reverse orientation on the adaxial surface reduces friction between surrounding leaves. This results in the

ability of the leaves to orient the adaxial surface of the leaves towards the sky to maximize photosynthesis, while grabbing onto suitable substrates with the abaxial surface [27, 52]. In this way, the arrangement of hooks has evolved to accommodate both photosynthesis, as well as climbing. Another more complex example of a leaf modification for climbing can be found in *Amphilophium crugigerum* (monkey's comb). In this species, after the initial growth of several nodes all with trifoliate leaves, complex leaves begin to form that are composed of a basal pair of foliate leaflets and bifurcated tendril-like leaflets [54]. When the soft hooks on the apical surface of the tendril-like leaflets contact a substrate and they begin to differentiate into callus-like adhesive pads and form intimate contact with the substrate [54]. This intimate contact serves as a signal for the coiling of the tendril-like leaflet, which further brings the stem closer to the substrate, at which point the tissue lignifies [54]. Unlike the adhesive pads that will be discussed for tendril and root climbers, the adhesive pad formed in the monkey's comb does not secrete a liquid adhesive.

### 2.4.3 Tendril climbers

Tendrils are long, slender filamentous organs derived from stems, leaves or flower peduncles and demonstrate movement and growth through contact stimuli [10, 18]. In most cases, tendrils develop into a spring-like support, going from a left-handed helix to a right-handed one, separated by a small internal segment (**Figure 2-1B**). This spring-like support is flexible, and resistant to high winds and weight bearing loads [55]. Tendril climbing was identified as the main mechanism of climbing in two latitudinal bands (35% in 0°-5°, 41% in 20°-25°) and the Americas, and second highest in all other latitudinal bands (19-29%) [42]. The prevalence of tendril climbing in the Americas may be attributed to species relatedness and the highly

conserved traits of climbing plant taxa [42]. Further, more tendril climbing plants have been shown to exist in early successional environments, forest edges, and in locations containing thinner host stem diameters, thus indicating a potential limitation of this strategy [56, 57].

In general, the tendril coiling strategy involves the elongation of the tendril to "search" for a substrate. After contacting a substrate the tendril rapidly coils around the substrate, termed "tip coiling", forming a strong point-of-contact. In some species, this initial coiling is followed by a secondary coiling termed "free coiling", during which the tendrils contract spirally dragging the plant closer to the substrate [57]. One example of a tendril coiling plant is *Luffa cylindrica* (towel gourd). In the towel gourd, free tendrils most often form left-handed helices; however, when contact is made, the tendril gradually reverses direction to form right-handed helices and wrap around a substrate [58]. Interestingly, the thigmotropic response driving coiling can be inhibited by the use of atropine, an inhibitor of acetylcholine, indicating that the towel gourd uses a similar electrical response mechanism seen in the nerve-muscle pathway of mammals [30]. Mechanistically, the reversal in direction of the tendril coil is controlled by alternate shrinking and swelling of cells in inner and outer layers of the tendril [58]. In this way deformation of the helical tendril can be derived from both the geometric and mechanical properties of the cells with hydraulic forces providing control over attachment [58]. Secondary to the initial tendril coiling, the towel gourd also undergoes free coiling, which drags the shoot upward and towards the substrate [59]. As a fail-safe to conserve water, considering the high energy cost of generating these hydraulic forces, it is not surprising that the tendrils will only undergo coiling upon contact with a surface [10].

While tendril coiling represents one elegant strategy used by tendril climbers to scale the canopy, another dominant strategy employs the secretion of adhesive from tendrils to form permanent attachment to substrates. The best studied examples of adhesive-secreting tendril climbers are *Parthenocissus* t*ricuspidata* (Boston ivy) and *Parthenocissus quinquefolia* (Virginia creeper). Both of these species are characterized by tendrils that originate from shoots at the base of foliate leaves [60, 61]. The morphology of the tendril branches are markedly different, however, with bulbous, oval tendril tips in Boston ivy, and elongated, forked, cylindrical tapered tips in Virginia creeper [62]. Further study has demonstrated that the tendrils represent terminal extensions of the shoot, with their own lateral branches that increase the surface area of the tendril [62]. In the event that a tendril contacts a surface, the tendril proceeds through four developmental stages [7, 63]. Upon shoot-surface contact, hooks are initiated for weak interaction with the surface, which, in turn, signals for differentiation of the swollen tendril tips with subsequent development of attachment pads [18, 63]. In stage I, the tip of the tendril swells to form the round/conical precursor to the differentiated attachment pad. During stage II, the pad changes morphology from centrisymmetric to bisymmetric, where the attachment pad begins to flatten at the point of contact with the substrate (**Figure 2-2**) [63]. Following stage II, the attachment pad continues to differentiate into a cap-like structure with bulging edges resembling a suction cup (stage III) (**Figure 2-2**). During stage III, epidermal cells in the periphery of the attachment pad differentiate into a papillate form and grow toward the substrate [63]. Closer examination of these cells shows an accumulation of numerous vacuoles of various sizes that contain electron-dense aggregates of tanniferous substances and insoluble carbohydrates that form the adhesive [7, 11]. As the attachment pad forms more intimate contact with the surface, the adhesive continues to accumulate within the concave region between the pad and surface and

eventually covers the entire contact area [63]. As the adhesive dries, the point at which the attachment pad ends and the surface begins becomes indistinguishable, demonstrating the strong bond formed between the tissue and surface by the adhesive. After all of the adhesive has been secreted, and most likely driven by the change in shape from this fluid loss, the adaxial surface of the attachment pad shrinks, pushing the attachment pad further toward the substrate [18, 63]. During the final stage of the attachment process, stage IV (lignification), the tissue in the attachment pad and tendril lignify, along with curing of the adhesive, leading to permanent contact between the tendril and substrate [18, 63].

Despite the reliance on a liquid adhesive for attachment in *Parthenocissus*, this attachment strategy is comparable to the other systems discussed previously (**Table 2-1**). The strong interfacial bond between the tissue and substrate generated by the secreted adhesive has led researchers to begin to examine the adhesive's chemical structure. Thus far, it has been found that the adhesive is primarily composed of mucopolysaccharides, including rhamnogalacturonan I (RGI), callose, and other mucilaginous pectins [7, 8, 11, 64, 65]. Further analysis of the metallic components of the adhesive revealed the presence of $K^+$, $Na^+$, $Mg^+$, Fe, Mn, which are all essential nutrients for growth, photosynthesis, and chlorophyll production [64]. Surprisingly, however, the most abundant metal present in the adhesive was $Ca^{2+}$, which is known to bind, with high affinity, to RGI [7, 66]. In other eukaryotic and prokaryotic adhesives, $Ca^{2+}$ has been demonstrated as an important cross-linking molecule to promote specific and non-specific binding to proteins and polysaccharides [67]. In this way, the presence of $Ca^{2+}$ in the polysaccharide rich adhesive may indicate a conserved strategy for bioadhesives between plants and animals.

Another example of an adhesive secreting tendril climbers are the passion flowers, *P. discophora*, *P. arbeliazii*, and *P. tryphostematoides*, which utilize attachment pads on branched tendrils to climb [68-70]. Whereas the majority of passion flowers climb using coiled tendrils, *P. discophora* climbs using multi-branched tendrils that emerge from the shoot and have adhesive pads on the terminus of each tendril [68, 71, 72]. Similar to *Parthenocissus*, attachment of *P. discophora* is a multistep process, utilizing intermittent contact prior to the formation of permanent attachment. While immature tendrils have a hook-shape, similar to other tendril climbers, the tip adheres to the surface using epicuticular wax crystals (**Figure 2-3**) [70]. This initial contact serves as a trigger for differentiation of epidermal cells at the apex into papillate cells, devoid of epicuticular wax [70]. These cells continue to grow and form a callus-like tissue (adhesive pad) that gradually fills the gaps between the pad and substrate, similar to the monkey's comb [70]. Unlike the monkey's comb, however, an extracellular adhesive is secreted as the pad presses against the surface. Surprisingly, the adhesive was found to be composed of cutin and lipids, with no mucopolysaccharides, callose, polysaccharides, or proteins, in stark contrast to the adhesives of *Parthenocissus* [70]. After deposition of the adhesive, the pad collapses, followed by lignification, which draws the tendril closer to the surface [70]. From this example, it can be seen that while the overall mechanism may be similar in adhesive tendril climbers, the adhesive is highly varied, which may have important evolutionary and structural implications.

### 2.4.4 Adventitious root climbers

The final category of climbing plants use clusters of adventitious roots that emerge from internodes to climb a variety of supports of nearly any diameter or texture (**Figure 2-1E**) [35].

Whereas tendril climbers use both adhesive and non-adhesive secreting climbing strategies, all adventitious root climbers secrete an adhesive for attachment [1, 12, 15, 17]. In a global analysis, adventitious root climbers were found to be in the least proportion of species across all latitudes, including the continents of Africa, the Americas, Asia and Australia [42]. However, root climbers were found to be in greater populations in forests with higher precipitation and reduced seasonality [73]. Additionally, a reduction of root climbers occurred when temperatures increased in tropical locations [73].

By far the most studied example of a root climber is English ivy [5, 12, 17]. The attachment of English ivy to natural and artificial substrates has been hypothesized to occur in a four-step process: initial physical contact with the substrate, intimate contact of the root with the substrate, chemical adhesion, and lignification with subsequent hook formation (**Figure 2-4**) [12]. Using real-time video microscopy, it was observed that prior to attachment, adventitious roots elongate with the tips oriented in multiple directions [17]. After contact, root hairs begin to rapidly grow posteriorly to the root cap, and begin to secrete adhesive onto the attaching surface [17]. While this is occurring, the adventitious root orients itself parallel to the substrate, bringing the root hairs into closer contact with the substrate and allowing the root hairs to penetrate into and bind to the substrate. Considering that each root hair is a single cell, elongation, vesicle formation, and secretion of the adhesive bears similarities to the papillate cells described for adhesive secreting tendril climbers. It is believed that the root hairs use the secreted adhesive to form a strong initial bond with the surface, which is further strengthened when the root hair lignifies. Upon lignification, the root hair undergoes a drastic change in morphology, where the previously flexible linear structure becomes a rigid hook (**Figure 2-4**). When the root hairs undergo this

change, root hairs inserted into small crevices/pores in the surface will pull the adventitious root into even closer contact. The combination of this chemical and physical attachment process is believed to contribute to the high strength of adventitious root climbers to rough/porous substrates (cork, tree bark, etc.) (**Table 2-1**) [5, 10]. This physicochemical mechanism may also explain why English ivy has a limited ability to effectively attach to smooth surfaces, such as glass and aluminum, while Boston ivy has no such difficulty [13]. The similarities in the attachment strategies of English ivy and Boston ivy warrants closer investigation into their comparative adhesive's chemical structures.

Recent studies have shown that the adhesive secreted by English ivy is a nanocomposite that is composed of nanoparticles and a liquid polymer matrix composed of polysaccharides [17, 74-76]. The nanoparticles have been characterized as highly uniform 50-80 nm spheres, and have been directly correlated with the adhesive secreted by the root hairs [17, 74, 75]. Similar to the results from analysis of the Boston ivy adhesive, the nanoparticles were shown to be composed of C, N, S, and O, indicating that the nanoparticles were primarily composed of biological macromolecules [76]. Unlike the Boston ivy adhesive, however, no metals appear to be associated with the ivy nanoparticles indicating a key difference in the composite adhesives. Further research into the structure of the ivy nanoparticles revealed that the ivy nanoparticles were primarily composed of a glycoprotein complex [76]. In order to determine if the nanoparticles alone could contribute to the adhesive strength of the ivy adhesive, a contact fracture mechanics model was tested, which determined van der Waals forces between the nanoparticles alone were not strong enough to produce the attachment strength observed experimentally [77]. Based on this evidence, cross-linking between the nanoparticles and the

polymer adhesive was hypothesized to be necessary for forming the strong bond between the root hairs and the contact surface. In this way the overall mechanism of the Boston ivy and English ivy adhesives appears to be similar, with $Ca^{2+}$ catalyzing cross-linking the polysaccharides in the Boston ivy adhesive, and the ivy nanoparticles cross-linking the English ivy adhesive. The prevalence of this bioadhesive strategy and implications to future applications and studies will be illustrated in the discussion.

## 2.5 Applications

While numerous examples exist for the translation of animal-inspired climbing and attachment mechanisms to develop engineered products, few examples exist for the translation of plant-based climbing and attachment into other fields. A prime example of the translational success of an animal-inspired attachment process can be observed with the development of the synthetic mussel adhesive Cell-Tak™ [78-80]. Cell-Tak™ utilizes recombinant mussel adhesive proteins combined with synthetic polymers to fabricate an adhesive that can be used in medicine to 'glue' tissue together. Relative to mussel adhesive, the adhesives secreted from Boston ivy, English ivy, and Virginia creeper appear to have product development potential. The adhesive secreted by mussels is a composite composed of adhesive proteins, a polysaccharide matrix (collagen), and an enzyme (catechol oxidase) for cross-linking the two components. In the marine polychaete *Phragmatopa californica*, a similar adhesive is used to glue grains of sand together to form tubular dwellings; however, in this case $Ca^{2+}$ is used to cross-link adhesive proteins with the polysaccharide matrix [81-84]. Clearly these two adhesives bear startling resemblance to the adhesives of Boston and English ivy, making both of these prime candidates for translation into other fields, including biomedicine, paints, synthetic adhesives, etc. Further, a plant-based

production system for adhesives and adhesive proteins has numerous advantages to animal-based systems. One of the greatest advantages is the ability to scale up production of adhesive by adapting climbers as crops.

Although liquid plant adhesives have been slow to make the transition to applications, there are a few examples of plant-inspired dry adhesive products on the market. The most successful example includes hook and loop enclosures, such as Velcro®, which was developed to mimic the thorns present on the seeds of the genus *Arctium* (burdock plants) [85]. Recently research has been conducted into developing hook and loop enclosures based on the hooked trichomes of cleavers with some success [53]. In addition to hook and loop enclosures, the robotics community has started to take note of the mechanics of attachment in climbing plants as a source of inspiration for grasping and climbing. One such example can be seen from the development of a kinematic model based on the tendrils of *Passiflora* [86]. Further studies into the application of tendril climbers have shown the feasibility of using Shape Memory Alloys to replicate the coiling behavior of tendrils [86]. Although these studies illustrate the feasibility of translating the mechanics of climbing and attachment in plants to real-world applications, there still exists a substantial deficit in research geared towards bio-inspired engineering from climbing plants.

## 2.6 Future research and perspectives

Plants have evolved numerous adaptive strategies for climbing, yet the translation of these plant innovations to human innovations has been minimal. In order to make the leap from fundamental understanding to engineered products, it is necessary to follow the path set forward by the

translation of animal climbing to numerous fields, including robotics, biomedical engineering, and even medicine. In the case of tendril coiling and twining plants, future research should focus on understanding how the tissue architecture, hydraulic forces, and frictional forces drive the process of attachment. While studies have focused on several of these aspects, for the engineering of a similar system, the tissue architecture and hydraulic flow must be better understood in order to mimic the system. Clearly the development of shape-changing alloys has opened the door for development of bio-inspired tendril and twining systems; however, a better fundamental understanding of the mechanics of movement in these systems must be the impetus for bio-inspiration. Perhaps the systems with the most potential for bio-inspiration are the adhesive secreting systems of adhesive tendril and root climbers. In these systems, the adhesive itself holds the most potential for translation into other fields. While some preliminary research has focused on understanding the chemical components of these adhesives, little progress has been made on developing synthetic adhesives mimicking their structures. Further research into understanding the chemical components and structure of these adhesives will surely speed the path to engineered systems. Also of interest is the potential to genetically engineer climbing plants or even heterologous "crops" to produce industrial quantities of bioadhesives. Any plant genetic engineering of this sort requires better understanding of the pathways and signaling involved in generating and secreting the adhesive, but has enormous potential in development of a system for harvesting large quantities of adhesive. Considering the depth of research into synthetic adhesives for bonding of wood components, a natural alternative that has evolved over centuries to specifically achieve this task would be a significant achievement. The numerous plant species and mechanisms distributed across a wide variety of plant taxa offer many potential research and economic opportunities.

## Acknowledgements

We thank the National Science Foundation CBET #0965877, the University of Tennessee, and the Ivan Racheff Chair of Excellence Endowment for funding.

## References

[1] Darwin, C. 1865 On the movements and habits of climbing plants. *Journal of the Linnean Society of London, Botany* **9**, 1-118. (doi:10.1111/j.1095-8339.1865.tb00011.x).

[2] Lee, H., Bruce, P.L. & Phillip, B.M. 2007 A reversible wet/dry adhesive inspired by mussels and geckos. *Nature* **448**, 338-341. (doi:10.1038/nature05968).

[3] Lin, Q., Gourdon, D., Sun, C., Holten-Andersen, N., Anderson, T.H., Waite, J.H. & Israelachvili, J.N. 2007 Adhesion mechanisms of the mussel foot proteins mfp-1 and mfp-3. *Proceedings of the National Academy of Sciences USA* **104**, 3782-3786. (doi:10.1073/pnas.0607852104).

[4] Zhang, M.J., Liu, M.Z., Bewick, S. & Suo, Z.Y. 2009 Nanoparticles to increase adhesive properties of biologically secreted materials for surface affixing. *Journal of Biomedical Nanotechnology* **5**, 294-299. (doi:10.1166/jbn.2009.1034).

[5] Sangeetha, R., Kumar, R., Venkatesan, R., Doble, M., Vedaprakash, L., Kruparatnam, Lakshmi, K. & Dineshram. 2010 Understanding the structure of the adhesive plaque of *Amphibalanus reticulatus*. *Materials Science and Engineering: C* **30**, 112-119. (doi:http://dx.doi.org/10.1016/j.msec.2009.09.007).

[6] Sullan, R.M.A., Gunari, N., Tanur, A.E., Chan, Y., Dickinson, G.H., Orihuela, B., Rittschof, D. & Walker, G.C. 2009 Nanoscale structures and mechanics of barnacle cement. *Biofouling* **25**,

263-275. (doi:10.1080/08927010802688095).

[7] Arzt, E., Gorb, S. & Spolenak, R. 2003 From micro to nano contacts in biological attachment devices. *Proceedings of the National Academy of Sciences* **100**, 10603-10606. (doi:10.1073/pnas.1534701100).

[8] Huber, G., Gorb, S.N., Hosoda, N., Spolenak, R. & Arzt, E. 2007 Influence of surface roughness on gecko adhesion. *Acta Biomaterialia* **3**, 607-610. (doi:10.1016/j.actbio.2007.01.007).

[9] Kesel, A.B., Martin, A. & Seidl, T. 2003 Adhesion measurements on the attachment devices of the jumping spider *Evarcha arcuata*. *Journal of Experimental Biology* **206**, 2733-2738. (doi:10.1242/jeb.00478).

[10] Kesel, A.B., Martin, A. & Seidl, T. 2004 Getting a grip on spider attachment: an AFM approach to microstructure adhesion in arthropods. *Smart Materials and Structures* **13**, 512-518. (doi:10.1088/0964-1726/13/3/009).

[11] Smith A, C.J.e. 2006 Properties, principles, and parameters of the gecko adhesive system. In *Biological Adhesives* (eds. A. Smith & J. Callow), pp. 225-256, Berlin Heidelberg, Germany: Springer.

[12] Awada, H., Mezzasalma, L., Blanc, S., Flahaut, D., Dagron‐Lartigau, C., Lyskawa, J., Woisel, P., Bousquet, A. & Billon, L. 2015 Biomimetic mussel adhesive inspired anchor to

design ZnO@ Poly (3‐hexylthiophene) hybrid core@ corona nanoparticles. *Macromolecular Rapid Communications* **36**, 1486-1491. (doi: 10.1002/marc.201500184).

[13] Kalouche, S., Wiltsie, N., Hai-Jun, S. & Parness, A. 2014 Inchworm style gecko adhesive climbing robot. In *IEEE/RSJ International Conference on Intelligent Robots and Systems (IROS)*, Chicago, USA, pp. 2319-2324. (doi:10.1109/IROS.2014.6942876).

[14] Palmer, L.R., Diller, E.D. & Quinn, R.D. 2009 Design of a wall-climbing hexapod for advanced maneuvers. In *IEEE/RSJ International Conference on Intelligent Robots and Systems (IROS),* St. Louis, USA, pp. 625-630. (doi: 10.1109/IROS.2009.5354753).

[15] Santos, D., Heyneman, B., Sangbae, K., Esparza, N. & Cutkosky, M.R. 2008 Gecko-inspired climbing behaviors on vertical and overhanging surfaces. In *IEEE International Conference on Robotics and Automation (ICRA)*, Pasadena, USA, pp. 1125-1131. (doi:10.1109/ROBOT.2008.4543355).

[16] Seo, S., Das, S., Zalicki, P., Mirshafian, R., Eisenbach, C.D., Israelachvili, J.N., Waite, J.H. & Ahn, B.K. 2015 Micro-phase behavior and enhanced wet-cohesion of synthetic copolyampholytes inspired by a mussel foot protein. *Journal of the American Chemical Society* **137**, 914-9217. (doi: 10.1021/jacs.5b03827).

[17] Gillies, A.G., Kwak, J. & Fearing, R.S. 2013 Controllable particle adhesion with a magnetically actuated synthetic gecko adhesive. *Advanced Functional Materials* **23**, 3256-3261.

(doi:10.1002/adfm.201203122).

[18] Paul, G. & Yavitt, J. 2011 Tropical vine growth and the effects on forest succession: A review of the ecology and management of tropical climbing plants. *The Botanical. Review* **77**, 11-30. (doi:10.1007/s12229-010-9059-3).

[19] Biernaskie, J.M. 2011 Evidence for competition and cooperation among climbing plants. *Proceedings of the Royal Society of London B: Biological Sciences* **278**, 1989-1996. (doi:10.1098/rspb.2010.1771).

[20] Gianoli, E. 2004 Evolution of a climbing habit promotes diversification in flowering plants. *Proceedings of the Royal Society of London B: Biological Sciences* **271**, 2011-2015. (doi:10.1098/rspb.2004.2827).

[21] Atala, C. & Gianoli, E. 2008 Induced twining in Convolvulaceae climbing plants in response to leaf damage. *Botany* **86**, 595-602. (doi:10.1139/B08-037).

[22] Atala, C., Quilodrán, M. & Molina-Montenegro, M.A. 2014 Induced twining in *Ipomoea purpurea* (L.) Roth.: response threshold and induction by volatiles and snail damage. *Gayana Botanica* **71**, 181-187. (doi: 10.4067/S0717-66432014000200001).

[23] Gianoli, E. 2015 The behavioural ecology of climbing plants. *AoB Plants* **7**. (doi:10.1093/aobpla/plv013).

[24] González‐Teuber, M. & Gianoli, E. 2008 Damage and shade enhance climbing and promote associational resistance in a climbing plant. *Journal of Ecology* **96**, 122-126. (doi:10.1111/j.1365-2745.2007.01321.x).

[25] Rowe, N., Isnard, S. & Speck, T. 2004 Diversity of mechanical architectures in climbing plants: An evolutionary perspective. *Journal of Plant Growth Regulation* **23**, 108-1128. (doi:10.1007/s00344-004-0044-0).

[26] Bell, P. 1958 Twining of the hop (*Humulus lupulus* L.). *Nature* **181**, 1009-1010. (doi:10.1038/1811009a0).

[27] Bowling, A.J., Maxwell, H.B. & Vaughn, K.C. 2008 Unusual trichome structure and composition in mericarps of catchweed bedstraw (*Galium aparine*). *Protoplasma* **233**, 223-230. (doi:10.1007/s00709-008-0006-7).

[28] Endress, A. & Thomson, W. 1976 Ultrastructural and cytochemical studies on the developing adhesive disc of Boston Ivy tendrils. *Protoplasma* **88**, 315-331. (doi:10.1007/BF01283255).

[29] Endress, A.G. & Thomson, W.W. 1977 Adhesion of the Boston ivy tendril. *Canadian Journal of Botany* **55**, 918-924. (doi: 10.1139/b77-112).

[30] Jaffe, M. & Galston, A. 1968 The physiology of tendrils. *Annual Review of Plant*

*Physiology* **19**, 417-434. (doi: 10.1146/annurev.pp.19.060168.002221).

[31] Steinbrecher, T., Danninger, E., Harder, D., Speck, T., Kraft, O. & Schwaiger, R. 2010 Quantifying the attachment strength of climbing plants: a new approach. *Acta biomaterialia* **6**, 1497-1504. (doi:10.1016/j.actbio.2009.10.003).

[32] González-Teuber, M. & Gianoli, E. 2008 Damage and shade enhance climbing and promote associational resistance in a climbing plant. *Journal of Ecology* **96**, 122-126. (doi:10.1111/j.1365-2745.2007.01321.x).

[33] Scher, J.L., Holbrook, N.M. & Silk, W.K. 2001 Temporal and spatial patterns of twining force and lignifcation in stems of *Ipomoea purpurea*. *Planta* **213**, 192-198.

[34] Gianoli, E. 2015 Evolutionary implications of the climbing habit in plants. *Ecology of Lianas*, 239-250. (doi:10.1002/9781118392409.ch18).

[35] Lenaghan, S.C. & Zhang, M.J. 2012 Real-time observation of the secretion of a nanocomposite adhesive from English ivy (*Hedera helix*). *Plant Science* **183**, 206-211. (doi:10.1016/j.plantsci.2011.08.013).

[36] Stevens, P. 2001 Angiosperm Phylogeny Website. Version 12. Accessed March 2016. http://www.mobot.org/MOBOT/research/APweb/.

[37] Melzer, B., Seidel, R., Steinbrecher, T. & Speck, T. 2012 Structure, attachment properties, and ecological importance of the attachment system of English ivy (*Hedera helix*). *Journal of Experimental Botany* **63**, 191-201. (doi:10.1093/Jxb/Err260).

[38] Melzer, B., Steinbrecher, T., Seidel, R., Kraft, O., Schwaiger, R. & Speck, T. 2009 Mechanics and structure of the attachment system of English ivy (*Hedera helix* L.). In *Proceedings of the 6th Plant Biomechanics Conference,* Cayenne, French Guyana, pp. 16-21.

[39] Melzer, B., Steinbrecher, T., Seidel, R., Kraft, O., Schwaiger, R. & Speck, T. 2010 The attachment strategy of English ivy: a complex mechanism acting on several hierarchical levels. *Journal of the Royal Society Interface* **7**, 1383-1389. (doi:10.1098/rsif.2010.0140).

[40] Zhang, M., Liu, M., Prest, H. & Fischer, S. 2008 Nanoparticles secreted from ivy rootlets for surface climbing. *Nano Letters* **8**, 1277-1280. (doi:10.1021/nl0725704).

[41] Durigon, J., Miotto, S.T. & Gianoli, E. 2014 Distribution and traits of climbing plants in subtropical and temperate South America. *Journal of Vegetation Science* **25**, 1484-1492. (doi:10.1111/jvs.12197).

[42] Gallagher, R.V. & Leishman, M.R. 2012 A global analysis of trait variation and evolution in climbing plants. *Journal of Biogeography* **39**, 1757-1771. (doi:10.1111/j.1365-2699.2012.02773.x).

[43] Schweitzer, J.A. & Larson, K.C. 1999 Greater morphological plasticity of exotic honeysuckle species may make them better invaders than native species. *Journal of the Torrey Botanical Society*, 15-23. (doi: 10.2307/2997251).

[44] Isnard, S., Cobb, A.R., Holbrook, N.M., Zwieniecki, M. & Dumais, J. 2009 Tensioning the helix: a mechanism for force generation in twining plants. *Proceedings of the Royal Society B: Biological Sciences*, **276,** 2643-2650. (doi: 10.1098/rspb.2009.0380).

[45] Isnard, S. & Silk, W.K. 2009 Moving with climbing plants from Charles Darwin's time into the 21st century. *American Journal of Botany* **96**, 1205-1221. (doi: 10.3732/ajb.0900045).

[46] Hu, L. & Li, M. 2013 Climbing capacity of the invasive vine *Mikania micrantha Kunth* on vertical artificial poles. *Biological Invasions* **16**, 295-302. (doi:10.1007/s10530-013-0518-8).

[47] Silk, W.K. & Hubbard, M. 1991 Axial forces and normal distributed loads in twining stems of morning glory. *Journal of Biomechanics* **24**, 599-606. (doi:10.1016/0021-9290(91)90292-U).

[48] Edwards, W., Moles, A.T. & Franks, P. 2007 The global trend in plant twining direction. *Global Ecology and Biogeography* **16**, 795-800. (doi:10.1111/j.1466-8238.2007.00326.x).

[49] Rowe, N. & Isnard, S. 2009 Biomechanics of climbing palms and how they climb. *Plant Signaling & Behavior* **4**, 875-877. (doi:10.3732/ajb.0700005).

[50] Corner, E.J.H. 1966 The Natural History of Palms. Berkeley, CA: University of California Press.

[51] Dransfield, J. 1978 Growth forms of rain forest palms. (Tomlinson, P, B,, Zimmermann, M, H ed (s). Tropical Tees as Living Systems. Cambridge, UK: Cambridge University Press.

[52] Putz, F. 1990 Growth habits and trellis requirements of climbing palms (*Calamus* spp) in North-Eastern Queensland. *Australian Journal of Botany* **38**, 603-608. (doi:10.1071/BT9900603).

[53] Isnard, S. & Rowe, N.P. 2008 The climbing habit in palms: biomechanics of the cirrus and flagellum. *American Journal of Botany* **95**, 1538-1547. (doi:10.3732/ajb.0700005).

[54] Bauer, G., Klein, M.-C., Gorb, S.N., Speck, T., Voigt, D. & Gallenmüller, F. 2010 Always on the bright side: the climbing mechanism of *Galium aparine*. *Proceedings of the Royal Society B: Biological Sciences* **278**, 2233-2239. (doi:10.1098/rspb.2010.2038).

[55] Andrews, H.G. & Badyal, J.P.S. 2014 Bioinspired hook surfaces based upon a ubiquitous weed (*Galium aparine*) for dry adhesion. *Journal of Adhesion Science and Technology* **28**, 1243-1255. (doi:10.1080/01694243.2014.891435).

[56] Dewalt, S.J., Schnitzer, S.A. & Denslow, J.S. 2000 Density and diversity of lianas along a chronosequence in a central Panamanian lowland forest. *Journal of Tropical Ecology* **16**, 1-19. (doi:null).

[57] Niklas, K.J. 2011 Climbing plants: attachment and the ascent for light. *Current Biology* **21**, R199-R201. (doi:http://dx.doi.org/10.1016/j.cub.2011.01.034).

[58] Seidelmann, K., Melzer, B. & Speck, T. 2012 The complex leaves of the monkey's comb (*Amphilophium crucigerum*, Bignoniaceae): a climbing strategy without glue. *American Journal of Botany* **99**, 1737-1744. (doi:10.3732/ajb.1200288).

[59] Wang, J.-S., Wang, G., Feng, X.-Q., Kitamura, T., Kang, Y.-L., Yu, S.-W. & Qin, Q.-H. 2013 Hierarchical chirality transfer in the growth of Towel gourd tendrils. *Scientific Reports* **3,** 3102. (doi:10.1038/srep03102).

[60] Jaffe, M.J. 1970 Physiological studies on pea tendrils VI characteristics of sensory perception and transduction. *Plant Physiology* **45**, 756-760. (doi:10.1104/pp.45.6.756).

[61] Jaffe, M.J. 1970 Reversible force transduction in tendrils of *Passiflora coerulea*. *Plant and Cell Physiology* **11**, 47-53.

[62] Critchfield, W.B. 1970 Shoot growth and leaf dimorphism in Boston ivy (*Parthenocissus tricuspidata*). *American Journal of Botany*, 535-542. (doi:http://www.jstor.org/stable/2441051).

[63] Yang, X. & Deng, W. 2013 Review on the adhesive tendrils of *Parthenocissu*s. *Chinese Science Bulletin* **59**, 113-124. (doi:10.1007/s11434-013-0037-0).

[64] Kim, I. 2014 Structural changes of adhesive discs during attachment of Boston Ivy. *Applied Microscopy* **44**, 111-116. (doi:10.9729/AM.2014.44.4.111).

[65] Wilson, T. & Posluszny, U. 2003 Complex tendril branching in two species of *Parthenocissus*: implications for the vitaceous shoot architecture. *Canadian Journal of Botany* **81**, 587-597. (doi:10.1139/b03-054).

[66] Junker, S. 1976 A scanning electron microscopic study on the development of tendrils of *Parthenocissus tricuspidata* sieb. & zucc. *New Phytologist* **77**, 741-746. (doi:10.1111/j.1469-8137.1976.tb04669.x).

[67] Tianxian, H., Zhang, L. & Wenli, D. 2011 Biological adhesion of *Parthenocissus tricuspidata*. *Archives of Biological Sciences* **63**, 393-398. (doi:10.2298/ABS1102393H).

[68] Bohn, H.F., Günther, F., Fink, S. & Speck, T. 2015 A passionate free climber: structural development and functional morphology of the adhesive tendrils in *Passiflora discophora*. *International Journal of Plant Sciences* 176, 294-305. (doi:10.1086/680231).

[69] Geesey, G.G., Wigglesworth‐Cooksey, B. & Cooksey, K.E. 2000 Influence of calcium and other cations on surface adhesion of bacteria and diatoms: A review. *Biofouling* **15**, 195-205. (doi:10.1080/08927010009386310).

[70] Scanlan, E.M., Mackeen, M.M., Wormald, M.R. & Davis, B.G. 2010 Synthesis and

solution-phase conformation of the RG-I fragment of the plant polysaccharide pectin reveals a modification-modulated assembly mechanism. *Journal of the American Chemical Society* **132**, 7238-7239. (doi:10.1021/ja9090963).

[71] Holm-Nielsen LB, Jørgensen PM, Lawesson JE, Harling G, Andersson L. 1988 *Part 126. Passifloraceae in* Harling G, Andersson L. (eds) *Flora of Ecuador:*, Göteborg University, Göteborg; Riksmuseum, Stockholm; and Pontificia Universidad Católica del Ecuador, Quito.

[72] Ulmer T, MacDougal JM, Ulmer B. 2004 *Passiflora: passion flowers of the world.* Portland, OR: Timber Press.

[73] Durigon, J., Durán, S.M. & Gianoli, E. 2013 Global distribution of root climbers is positively associated with precipitation and negatively associated with seasonality. *Journal of Tropical Ecology* **29**, 357-360. (doi:10.1017/S0266467413000308).

[74] Holm-Nielsen, L.B. & Jorgensen, P. 1986 *Passiflora tryphostemmatoides* and its allies. *Phytologia* **60**, 119-124. (doi: http://dx.doi.org/10.5962/bhl.part.3796).

[75] Jørgensen, P., Holm‐Nielsen, L.B. & Lawesson, J. 1987 New species of *Passiflora subg. Plectostemma and subg. Tacsonia* (Passifloraceae). *Nordic Journal of Botany* **7**, 127-133. (doi:10.1111/j.1756-1051.1987.tb00925.x).

[76] Xia, L., Lenaghan, S.C., Zhang, M., Zhang, Z. & Li, Q. 2010 Naturally occurring nanoparticles from English ivy: an alternative to metal-based nanoparticles for UV protection. *Journal of Nanobiotechnology* **8**, 12. (doi:10.1186/1477-3155-8-12).

[77] Xia, L.J., Lenaghan, S.C., Zhang, M.J., Wu, Y., Zhao, X., Burris, J.N. & Stewart, C.N. 2011 Characterization of English ivy (*Hedera helix*) adhesion force and imaging using atomic force microscopy. *Journal of Nanoparticle Research* **13**, 1029-1037. (doi:10.1007/s11051-010-0091-3).

[78] Benedict, C.V. & Picciano, P.T. 1989 Adhesives from marine mussels. *Adhesives from Renewable Resources* **385**, 465-483. (doi:10.1021/bk-1989-0385.ch033).

[79] Lenaghan, S.C., Burris, J.N., Chourey, K., Huang, Y.J., Xia, L.J., Lady, B., Sharma, R., Pan, C.L., LeJeune, Z., Foister, S., et al. 2013 Isolation and chemical analysis of nanoparticles from English ivy (*Hedera helix* L.). *Journal of the Royal Society Interface* **10**, 20130392. (doi:10.1098/rsif.2013.0392).

[80] Wu, Y., Zhao, X.P. & Zhang, M.J. 2010 Adhesion mechanics of ivy nanoparticles. *Journal of Colloid and Interface Science* **344**, 533-540. (doi:10.1016/j.jcis.2009.12.041).

[81] Coombs, T.L. & Keller, P.J. 1981 *Mytilus* byssal threads as an environmental marker for metals. *Aquatic Toxicology* **1**, 291-300. (doi:http://dx.doi.org/10.1016/0166-445X(81)90023-0).

[82] Fant, C., Elwing, H. & Hook, F. 2002 The influence of cross-linking on protein-protein interactions in a marine adhesive: the case of two byssus plaque proteins from the blue mussel. *Biomacromolecules* **3**, 732-741. (doi:bm025506j [pii]).

[83] Hwang, D.S., Gim, Y., Kang, D.G., Kim, Y.K. & Cha, H.J. 2007 Recombinant mussel adhesive protein mgfp-5 as cell adhesion biomaterial. *Journal of Biotechnology* **127**, 727-735. (doi:10.1016/j.jbiotec.2006.08.005).

[84] Hwang, D.S., Yoo, H.J., Jun, J.H., Moon, W.K. & Cha, H.J. 2004 Expression of functional recombinant mussel adhesive protein Mgfp-5 in *Escherichia coli*. *Applied and Environmental Microbiology* **70**, 3352-3359. (doi:10.1128/AEM.70.6.3352-3359.2004).

[85] Stevens, M.J., Steren, R.E., Hlady, V. & Stewart, R.J. 2007 Multiscale structure of the underwater adhesive of *Phragmatopoma californica:* a nanostructured latex with a steep microporosity gradient. *Langmuir* **23**, 5045-5049. (doi:10.1021/la063765e).

[86] Szefer, P., Ikuta, K., Kushiyama, S., Szefer, K., Frelek, K. & Geldon, J. 1997 Distribution and association of trace metals in soft tissue and byssus of *Mytilus edulis* from the east coast of Kyushu Island, Japan. *Archives of Environmental Contamination and Toxicology* **32**, 184-190. (doi:10.1007/s002449900173).

# Appendix

## Table and Figure

**Table 2-1.** Examples of climbing plants in each of the four categories (tendrils, twining, adventitious roots, and hooks or thorns) and their associated attachment strengths (the maximum force at failure and average values of maximum forces (± standard deviation)).

| Structural category | Species | Common name | Attachment strength (Force (F)) | Reference |
|---|---|---|---|---|
| **Tendrils** | | | | |
| | *Parthenocissus tricuspidata* | Boston ivy | 7.59 ±2.53 N, Fmax=14.03 N | [11] |
| | *Campsis radicans* | Trumpet vine | 18.26 ±6.00 N, Fmax=25.18 N | [11] |
| **Twining** | | | | |
| | *Dioscorea bulbifera* | Air potato | 100-300 mN (squeezing force) | [43] |
| | *Ipomoea purpurea* | Morning glory | 167 ±46 mN (slender pole) | [44] |
| **Adventitious roots** | | | | |
| | *Hedera helix* | English ivy | 3.81 ±2.41 N, Fmax=7.07 N | [11] |
| **Hooks or thorns** | | | | |
| | *Galium aparine* | Cleaver | 21.9 ±13.4 mN foam plastic (adaxial leaf surface) | [53] |
| | | | 33.3 ±15.1 mN foam plastic (abaxial leaf surface) | [53] |

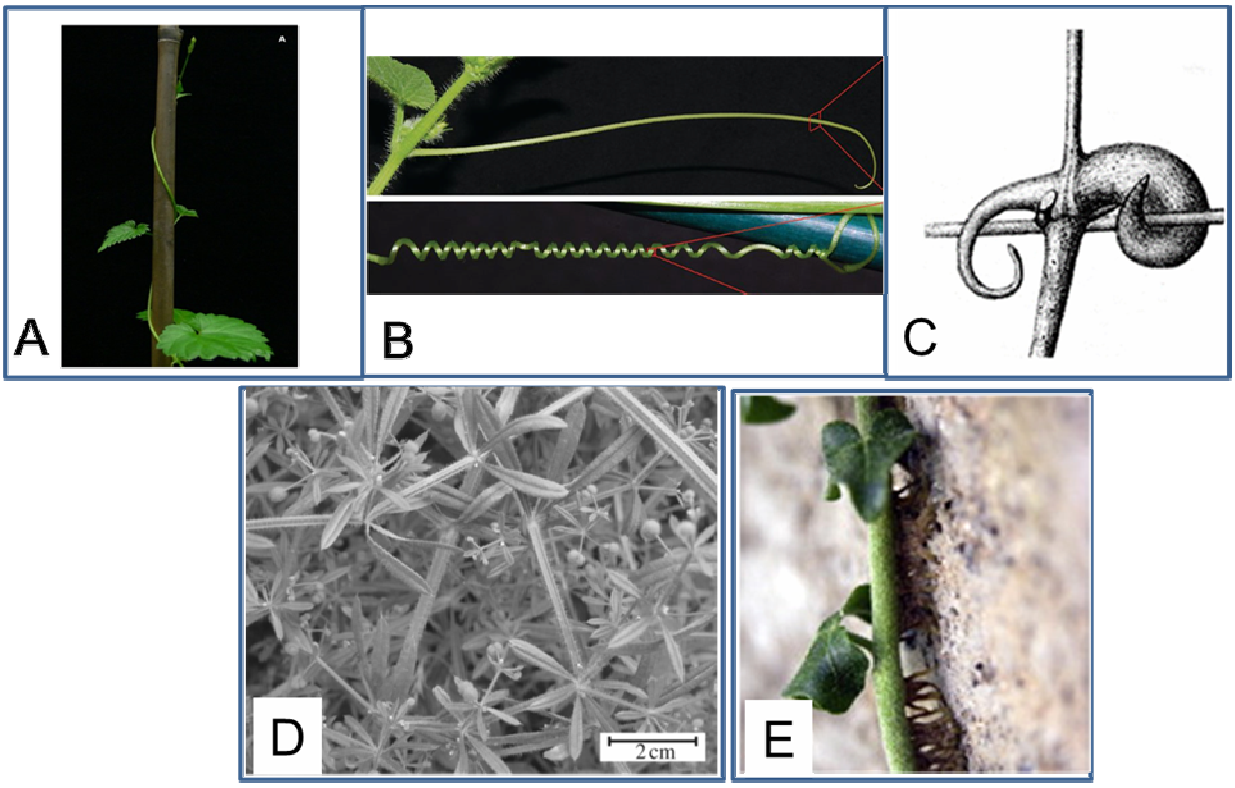


**Figure 2-1.** Example of each climbing strategy identified by Darwin. A) twining (*Humulus lupulus*), B) tendril bearers (*Cucumis sativus*), C) hook-climbers (*Uncaria ovalifolia*), D) leaf-angle climbers (*Galium aparine*), and E) adventitious root climbers (*Hedera helix*). Figure compiled from [1, 11, 42, 53, 91, 92].

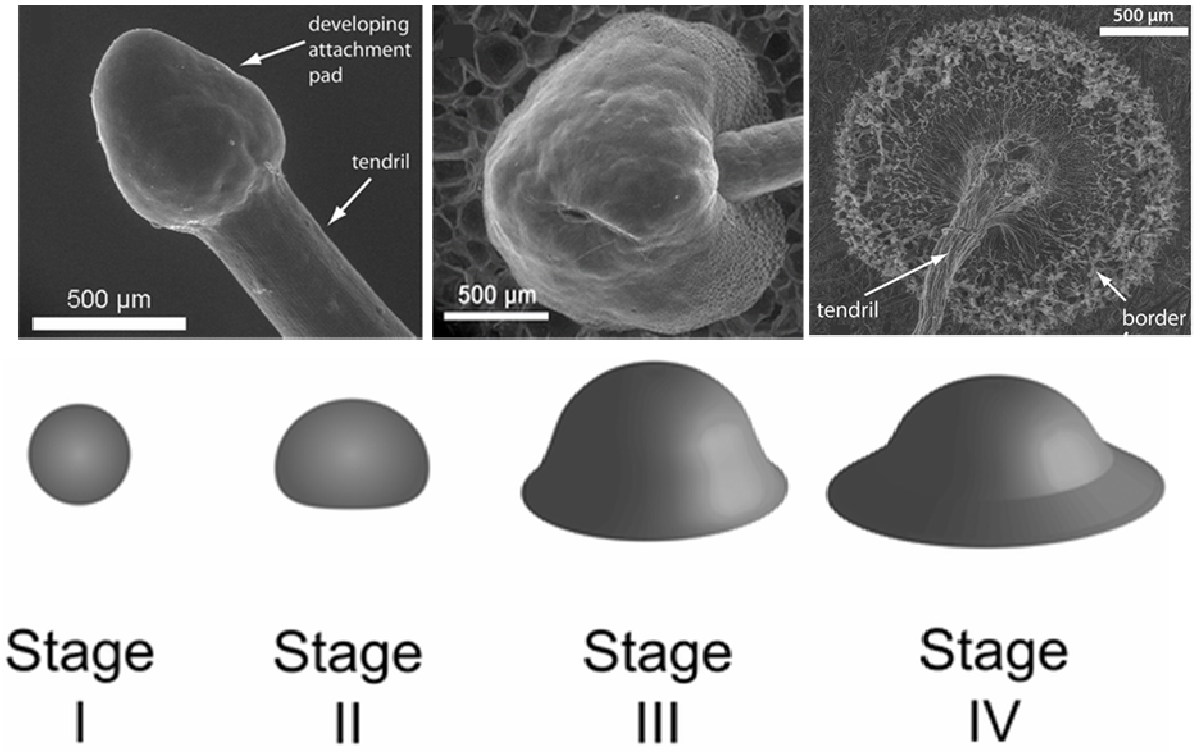


**Figure 2-2.** Structure and morphology of the attachment system of *Parthenocissus triscuspidata* (Boston ivy). A) Swollen tip of a developing attachment pad, B) Freshly attached pad to a sponge, and C) Lignified attachment pad on to cardboard. D) Stage I- II, undifferentiated attachment pad through initial development. Stage III, differentiation of attachment pad to cap-like structure with eventual flattening. Stage IV, lignification of attachment pad surrounded by a border. Modified from [18].

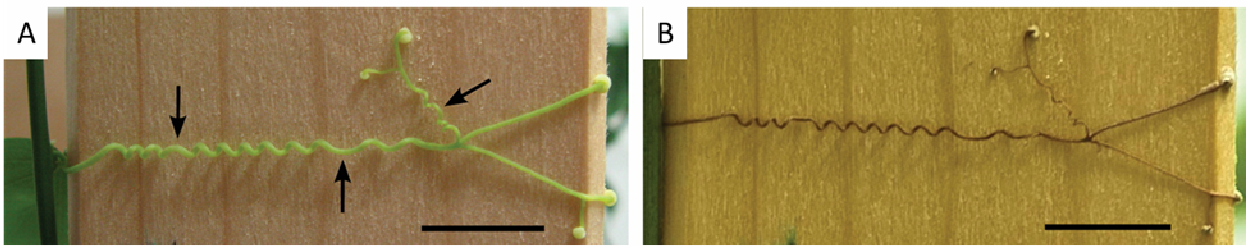


**Figure 2-3**. Development of adhesive tendrils in *Passiflora discophora* (passion flower). A) Fully developed tendril with adhesive pads and coiled axes before senescence and B) following senescence. Scale bar: 10 mm. Arrows indicate a shift of handedness in coils. Modified from [72].

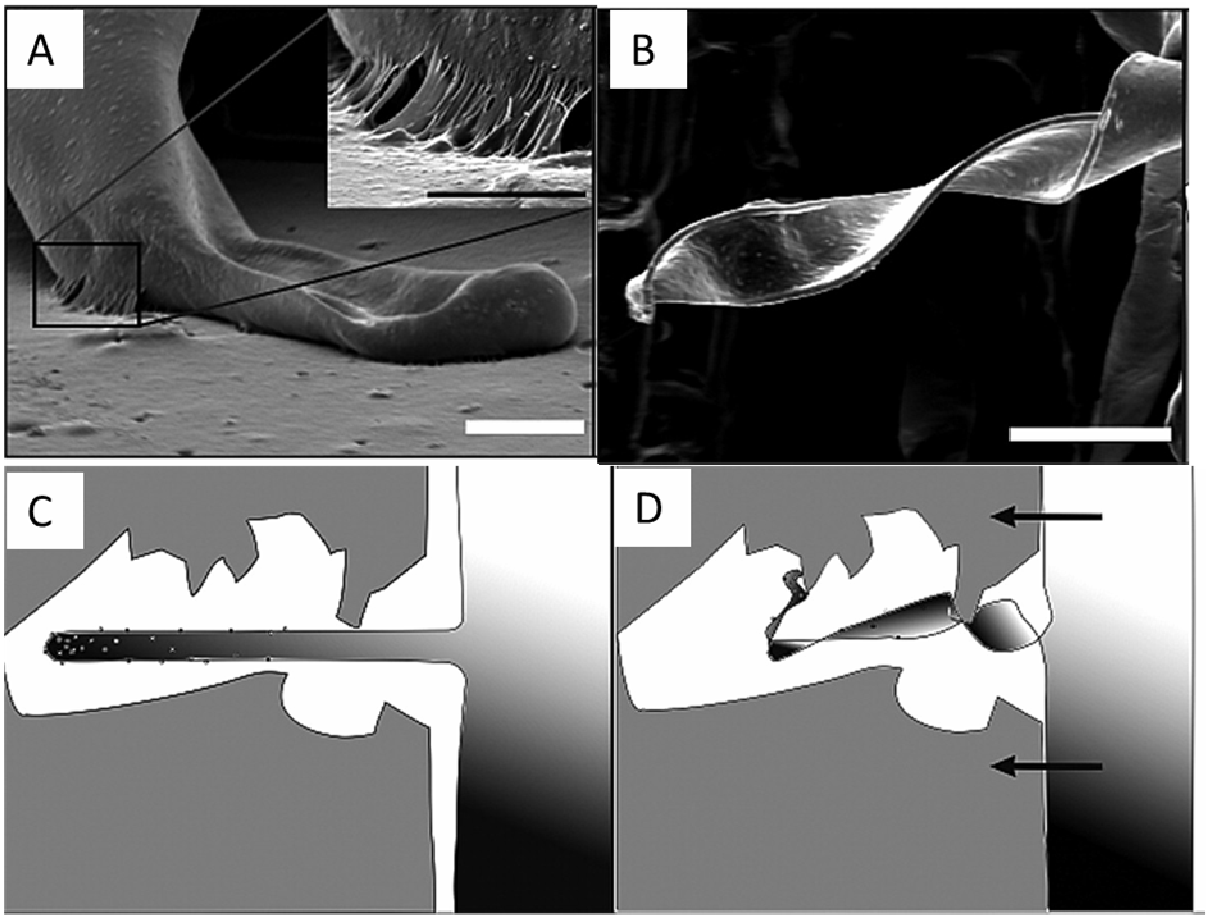


**Figure 2-4.** Participation of root hair in attachment strategy of English ivy. A) SEM of root hair demonstrating point of contact between the secreted adhesive and the substrate. B) SEM of root hair demonstrating the helical from created upon lignification and dehydration. C&D) Schematic of the process of dehydration and hook formation of a root hair, further drawing the shoot into close contact with the substrate. Scale bar on overview 10 µm; scale bar on inset 5 µm. Modified from [39].

# Chapter 3. Nanoparticle biofabrication using English ivy (*Hedera helix*)

Adapted from:

Jason N. Burris, Scott C. Lenaghan, Mingjun Zhang, and C. Neal Stewart, Jr. Nanoparticle biofabrication using English ivy (*Hedera helix*). Journal of Nanobiotechnology 10:41. doi:10.1186/1477-3155-10-41

I designed, executed and analyzed the experiments and wrote the manuscript.

## 3.1 Abstract

**Background**

English ivy (*Hedera helix*) is well known for its adhesive properties and climbing ability. Essential to its ability to adhere to vertical surfaces is the secretion of a nanocomposite adhesive containing spherical nanoparticles, 60-85 nm in diameter, produced exclusively by root hairs present on adventitious roots. These organic nanoparticles have shown promise in biomedical and cosmetic applications, and represent a safer alternative to metal oxide nanoparticles currently available.

**Results**

It was discovered that the maximum adventitious root production was achieved by a 4 h application of 1 mg/ml indole-3 butyric acid (IBA) to juvenile English ivy shoot segments cultured in custom vessels. After incubation of the shoots under continuous light at 83 μmol/$m^2$ s at 20 °C for 2 wk, the adventitious roots were harvested from the culture system and it was possible to isolate 90 mg of dry weight nanoparticles per 12 g of roots. The nanoparticle morphology was characterized by atomic force microscopy, and found to be similar to previous studies.

## Conclusions

An enhanced system for the production of English ivy adventitious roots and their nanoparticles by modifying GA7 Magenta boxes and identifying the optimal concentration of IBA for adventitious root growth was developed. This system is the first such platform for growing and harvesting organic nanoparticles from plants, and represents an important step in the development of plant-based nanomanufacturing. It is a significant improvement on the exploitation of plant systems for the formation of metallic nanoparticles, and represents a pathway for the generation of bulk ivy nanoparticles for translation into biomedical applications.


## Keywords

English ivy, nanoparticles, biofabrication, adventitious root production

## 3.2 Introduction

A wide variety of plants across several taxa have been shown to produce metal nanoparticles with interesting properties when combined with silver nitrate or gold (III) chloride. Nanoparticle production, without the need for silver or gold, has been demonstrated in sundew [1] and English ivy (*Hedera helix* L.; family, Araliaceae) [2-5], a climbing plant well known for its ability to adhere to vertical surfaces [6]. Recent research has demonstrated that the adventitious roots of English ivy are responsible for the production of an adhesive compound composed of polysaccharide and spherical nanoparticles 60-85 nm in diameter [4-5]. These organic nanoparticles have an optical absorption and light scattering properties that make them attractive candidates for sunscreen fillers, especially in light of the toxicity concerns over currently available $TiO_2$ and ZnO nanoparticles [7-8]. In addition to sunscreen applications, the strong adhesive properties of the nanocomposite adhesive formed from the English ivy nanoparticles and surrounding polysaccharide matrix have been implicated in both biomedical and traditional adhesive applications. In both cases, natural nanoparticles produced in plants might be attractive alternatives to currently-used metal nanoparticles [7-8].

Prior to this study it has been laborious to obtain sufficient homogeneous nanoparticles for research purposes. Therefore, our goal was to develop an effective system for nanoparticle production using English ivy as a bioproduction factory. In this work, special attention has been paid to the effect of exogenous auxin application, in this case as a stem soak of indole-3 butyric acid (IBA), to optimize adventitious root and nanoparticle production. Further, a growth-culture system for nanoparticle production using modified Magenta GA7 tissue culture vessels was developed

## 3.3 Results and discussion

Figure 1 demonstrates *Hedera helix* adventitious root production after an incubation of 2 wk from shoots cut into 12.5 cm segments and treated with either low concentrations of IBA 0.0, 0.1, 0.2, 0.3, 0.4, 0.5, 0.6 mg/ml for 16 h or high concentrations of IBA 0, 10, 20, 30, 40, 50, 60, mg/ml after 4 h. Delaying the processing of stems beyond the day received was shown to affect the production of adventitious roots, likely due to abiotic stress (data not shown). Maximum adventitious root production (frozen weight) was achieved by soaking juvenile stems in IBA at a concentration of 1 mg/ml for 4 h, producing approximately 8 g adventitious roots per 5 GA7 vessels (**Figures 3-1, 3-2**) or approximately 100 roots per stem (data not shown). Adventitious root production was optimal under a relatively high IBA concentration of 1 mg/ml for 4 h periods (**Figure 3-2**). However, toxic effects of IBA were observed (necrosis or yellowing of the leaf tissue) when stems were treated with higher concentrations of IBA overnight (**Figure 3-1B**) leading to a decrease in adventitious root production (**Figure 3-2**). Adventitious roots produced using the 1 mg/ml soak over 4 h led to normal adhesive material release with adhesion to the GA 7 wall (**Figure 3-3**). Similar to observations by previous researchers [5], no root hairs were observed to be produced at the tips of roots (**Figures 3-3B, 3-4A**).

Two types of roots are produced from *H. helix*—adventitious and subterranean (**Figure 3-4**). Subterranean roots show a lack of root hairs and produce a branching pattern not shown in adventitious roots (**Figure 3-4**). Previous research, employing a real-time observation system, demonstrated nanoparticles are released specifically from adventitious root hairs [5]. Therefore, we created a system designed for the enhanced production of adventitious roots and associated root hairs. Researchers have hypothesized that English ivy attachment to vertical surfaces occurs

in four stages [9], and a recent researchers [5] have determined the secretion process took approximately 4 to 6 h, and observed that adhesive droplets from multiple root hairs in close proximity fused to form larger adhesive droplets. Similarly, we observed the formation of adhesive droplets on the adventitious roots. The morphology of English ivy nanoparticles was analyzed by atomic force microscopy and dynamic light scattering (**Figure 3-5**) and showed similar results to what has been previously shown from both natural and tissue culture produced roots [1-5].

In natural conditions in the absence of root-to-surface contact, adventitious roots can grow unbranched to lengths 1-15 mm [9]. We have observed root growth of greater than 30 mm without the release of nanoparticles in the GA7 boxes, due to the artificial conditions placed on the stems and excess humidity provided by our rooting chambers. Adventitious rooting cuttings are normally placed under intermittent misting systems that spray water for 2 ½ sec every 5 min to ensure humidity is kept high [10]. By omitting the need for misting and soil/media substrate we have created ideal conditions where cultivated roots produce intact nanoparticles until harvest or until application of mechanical stimulus for natural release. In our observations of roots produced on potted plants, roots that do not come in contact with an attachable surface will dehydrate and abort. Therefore, a high humidity system is required for optimal adventitious root and nanoparticle production. Under high humidity, roots grow unabated for at least one month.

While the composition of the nanoparticle and polysaccharide components in English ivy are unknown, Virginia creeper (*Parthenocissus quinquefolia* L.; family, Vitaceae) exudes a debranched rhamnogalacturonan (RG) I, which allows its attachment to vertical surfaces [11-12].

In order to characterize the chemical composition of English ivy nanoparticles and secreted polysaccharides, it is necessary to produce sufficient quantities of secreted materials for chemical and physical analysis. As such, it was necessary to develop a production and purification system as a means of producing large quantities of adventitious roots and nanoparticles. Here we designed and manufactured a simple rooting chamber for English ivy adventitious root production. In the past, *H. helix* has been examined for its adventitious rooting properties for the production of cuttings for the ornamental horticulture industry [13-14], whereby adventitious roots were produced at very low concentrations, 12 to 22 roots per stem, based upon the treatment applied [10, 14]. Prior research examined the cuttings for production in a horticultural setting through the use of a potting media with and without a misting system [10]. In this study, the addition of IBA and the development of ivy rooting chambers was a significant advancement allowing for the production of large quantities of adventitious roots, and thus ivy nanoparticles.

## 3.4 Methods

Initial English ivy propagules were provided by David Gilmore (Swan Valley Farms, Mount. Vernon, Washington, USA). Stems were segmented to 12.5 cm linear sections and leaves were removed except for one leaf at each stem's apex. IBA potassium salt (Sigma, St. Louis, Missouri, USA) stock solutions were prepared at 50 mg/ml. Two types of IBA soak procedures were performed: an overnight 16 h soak at a low concentration and a 4 h soak with a high concentration. For each concentration, the appropriate amount of a stock solution of 50 mg/ml IBA was added to deionized water for a final volume of 100 ml. For the low concentration soak, concentrations of 0, 0.1, 0.2, 0.3, 0.4, 0.5 and 0.6 mg/ml of IBA were used. For the high concentration soak, concentrations of 0, 1, 2, 3, 4, 5, and 6 mg/ml of IBA were used. Stems were

placed in 150 ml beakers so that the solution covered 75% of the stems (apex was dry) and were incubated in a darkened room overnight. Post-treatment, four stem segments were placed per Magenta GA7 box (Fisher, Waltham, Massachusetts, USA) in an incubator for continuous light at 83 μmol/$m^2$ s at 20 °C for 2 wk. Magenta boxes were converted to ivy rooting chambers by drilling lids with four 13 mm holes. Each hole was centered 1.5 mm from respective corners and a foam plug that has been cut to the center was placed into each hole. Stems were placed into the foam plugs and the bottom of stems rested on the bottom of the Magenta box. Fifty milliliters of water were placed in each box to provide humidity and moisture.

Following 2 wk growth, roots were harvested from stems, flash frozen in liquid nitrogen and fresh weights were recorded. Nanoparticles were extracted from 12 g of frozen adventitious rootlets and macerated as described in [8]. Macerated tissue was squeezed using a glass dounce tissue grinder, only the liquid from the tissue was collected (approximately 10 ml), centrifuged at 5000 x g for 10 min and filtered through a 0.22 μm filter. Nanoparticles were then dialyzed in Spectra cellulose ester dialysis membranes MWCO 300,000 against DI water overnight with 3 DI water changes. Solutions were frozen at -80 C, lyophilized (FreeZone 12 L, Labconco) and dry weights were recorded. The presence and morphology of ivy nanoparticles produced using the system described above were analyzed by atomic force microscopy and dynamic light scattering, as defined in [7-8].

Data were analyzed as a completely randomized design with two replicates by analysis of variance (ANOVA) using the general linear model (SAS 9.3, SAS Institute, Cary, NC). Least significant differences (LSD) were used to compare treatment mean values when significant

differences ($p<0.05$) were found.

## Authors' contributions

JB and SCL designed the project. JB performed the adventitious root and nanoparticle production and wrote the manuscript with SCL. SCL performed the imaging and characterization of the nanoparticles. CNS and MZ contributed to the overall project development and manuscript preparation. All authors read and approved the manuscript.

## Acknowledgements

This research was supported by the National Science Foundation and the Tennessee Agricultural Experiment Station. The authors wish to thank Basmah Kadambalath for her assistance in cutting shoots during the ivy manufacturing process and David Gilmore for providing the shoots.

## References

1. Zhang M, Lenaghan SC, Xia L, Dong L, He W, Henson WR, Fan X: Nanofibers and nanoparticles from the insect capturing adhesive of the sundew (*Drosera*) for cell attachment. *J Nanobiotechnol* 2010, 8:20.

2. Zhang M, Liu M, Prest H, Fischer S: Nanoparticles secreted from ivy rootlets for surface climbing. *Nano Letters* 2008, 8:1277-1280.

3. Wu Y, Zhao X, Zhang M: Adhesion mechanics of ivy nanoparticles. *J Colloid Interface Sci* 2010, 344:533-540.

4. Xia L, Lenaghan SC, Zhang M, Wu Y, Zhao X, Burris JN, Stewart Jr. CN: Characterization of English ivy (*Hedera helix*) adhesion force and imaging using atomic force microscopy. *J Nanopart Res* 2011, 13(3):1029-1037.

5. Lenaghan S, Zhang M: Real-time observation of the secretion of a nanocomposite adhesive from English ivy (*Hedera helix*). *Plant Sci* 2012, 183:206-211.

6. Ackerfield J, Wen J: Evolution of *Hedera* (the ivy genus, Araliaceae): insights from chloroplast DNA data. *Int J Plant Sci* 2003, 164(4):593-602.

7. Li Q, Xia L, Zhang Z, Zhang M: Ultraviolet extinction and visible transparency by ivy nanoparticles. *Nanoscale Res Letters* 2010, 5:1487-1491.

8. Xia L, Lenaghan SC, Zhang M, Zhang Z, Li Q: Naturally occurring nanoparticles from English ivy: an alternative to metal-based nanoparticles for UV protection. *J Nanobiotechnol* 2010, 8:12.

9. Melzer B, Steinbrecher T, Seidel R, Kraft O, Schwaiger R, Speck T:
The attachment strategy of English ivy: a complex mechanism acting on several hierarchical levels. *J Royal Society Interface* 2010, 7:1383-1389.

10. Dirr M: Effects of P-ITB and IBA on the rooting response of 19 landscape taxa. *J Environ Hort* 1990, 8(2): 83-85.

11. Bowling AJ, Vaughn KC: Structural and immunocytochemical characterization of the adhesive tendril of Virginia creeper (*Parthenocissus quinquefolia* [L.] Planch.). *Protoplasma* 2008, 232(3-4):153-63.

12. Steinbrecher T, Beuchle G, Melzer B, Speck, T, Kraft O, Schwaiger R: Structural development and morphology of the attachment system of *Parthenocissus tricuspidata. Int J Plant Sci* 2011, 172(9):1120-1129.

13. Richardson SA, Humphries RN: The rooting of the juvenile form of Hedera helix L. from shoot cuttings. *Sci Hortic* 1982, 33:136-139.

14. Blythe E, Sibley J, Tilt K: Cutting propagation with auxin applied via a stabilized organic

rooting substrate. *Comb Proc-Int Plant Propag Soc* 2003, 53:275-283.

# Appendix

## Figures

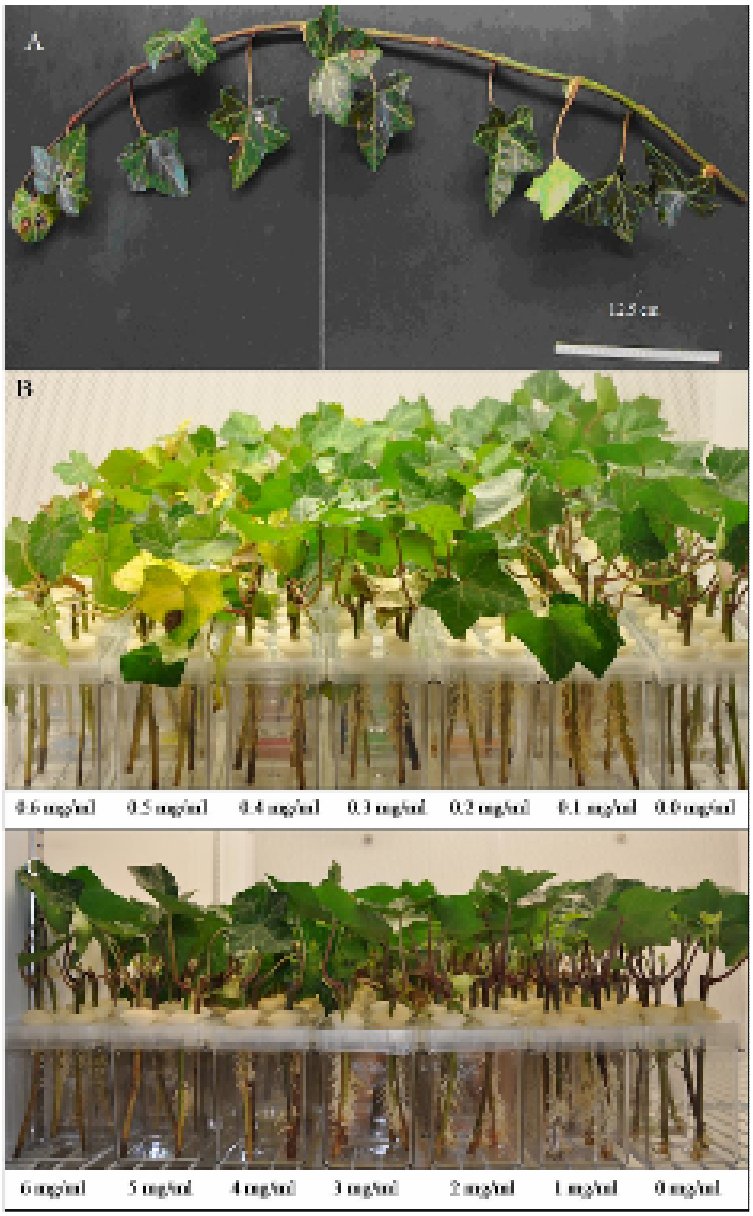


**Figure 3-1.** *H. helix* adventitious root production after 2 wk. A. Initial 50 cm stems were cut into 12.5 cm pieces and treated with either B. low levels of IBA overnight or C. high levels of IBA for 4 h. Necrosis was observed in leaves where stems were treated with >0.4 mg/ml of IBA overnight.

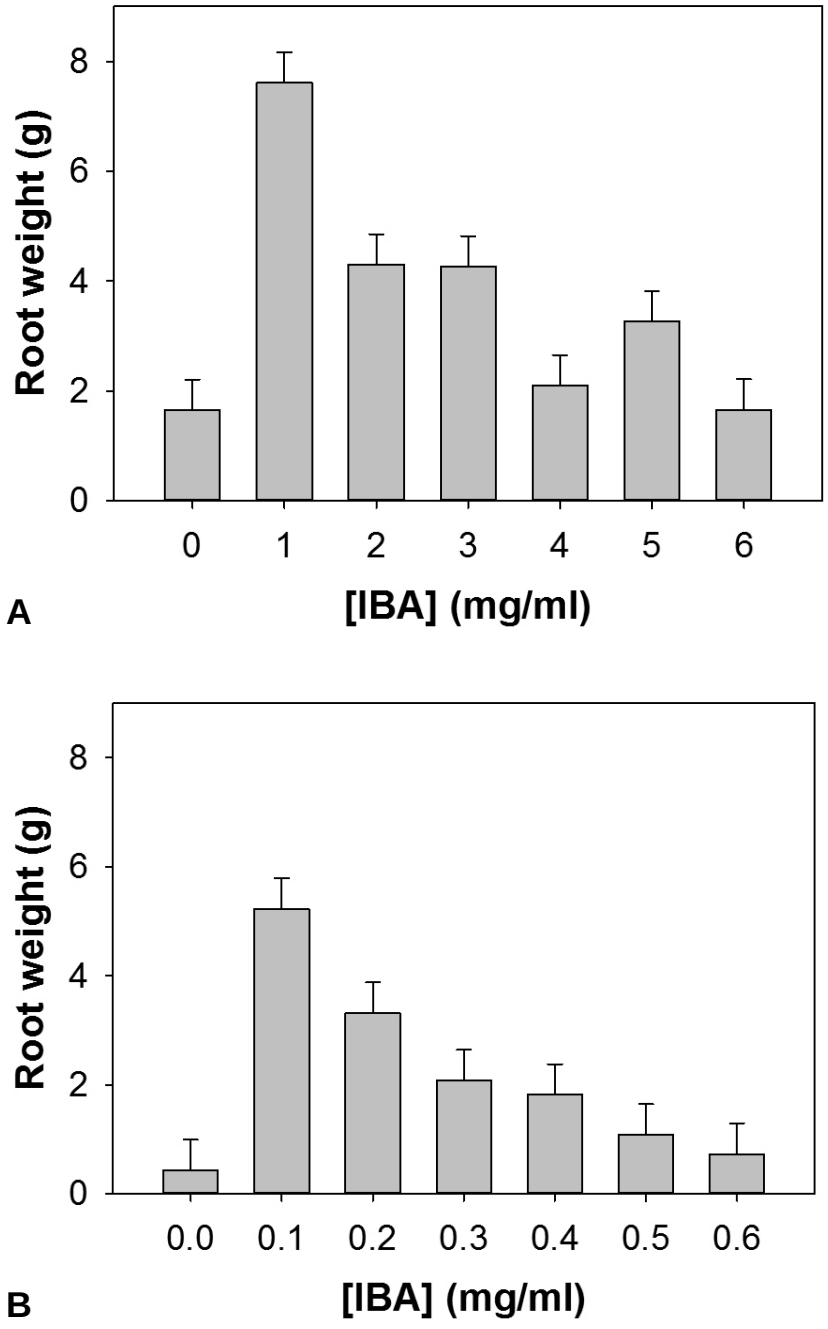


**Figure 3-2.** *H. helix* adventitious root production by weight (g) treated with either A. high levels of IBA ([0-6 mg/ml]) for 4 h or B. low levels of IBA ([0-0.6 mg/ml]) for 16 h. Error bars represent 95% confidence intervals using least significant differences ($P<0.05$).

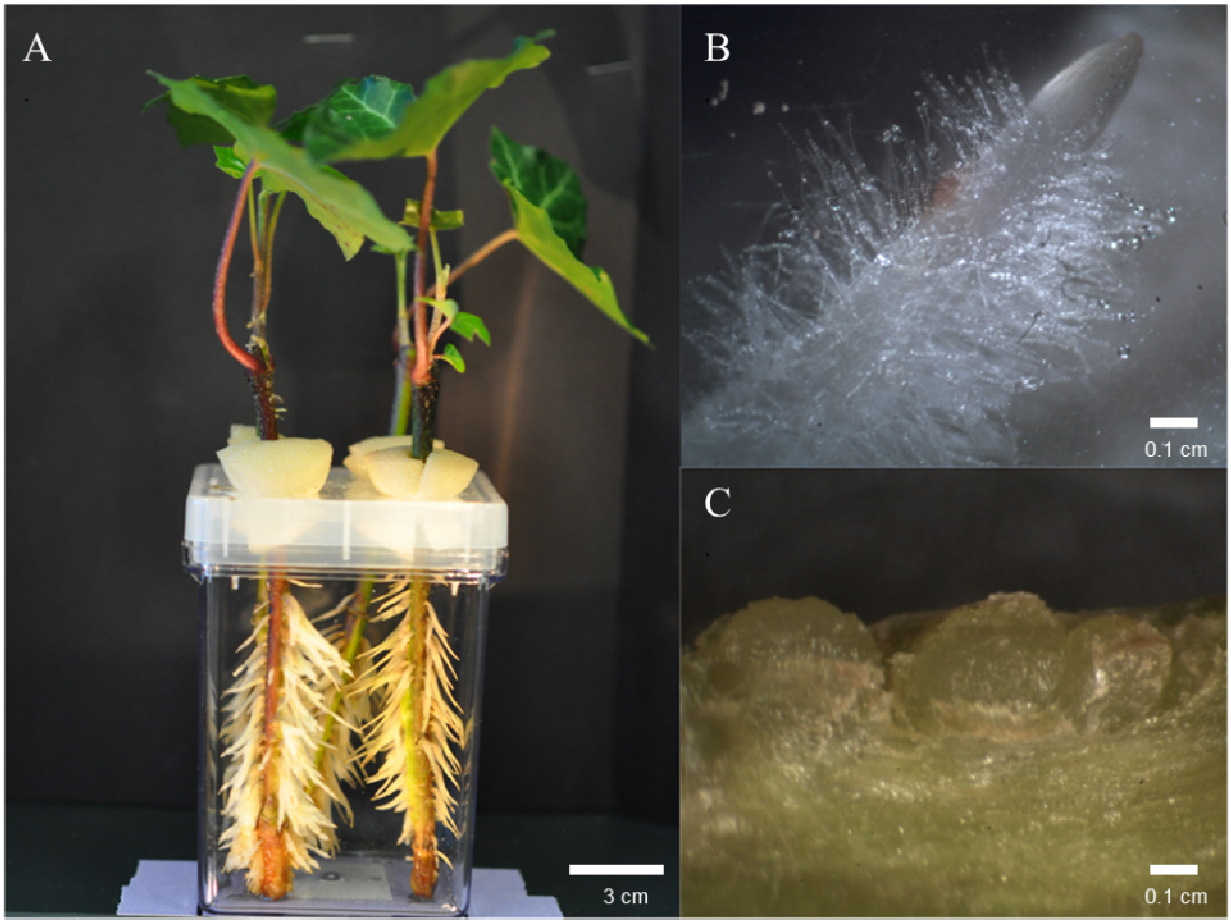


**Figure 3-3.** Adventitious roots produced from *H. helix* A. after 2 wk treated with 100 mg IBA for 4 h, B. adventitious roots releasing adhesive, and C. root primordial after 1 wk.


**Figure 3-4.** Two root types produced by *H.* helix. A. adventitious and B. subterranean roots as viewed under a light microscope. C. High levels of IBA shoots and D. subterranean roots.

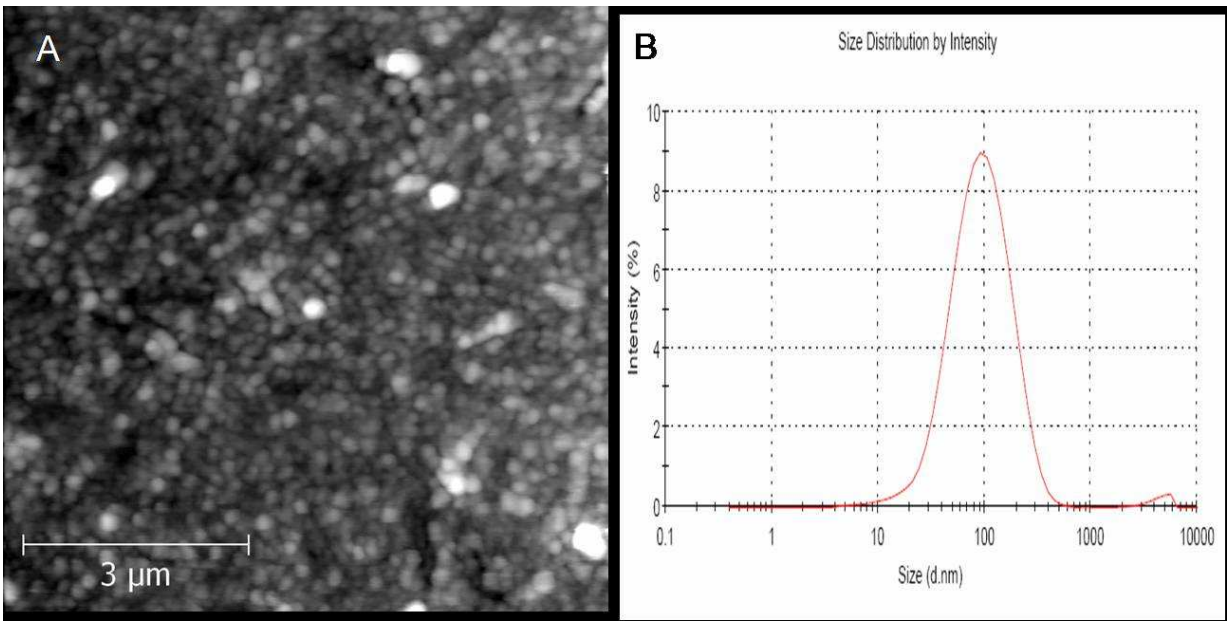


**Figure 3-5.** AFM and DLS of isolated ivy nanoparticles. A. AFM micrograph of ivy nanoparticles. B. DLS of ivy nanoparticles, with a mean diameter of 109.8 ± 5.6 nm.

# Chapter 4. Isolation and chemical analysis of nanoparticles from English ivy (*Hedera helix* L.)

Adapted from:

Scott C. Lenaghan, Jason N. Burris, Karuna Chourey, Yujian Huang, Lijin Xia, Belinda Lady, Rittin Sharma, Chongle Pan, Zorabel LeJeune, Shane Foister, Robert L. Hettich, C. Neal Stewart, Jr., and Mingjun Zhang. 2013. Journal of Royal Interface. 10(87), 20130392.

I designed, executed and analyzed the experiments relating to the protein isolation and helped to write and edit the manuscript. Specifically, I ran and stained the protein gel found in the manuscript, but also performed many experiments not included in the manuscript to determine the protein composition of the nanoparticle (see Supplemental)

## 4.1 Abstract

Bio-inspiration for novel adhesive development has drawn increasing interest in recent years with the discovery of the nano-scale morphology of the gecko footpad, and mussel adhesive proteins. Similar to these animal systems, it was discovered that English ivy (*Hedera helix* L.) secretes a high strength adhesive containing uniform nanoparticles. Recent studies have demonstrated that the ivy nanoparticles not only contribute to the high strength of this adhesive, but also have UV protective abilities, making them ideal for sunscreen and cosmetic fillers, and may be used as nanocarriers for drug delivery. To make these applications a reality, the chemical nature of the ivy nanoparticles must be elucidated. In the current work, a method was developed to harvest bulk ivy nanoparticles from an adventitious root culture system, and the chemical composition of the nanoparticles was analyzed. Ultraviolet/visible (UV/Vis) spectroscopy, inductively coupled plasma mass spectrometry (ICP-MS), fourier transform infrared

spectroscopy (FTIR), and electrophoresis were used in this study to identify the chemical nature of the ivy nanoparticles. Based on this analysis, we conclude that the ivy nanoparticles are proteinaceous.

## 4.2 Introduction

Recent studies showed that the root hairs from the adventitious roots of English ivy (*Hedera helix* L.) secrete a nanocomposite adhesive composed of nanoparticles and a liquid polymer matrix [1-2]. The naturally secreted nanoparticles are highly uniform with a diameter of 50-80 nm, as measured by atomic force microscopy (AFM), and were hypothesized to contribute to the high adhesive strength of English ivy [2-4]. Force spectroscopy conducted on the freshly secreted adhesive found that the strength of the ivy adhesive was much greater than similar bioadhesives [4]. In order to determine the potential contribution of the ivy nanoparticles to the generation of the measured adhesive force, a contact fracture mechanics model was developed to predict the attachment strength of the nanoparticles [3]. Based on the model, it was discovered that van der Waals forces between the nanoparticles alone were not strong enough to generate the attachment strength observed experimentally. The data led to the hypothesis that the interaction between the nanoparticles and the polymer matrix generates cross-linking reactions that lead to an increased strength of adhesion. This hypothesis is consistent with the mechanism of other bioadhesives, such as the marine mussels and barnacles, where adhesive proteins interact with divalent cations and polysaccharides to generate a stable water resistant adhesive [5].

In addition to the role of ivy nanoparticles in the formation of strong adhesive forces, the

nanoparticles have also demonstrated unique optical properties. A recent study demonstrated, through UV/Vis spectroscopy, that the ivy nanoparticles exhibit a strong UV absorbance from 200-400 nm [6-7]. Comparison of the ivy nanoparticles with similar concentrations of ZnO and $TiO_2$ nanoparticles demonstrated an increased ability to block UV light, indicating a potential role for the ivy nanoparticles as sunscreen protective agents [3]. In the same study, the ivy nanoparticles were shown to be less toxic to mammalian cells, when compared to similar concentrations of $TiO_2$ nanoparticles [7]. The reduced toxicity was speculated to be attributed to the organic nature of the nanoparticles, compared to the metallic nature of the $TiO_2$ nanoparticles; however, the chemical nature of the ivy nanoparticles was not known at the time of this study.

There are a number of potential applications for which the ivy nanoparticles are ideally suited [3, 7-8]; however, several issues exist before they can be used for large scale applications. First, a method must be developed for isolating ivy nanoparticles from the root hairs of adventitious roots. Second, enough ivy nanoparticles should be collected for chemical analysis, to determine the chemical nature of the ivy nanoparticles, and the chemical components that makeup the nanoparticles. In this work, we have achieved both of these goals, first by developing a procedure for the production of ivy nanoparticles, and second, by using this method to collect gram quantities of nanoparticles for chemical analysis.

## 4.3 Results and discussion

### 4.3.1 Production of ivy nanoparticles

A significant challenge to the collection of ivy nanoparticles was the small size of the root hairs (~10 um in diameter). In the natural system, when the root cap of an adventitious root contacts a surface, the root hairs begin to elongate and secrete adhesive [1, 9]. As mentioned earlier, it has been proven in previous studies that this secreted adhesive contains nanoparticles [1]. Since the root hairs are the only known structures involved in the generation of the nanocomposite adhesive [1], the first step in the development of a procedure for nanoparticle production was to maximize the production of root hairs, while preventing any external contamination. As a result, a tissue culture method was developed for growing the adventitious roots from cut shoots in sterile Magenta® GA-7 (MAG) plant culture boxes. Ivy shoots used for tissue culture were donated by Swan Valley Farms (Bow, Washington) on a weekly basis. Briefly, shoots were cut to approximately 6 inches with one leaf remaining on the top of the shoot. The external surfaces of the shoots were then sterilized and the shoots placed upright into MAG boxes containing nutrient media. The boxes were then sealed and placed into a plant growth chamber with controlled light and temperature. By sealing the MAG boxes, it was possible to achieve 100% humidity in the boxes, which was crucial for maintaining the hydration of the adventitious roots. Using this culture method, it was possible to generate harvestable adventitious roots every two weeks. In addition, adventitious roots grew much denser in the culture system when compared to uncultured plants. Further, the adventitious roots had a much higher concentration of root hairs, owing to the high humidity and the increased availability of nutrients. Development of this culture system greatly increased the ability to generate the tissue for nanoparticle secretion, leading to further advances in the design of a robust method for ivy nanoparticle isolation.

With the stable, scalable tissue culture system described above, the next step was to harvest the tissue for isolation of the nanoparticles. Considering the small diameter of the root hairs and the rapid dehydration of the tissue when separated from the adventitious roots, the entire adventitious root was collected for harvesting the nanoparticles. To preserve the integrity of the tissue during the time required for harvesting, the adventitious roots were excised directly into a liquid nitrogen cooled container resulting in an immediate snap freezing of the tissue. After collection of bulk adventitious roots, the roots were stored at -80°C. Once an appropriate amount of tissue (> 1 g) was collected for nanoparticle isolation, the tissue was homogenized at 4°C using a mortar and pestle. Manual homogenization was conducted with only a minimum amount of ultrapure water to allow the solution to be easily pipetted out of the mortar. After homogenization, the solution containing a large amount of cell debris, proteins, the polymer adhesive, and nanoparticles was obtained. To remove the large debris, the solution was filtered through a 0.2 µm syringe filter and then centrifuged at 1,000 x g to remove any remaining debris. Finally, the sample was dialyzed through a 300 kD Spectra/Por cellulose ester (CE) dialysis membrane overnight at 4°C with constant stirring. This high molecular weight (MW) dialysis membrane was effective for removing most proteins, and also salts present in the sample. Smaller MW dialysis membranes were tested; however, the nanoparticles isolated using the 300 kD membrane represented the purest fraction through elimination of extraneous lower MW compounds, thus this membrane was used for further purification. After dialysis, samples were run on an SEC-HPLC column for separation of the ivy nanoparticles from the other components.

Previous studies using freshly secreted ivy nanoparticles indicated that the nanoparticles absorbed UV light over the range of 200-400 nm [6-7]. Since the UV absorbance and

morphology of the ivy nanoparticles were known, samples eluted from the SEC-HPLC column were collected every minute and scanned using an AFM. In addition, a UV detector was used to constantly measure the UV absorbance at both 280 and 320 nm during the entire elution. Based on the AFM images, it was determined that the ivy nanoparticles were contained in the fraction collected from 10-11 minutes. The nanoparticles collected in this fraction had the same morphology as those secreted directly from the plant (**Figure 4-1A, 4-1B**). Further analysis of the morphology of individual nanoparticles was carried out by examining diluted samples using both AFM and SEM (**Figure 4-1C**). In addition to these techniques, DLS and Zeta Potential analysis were performed to determine the size distribution and stability of the hydrated nanoparticles (**Figure 4-2A, 4-2B**). DLS conducted on nanoparticles obtained from three separate batches of adventitious roots confirmed the presence of the ivy nanoparticles in the solution collected from the 10-11 min fraction with a mean diameter of 95.69 ±5.56 nm (**Figure 4-2A**). As expected, the nanoparticle diameter measured by DLS was larger than that using the AFM and SEM, due to the hydrodynamic radii present in solution [10]. In addition, Zeta Potential analysis indicated that the ivy nanoparticles did not form a stable solution in ultrapure water (**Figure 4-2B**). This was expected, since the ivy nanoparticles have been observed to slowly precipitate in neutral solutions.

In addition to the physical structure of the isolated ivy nanoparticles, the data from the UV detector showed a high intensity peak at ~10.5 min at both 280 and 320 nm (**Figure 4-3A, 4-3B**). These peaks were positively correlated with the AFM and DLS data, and confirmed the presence of the ivy nanoparticles. In previous studies, determination of the concentration of ivy nanoparticles in solution could only be estimated, due to the limited quantity of nanoparticles [6].

Using the method developed above, after collecting the concentrated ivy nanoparticles, the samples were pooled and lyophilized to get an accurate measure of the dry weight of the ivy nanoparticles. To confirm that the previously observed UV/Vis absorbance spectra [6-7] was due to the ivy nanoparticles alone, it was necessary to analyze the concentration dependent effect of the ivy nanoparticles using UV/Vis spectroscopy. As shown in **Figure 4-4A**, when the concentration of the ivy nanoparticles decreased, the resulting absorbance decreased. A plot of the UV absorbance at 283 nm showed a linear increase between the concentration of the ivy nanoparticles and the absorbance value measured by the UV/Vis spectrometer. This linear increase in absorbance demonstrated that the UV absorbance spectra obtained was from the ivy nanoparticles. After thorough validation of the method described above for the generation of ivy nanoparticles, the above procedure was repeated to collect enough nanoparticles for subsequent chemical analysis.

### 4.3.2 Chemical analysis of the ivy nanoparticles

The first step in chemical analysis of the ivy nanoparticles was to confirm that the nanoparticles are organic and did not contain any metals. This is especially important when considering the large number of metallic nanoparticles that can be formed naturally from heavy metal substrates. Numerous studies have demonstrated the potential for plants, including English ivy, to generate nanoparticles from tetrachloroaurate ($HAuCl_4$), silver nitrate ($AGNO_3$), chloroplatinic acid hexahydrate ($H_2PtCl_6 \cdot 6H_2O$), and iron (III) chloride hexahydrate ($FeCl_3 \cdot 6H_2O$) [11-14]. Since the ivy shoots were grown in a cultured environment, and were not exposed to variable soil conditions, it was also expected that this would reduce the availability of heavy metal substrates. To rule out the possibility of the ivy nanoparticles containing metallic components, 48.78 mg of ivy nanoparticles were analyzed using inductively coupled plasma mass spectrometry (ICP-MS).

This technique can be used to detect trace levels of metals in a sample, and has recently been expanded to the analysis of metallo-biomolecules, including metalloproteins [15-16]. The ivy nanoparticles were analyzed independently by Galbraith Laboratories, Inc. The results indicated that 47 out of 57 elements tested were below the limit of detection of the test at less than 2 parts per million (ppm). These included the most common metals used for the synthesis of nanoparticles from plant extracts, gold, silver, platinum, and iron. In addition to the metals that were below the detection limit, only manganese and zinc were found above 30 ppm, and both were still at below trace concentrations (**Figure 4-5**). Since no metals were detected above trace levels, it can be concluded that the ivy nanoparticles are, in fact, organic nanoparticles.

After confirmation of the organic nature of the ivy nanoparticles, the next step was to analyze what type of molecules may be responsible for the formation of the nanoparticles. In previous studies of Boston ivy (*Parthenocissus tricuspidata*) and Virginia creeper (*Parthenocissus quinquefolia*), it was found, through immunocytochemical analysis, that the majority of the components in the secreted adhesives were mucilaginous pectins, callose, tanniferous substances, and acid mucopolysaccharides [17-19]. However, nanoparticles were not observed in either of these studies, potentially due to the techniques employed at the time of the studies. In other biological systems, such as the marine mussel *Mytilus edulis* and polychaete *Phragmatopa californica*, proteins are considered as the main building blocks that lead to the generation of strong adhesive forces [20-22]. In these two systems, unlike *Parthenocissus sp.*, the adhesives secreted from these organisms have shown the presence of nanoparticles, mainly thought to form from the interactions of negatively charged proteins with divalent cations, forming three dimensional nanoparticles [22]. Based on this information, we established a series of

experiments to determine the organic components involved in the formation of the ivy nanoparticles.

The first experiment conducted was elemental analysis to determine the amount of carbon, nitrogen, and sulfur present in the ivy nanoparticles. It was found that the nanoparticles were composed of 51.77% carbon and 4.72% nitrogen (**Figure 4-5**). This was a relatively high carbon to nitrogen ratio ~10:1, and was indicative of a biomolecule such as DNA, RNA, or protein. In addition, the nanoparticles contained 0.32% sulfur, which again would be expected for a biomolecule, such as a protein, where disulfide bonds play an important role in folding and stability, especially in secreted proteins [23]. While this evidence strongly pointed to the presence of proteins in the nanoparticles, it could not rule out that other biomolecules, such as polysaccharides, may still contribute to the overall structure. In addition, since nanoparticles were isolated, and not an individual chemical component, it was possible that the C:N ratio could have been skewed by the presence of multiple components. As a result, FTIR was conducted on lyophilized nanoparticles to obtain further information on the chemical structures of the nanoparticles.

As demonstrated in **Figure 4-6**, the FTIR spectra of the ivy nanoparticles was compared with the spectra generated from a typical protein sample, bovine serum albumin (BSA), and also a popular polysaccharide used in the fabrication of nanomaterials, chitosan. All three samples showed a peak at 1,653 $cm^{-1}$ indicating vibration around C=O and C-N, along with peaks at 1,384-1,385 $cm^{-1}$, indicating C-H bending in aliphatic side groups [24-25]. Additionally, shared peaks at 2928 $cm^{-1}$ for both ivy nanoparticles and chitosan, and 2932 $cm^{-1}$ for BSA, indicate the

vibration of C-H present in all samples. When compared to the BSA spectra, the ivy nanoparticles also shared a peak around 1518 $cm^{-1}$ for BSA, and 1539 $cm^{-1}$ for ivy. This peak represents the amide II band, and is a standard protein peak, indicating the presence of in-plane N-H bending, and the stretching vibrations of C-N and C-C [25]. In standard protein samples, this amide II band often shows similar intensity to the amide I band, as shown for BSA, but the complexity of this band leads to variable intensity and shifts of this peak. In addition to the peak shared by the BSA and ivy nanoparticle sample, the chitosan and ivy nanoparticles shared a peak at 1071 $cm^{-1}$ for chitosan, and 1076 $cm^{-1}$ for the ivy nanoparticles, indicating the presence of glycoconjugates. This peak was associated with vibration of the CO-C bond typically found in carbohydrates [24-25], and thus was not present in the BSA sample. The broad peak present at 3329 $cm^{-1}$ in the BSA sample, indicates the vibration of N-H, and is similar to the broad peaks for chitosan, 3433 $cm^{-1}$, and the ivy nanoparticles, 3407 $cm^{-1}$, where the shift is due to the addition of vibration from O-H [24]. Based on the FTIR data, in combination with the elemental analysis, we believed that the most likely component of the nanoparticles was glycoprotein, due to the shared amide II band with the BSA spectra, and the shared CO-C band with the chitosan spectra. In addition, the shift in the broad peak at 3407 $cm^{-1}$, indicated that O-H bonds were present, further suggesting the presence of carbohydrate. Based on this data, individual proteins and glycoproteins were believed to form the ivy nanoparticles, and thus we conducted gel electrophoresis to identify individual proteins.

Several different gel electrophoresis techniques were evaluated in this study to determine if the proteins and glycoproteins could be separated from the ivy nanoparticles. It was determined that SDS-PAGE with a 5% stacking gel and 10% resolving gel yielded the best results for the ivy

nanoparticles. In addition, the samples were pre-treated with 2 M thiourea, 8 M urea, and 3% SDS, to completely solubilize the nanoparticles, which reduced the background staining. After electrophoresis for 4 hours at 180 V, duplicate gels were stained with either the Pro-Q Emerald 300 Glycoprotein Stain Kit (Molecular Probes, Inc., Eugene, OR) or the PlusOne Silver Staining Kit (AP Biotech). For reproducibility, ivy nanoparticles isolated from three different isolation procedures with two different researchers were tested. Surprisingly, only one high molecular weight band (> 460 kD) was observed in all of the ivy nanoparticle samples, despite the harsh denaturing conditions used, **Figure 4-7**. This high molecular weight band stained positive for protein, using the silver stain, and glycoprotein, using the Pro-Q Glycoprotein stain, **Figure 4-7**. When comparing the two stains, it was observed that the glycoprotein stain did not cross-react with the non-glycosylated proteins present in the protein ladder, **Figure 4-7**. To ensure that the presence of the glycoprotein band was always associated with the ivy nanoparticles, three separate isolations were conducted using different batches of adventitious roots. As shown in **Figure 4-7**, the band was consistent across all three samples. This confirmed that the ivy nanoparticles were composed of at least one, if not several glycoproteins. Due to the high molecular weight of the band, and the potential for the ivy nanoparticles to have survived the denaturing conditions, the possibility still exists, that the ivy nanoparticles are composed of multiple proteins and glycoproteins. Further studies are necessary to determine the three dimensional crystal structure of the ivy nanoparticles, and to identify if multiple copies of a single protein, or multiple proteins combine to form the ivy nanoparticles. In either case, the discovery that ivy nanoparticles are non-metallic and proteinaceous, represents a significant finding, and opens the door for further analysis of the structure of these novel nanoparticles.

## 4.4 Conclusion

In this study, we have developed a method for the production of ivy nanoparticles, and demonstrated the scalability of this process. Briefly, bulk ivy nanoparticles were harvested from cultured adventitious roots through homogenization, filtration, and separation through an SEC column. The development of this method was crucial for demonstrating the ability to collect bulk nanoparticles for use in biomedical applications, and also to obtain enough nanoparticles for subsequent chemical analysis. Through experiments conducted using ICP-MS, we were able to prove that the ivy nanoparticles did not contain any metallic components, confirming the earlier hypothesis that the ivy nanoparticles were organic. Elemental analysis revealed a high, ~10:1, C:N ratio, and further analysis by FTIR confirmed the presence of peaks related to C-N bonding. Comparison of the ivy nanoparticle FTIR spectra with a polysaccharide standard, chitosan, and protein standard, BSA, demonstrated that the ivy nanoparticles shared similar structure to both samples, indicating that the nanoparticles were most likely composed of glycoproteins. Using gel electrophoresis, the ivy nanoparticles formed a single high molecular weight band, which stained positive for both proteins and glycoproteins through silver and glycoprotein specific stains. At this stage, it is not possible to identify the exact interactions between proteins that lead to the structural formation of the three dimensional nanoparticles; however, further studies based on identification of the sequence of these proteins will provide information on how they may be arranged. It is expected that continued research into these proteins will aid in the development of new high strength adhesives. Further, it will also be possible to scale-up the procedure developed in this work to collect enough ivy nanoparticles for future applications in drug delivery and cosmetics.

## 4.5 Experimental

### 4.5.1 Isolation and physical analysis of the ivy nanoparticles

Previously, a method was developed for generating bulk adventitious roots from the shoots of English ivy, specifically for the production of viable nanoparticle containing tissue [26]. This method was employed to grow harvestable amounts of adventitious roots for use in this study. Since the adventitious roots and root hairs that branch off of the rootlet are the only structures involved in secretion of the adhesive, these structures were removed from fresh shoots using a razor blade. Adventitious roots were harvested directly into liquid nitrogen before attaching. Homogenization of the cleaned rootlets was accomplished with the use of a pellet pestle (Kimble Chase Kontes) designed for use in 1.5 ml microfuge tubes. The supernatant was removed from the homogenate and centrifuged at 1000 x g for 10 minutes to remove large debris. The supernatant from this treatment was then filter-sterilized through a 0.2 µm syringe filter to remove debris larger than 200 nm, and also to remove bacteria that may have been present in the sample. The filtrate was then dialyzed overnight at 4°C with distilled water using a Spectra/Por® Biotech Cellulose Ester dialysis membrane that allowed removal of small chemicals and proteins with a molecular weight of less than 300,000 daltons.

After removing most of the components from the rootlet extract it was possible to run the extract on a Phenomenex® Biosep-SEC-S 4000 silica gel filtration column attached to an Agilent High-Performance Liquid Chromatography (HPLC 1100) equipped with a diode array detector (DAD) and an evaporative light scattering detector (ELSD). The column was equipped with a SecurityGuard™ Cartridge to prevent any remaining debris from entering the column. Similar SEC-HPLC setups have been used to separate and isolate a wide range of nanoparticles [27-29].

200 µl of the cleaned extract was run on the column using a flow-rate of 0.5 ml/min. The eluate was constantly monitored with a dual wavelength UV detector measuring at 280 and 320 nm. Ivy nanoparticle fractions were known to absorb UV at these wavelengths based on previous studies [6-7]. Fractions were also collected every minute over the course of 60 minutes for analysis by AFM. For AFM analysis, 20 µl of each fraction was drop deposited on freshly cleaved mica or a cleaned glass cover slip and allowed to dry overnight. AFM imaging was conducted using an Agilent 6000 ILM/AFM equipped with Nanosensors™ PPP-NCHR-20 silicon cantilevers with spring constants of 4-20 N/m. All imaging was conducted in AC mode to prevent contamination on the tip, and also to prevent the tip from dislodging the nanoparticles from the surface. To determine the presence of the nanoparticles in solution, DLS was performed on the nanoparticle fractions using a Malvern ZetaSizer Nano ZS (Malvern Instruments Ltd). This instrument was also used to determine the Zeta Potential of the ivy nanoparticle solution. After identifying the fraction that contained the nanoparticles, the fraction was frozen in a -80°C freezer and lyophilized overnight to remove the liquid components and concentrate the nanoparticles. The lyophilized powder was then resuspended in ultrapure water and drop deposited on silica wafer before examination using SEM. SEM was used to determine the size and shape of the nanoparticles, and also to scan a larger area to determine the relative purity of the sample.

### 4.5.2 Chemical analysis

UV/Vis spectroscopy was conducted on the liquid fraction collected from the column and also on the lyophilized powder resuspended in ultrapure water, using a Thermo Scientific Evolution 600 spectrophotometer. The samples were analyzed over wavelengths from 200-500 nm, and the

absorbance was measured. The absorbance versus concentration was plotted by conducting a serial dilution of the resuspended nanoparticle powder. FTIR was conducted on the lyophilized powder to determine the functional groups found in the nanoparticles using a Bio-RAD FTS6000 FTIR spectrometer. Both ICP-MS and the elemental analysis of the ivy nanoparticles were conducted at Galbraith labs Inc., which allowed for an unbiased examination of the specimen. Finally, 5 mg of lyophilized nanoparticles were rehydrated in 1 ml of 0.5 M Tris-HCl (pH 6.8). Seventy-five µl of nanoparticle solution was then mixed with 25 µl of 4x LDS sample buffer (Life Technologies, Grand Island, NY). Eight µl of the sample was then mixed with 10 µl reducing buffer (2M thiourea, 8M urea, and 3% SDS) and boiled for 10 min. After denaturation, samples were run on 5%/10% SDS-PAGE at 180 V for 4 h at 4$^{o}$C in SDS-Tris-Glycine running buffer. Gels were subsequently stained using Pro-Q Emerald 300 glycoprotein stain kit (Molecular Probes, Inc., Eugene, OR) or the PlusOne silver staining kit (AP Biotech).

## Acknowledgements

This research is partially sponsored by the Army Research Office (W911NF-10-1-0114) and the National Science Foundation (CMMI: 1029953, CBET: 0965877). The authors are grateful for the support. R. Sharma acknowledges graduate stipend support from the Genome Science and Technology Graduate School at UT-Knoxville. Financial support to K. Chourey, C. Pan and R.L. Hettich was provided by the U.S. Department of Energy, Biological and Environmental Research Division, Genome Sciences Program. Oak Ridge National Laboratory is managed by University of Tennessee-Battelle LLC for the Department of Energy.

## References

1. Lenaghan, S. C. and Zhang, M. 2012 Real-time observation of the secretion of a nanocomposite adhesive from English ivy (*Hedera helix*). *Plant Sci.* **183**, 206-211.

2. Zhang, M., Liu, M., Prest, H., and Fischer, S. 2008 Nanoparticles secreted from ivy rootlets for surface climbing. *Nano Lett.* **8**, 1277-1280.

3. Wu, Y., Zhao, X., and Zhang, M. 2010 Adhesion mechanics of ivy nanoparticles. *J. Colloid Interf. Sci.* **344**, 533-540.

4. Xia, L., Lenaghan, S., Zhang, M., Wu, Y., Zhao, X., Burris, J., and Neal Stewart, C. 2010 Characterization of English ivy (*Hedera helix*) adhesion force and imaging using atomic force microscopy. *J. Nanopart. Res.* **13**, 1029-1037.

5. Coombs, T. L. and Keller, P. J. 1981 *Mytilus* byssal threads as an environmental marker for metals. *Aquat. Toxicol.* **1**, 291-300.

6. Li, Q., Xia, L., Zhang, Z., and Zhang, M. 2010 Ultraviolet Extinction and Visible Transparency by Ivy Nanoparticles. *Nanoscale Res. Lett.* **5**, 1487-1491.

7. Xia, L., Lenaghan, S., Zhang, M., Zhang, Z., and Li, Q. 2010 Naturally occurring nanoparticles from English ivy: an alternative to metal-based nanoparticles for UV protection. *J. Nanobiotechnol.* **8**, 12.

8. Zhang, M., Liu, M., Bewick, S., and Suo, Z. 2009 Nanoparticles to Increase Adhesive Properties of Biologically Secreted Materials for Surface Affixing. *J. Biomed. Nanotechnol.* **5**, 294-299.

9. Melzer, B., Steinbrecher, T., Seidel, R., Kraft, O., Schwaiger, R., and Speck, T. 2010 The attachment strategy of English ivy: a complex mechanism acting on several hierarchical levels. *J. Roy. Soc. Interface*. **7**, 1383-1389.

10. Hoo, C., Starostin, N., West, P., and Mecartney, M. 2008 A comparison of atomic force microscopy (AFM) and dynamic light scattering (DLS) methods to characterize nanoparticle size distributions. *J. Nanopart. Res.* **10**, 89-96.

11. Chandran, S. P., Chaudhary, M., Pasricha, R., Ahmad, A., and Sastry, M. 2006 Synthesis of Gold Nanotriangles and Silver Nanoparticles Using Aloevera Plant Extract. *Biotechnol. Progr.* **22**, 577-583.

12. Njagi, E. C., Huang, H., Stafford, L., Genuino, H., Galindo, H. M., Collins, J. B., Hoag, G. E., and Suib, S. L. 2010 Biosynthesis of Iron and Silver Nanoparticles at Room Temperature Using Aqueous Sorghum Bran Extracts. *Langmuir*. **27**, 264-271.

13. Shankar, S. S., Ahmad, A., Pasricha, R., and Sastry, M. 2003 Bioreduction of chloroaurate ions by geranium leaves and its endophytic fungus yields gold nanoparticles of

different shapes. *J. Mater. Chem.* **13**, 1822-1826.

14. Song, J. Y., Kwon, E. Y., and Kim, B. S. 2010 Biological synthesis of platinum nanoparticles using *Diopyros kaki* leaf extract. *Bioprocess. Biosyst. Eng.* **33**, 159-164.

15. Ellis, J., Del Castillo, E., Montes Bayon, M., Grimm, R., Clark, J. F., Pyne-Geithman, G., Wilbur, S., and Caruso, J. A. 2008 A Preliminary Study of Metalloproteins in CSF by CapLC-ICPMS and NanoLC-CHIP/ITMS. *J. Proteome Res.* **7**, 3747-3754.

16. Garcia, J. S., Magalhães, C. S., and Arruda, M. A. 2006 Trends in metal-binding and metalloprotein analysis. *Talanta*. **69**, 1-15.

17. Bowling, A. J. and Vaughn, K. C. 2008 Structural and immunocytochemical characterization of the adhesive tendril of Virginia creeper (*Parthenocissus quinquefolia* [L.] Planch.). *Protoplasma*. **232**, 153-163.

18. Endress, A. G. and Thomson, W. W. 1976 Ultrastructural and cytochemical studies on the developing adhesive disc of Boston Ivy tendrils *Protoplasma*. **88**, 315-331.

19. Endress, A. G. and Thomson, W. W. 1977 Adhesion of the Boston ivy tendril. *Can. J. Bot.* **55**, 918-924.

20. Fant, C., Elwing, H., and Hook, F. 2002 The influence of cross-linking on protein-protein

interactions in a marine adhesive: the case of two byssus plaque proteins from the blue mussel. *Biomacromolecules*. **3**, 732-741.

21. Ninan, L., Stroshine, R. L., Wilker, J. J., and Shi, R. 2007 Adhesive strength and curing rate of marine mussel protein extracts on porcine small intestinal submucosa. *Acta Biomater.* **3**, 687-694.

22. Stevens, M. J., Steren, R. E., Hlady, V., and Stewart, R. J. 2007 Multiscale Structure of the Underwater Adhesive of *Phragmatopoma Californica*:a Nanostructured Latex with a Steep Microporosity Gradient. *Langmuir*. **23**, 5045-5049.

23. Sevier, C. S. and Kaiser, C. A. 2002 Formation and transfer of disulphide bonds in living cells. *Nat. Rev. Mol. Cell. Biol.* **3**, 836-847.

24. Bhattarai, S., Kc, R., Kim, S., Sharma, M., Khil, M., Hwang, P., Chung, G., and Kim, H. 2008 N-hexanoyl chitosan stabilized magnetic nanoparticles: Implication for cellular labeling and magnetic resonance imaging. *J. Nanobiotechnol.* **6**, 1.

25. Wang, T. D., Triadafilopoulos, G., Crawford, J. M., Dixon, L. R., Bhandari, T., Sahbaie, P., Friedland, S., Soetikno, R., and Contag, C. H. 2007 Detection of endogenous biomolecules in Barrett's esophagus by Fourier transform infrared spectroscopy. *Proc. Natl. Acad. Sci. U.S.A.* **104**, 15864-15869.

26. Burris, J., Lenaghan, S., Zhang, M., and Stewart, C. 2012 Nanoparticle biofabrication using English ivy (*Hedera helix*). *J. Nanobiotechnol.* **10**, 41.

27. Sivamohan, R., Takahashi, H., Kasuya, A., Tohji, K., Tsunekawa, S., Ito, S., and Jeyadevan, B. 1999 Liquid chromatography used to size-separate the amphiphilic-molecules stabilized nano-particles of cds in the 1-10nm range. *Nanostruct. Mater.* **12**, 89-94.

28. Wang, S., Mamedova, N., Kotov, N. A., Chen, W., and Studer, J. 2002 Antigen/Antibody Immunocomplex from CdTe Nanoparticle Bioconjugates. *Nano Lett.* **2**, 817-822.

29. Wei, G. T. and Liu, F. K. 1999 Separation of nanometer gold particles by size exclusion chromatography. *J. Chromatogr. A.* **836**, 253-260.

## Appendix

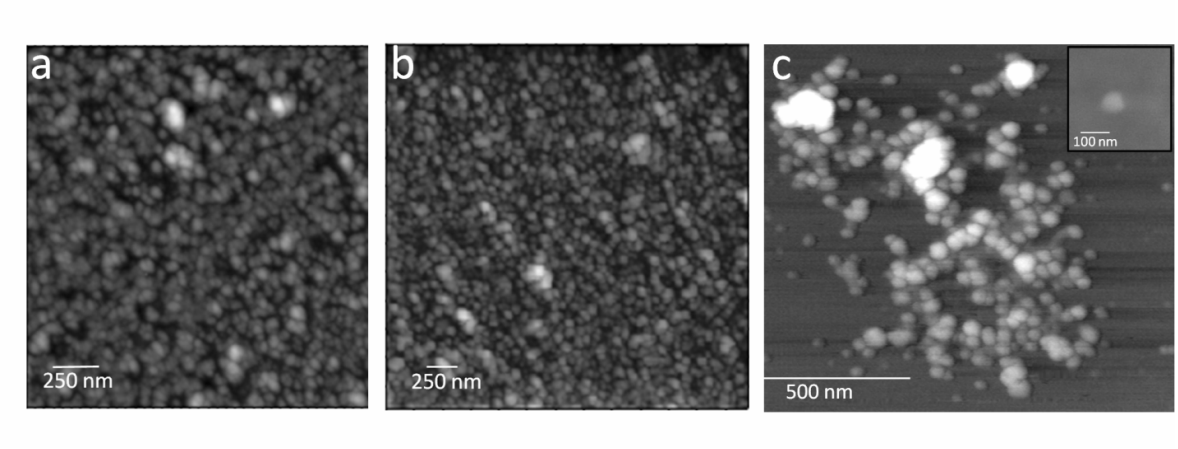


**Figure 4-1.** AFM and SEM images of ivy nanoparticles. a) AFM scan of dense ivy nanoparticles secreted directly from an adventitious root. b) AFM scan of dense ivy nanoparticles isolated using the procedure developed in this study. c) Small cluster of ivy nanoparticles imaged by AFM after dilution from the concentrated sample collected from the column. The inset of c) shows an SEM image of a single ivy nanoparticle prepared the same as the diluted AFM sample. Note that the size of an individual nanoparticle is slightly smaller by AFM, however, artifacts related to tip-particle interactions can greatly affect size measurements using AFM.

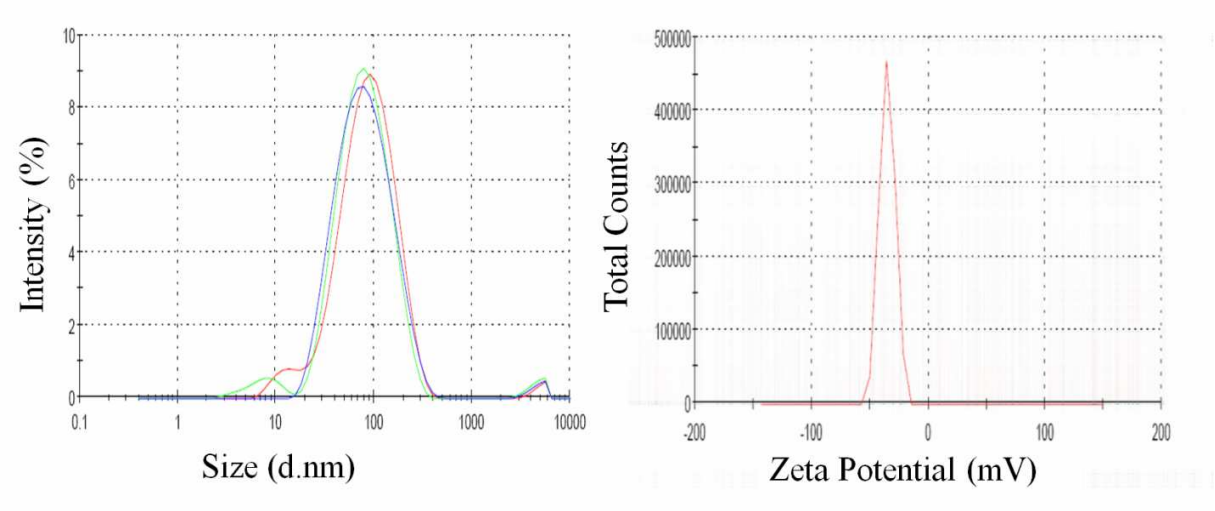


**Figure 4-2.** DLS and Zeta Potential analysis of the isolated ivy nanoparticles. a) DLS of the nanoparticles collected from three separate isolations showed a similar distribution, with a mean diameter of 95.69 ±5.56 nm. b) The Zeta potential of the ivy nanoparticles was found to be -35.3 mV, indicating that the ivy nanoparticles did not form stable solution in ultrapure water.

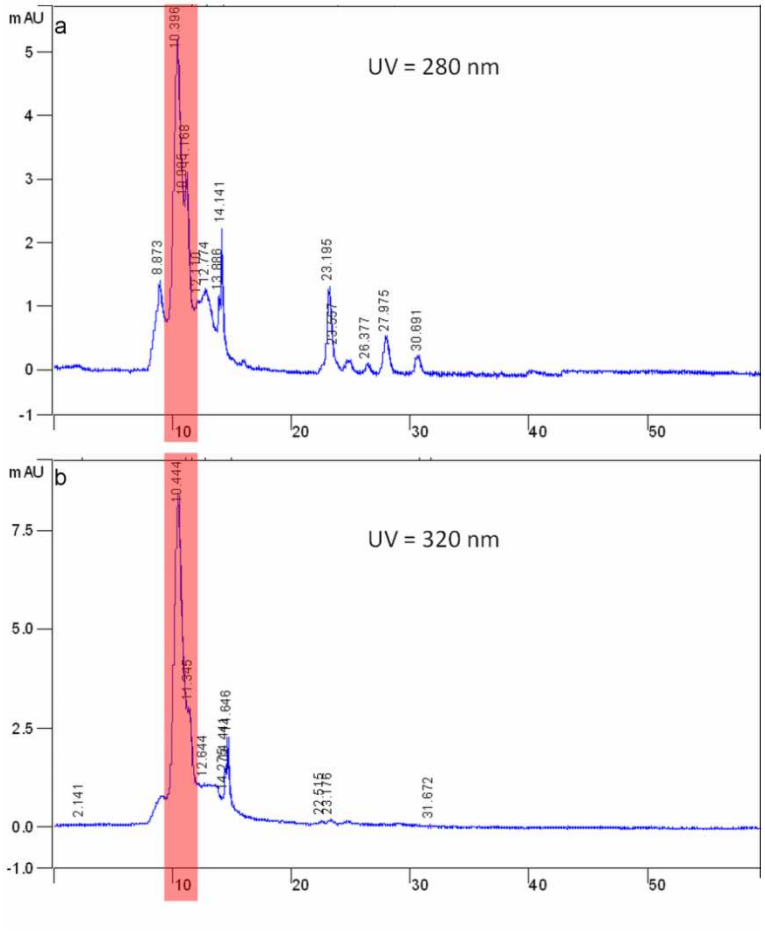


**Figure 4-3.** Peaks observed from UV detector of the ivy extract. A prominent peak was observed in both wavelengths (highlighted in red) during the 10-11 minute fraction. This fraction corresponded to the presence of nanoparticles, as indicated by AFM. Peaks with lower intensity were imaged, but were found not to contain any nanoparticles.

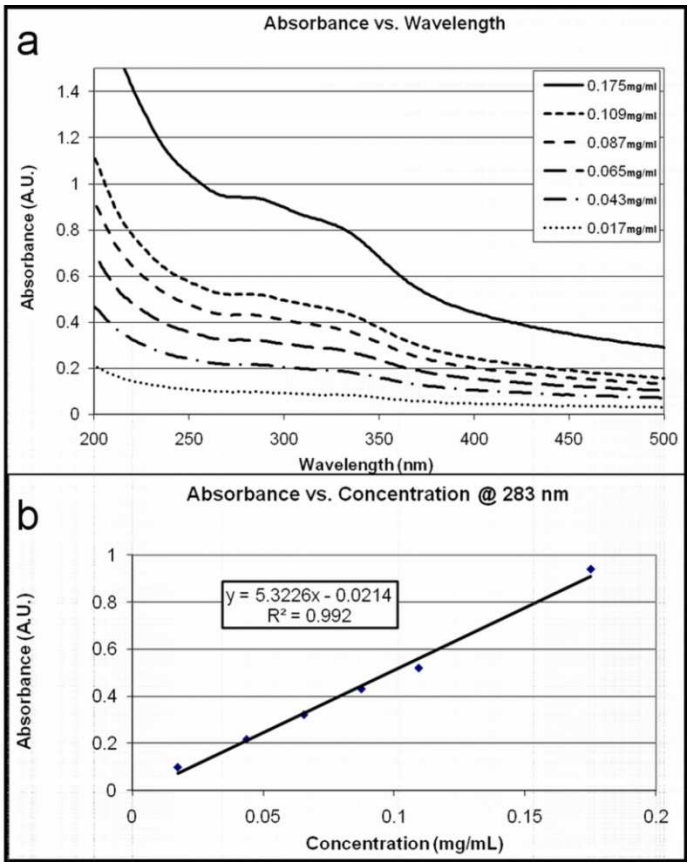


**Figure 4-4.** UV/vis spectra of the ivy nanoparticle fraction collected directly from the HPLC column. A) Note the wide absorbance from 200-350 nm, before dropping off in the visible spectra. B) A plot of absorbance versus concentration at 283 nm clearly shows the direct effect of the nanoparticle concentration on the absorbance.

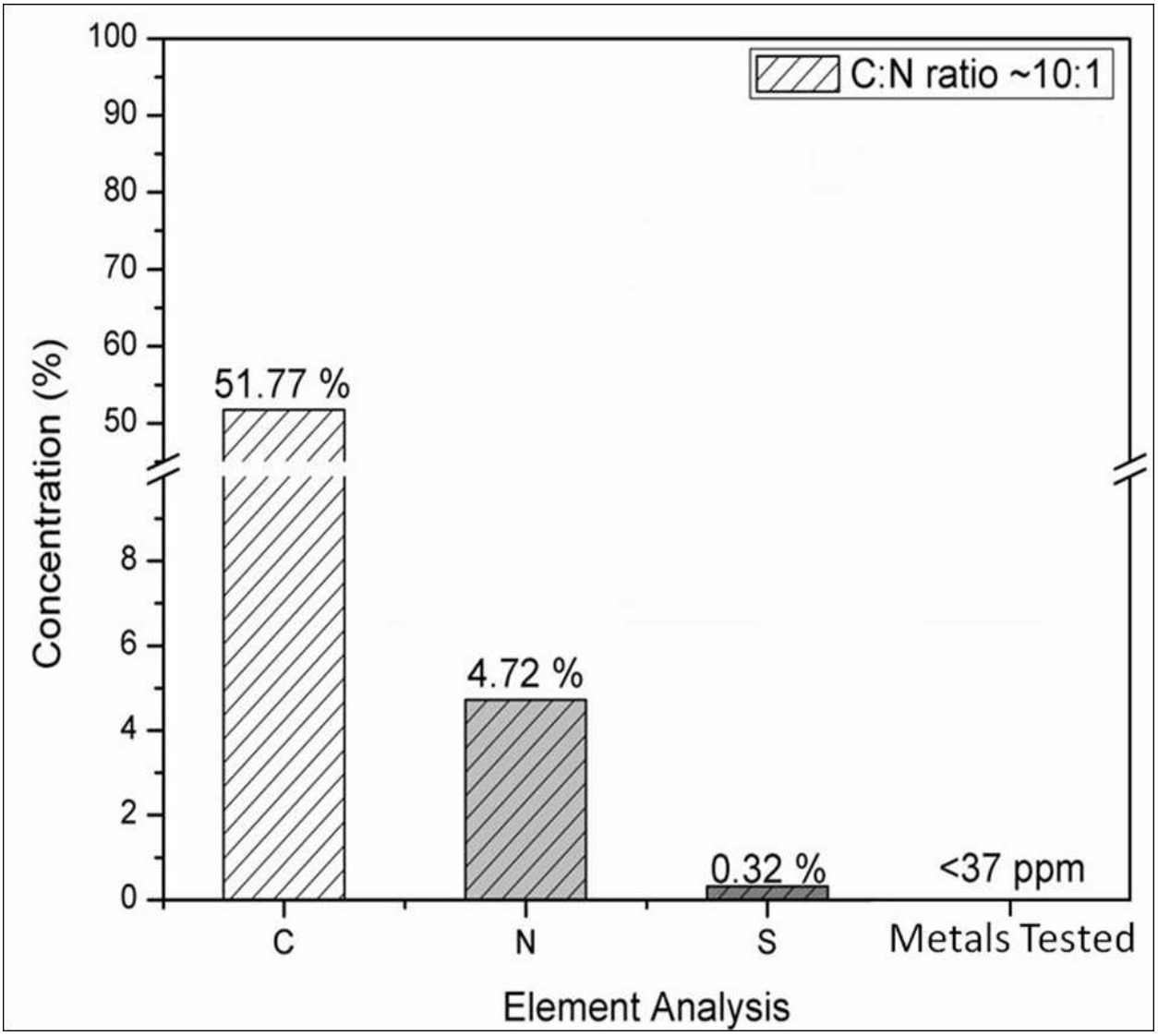


**Figure 4-5.** Diagrammatic representation of the results from the ICP-MS and elemental analysis. As indicated, the C:N ratio was ~10:1, indicating that the nanoparticles were composed of biomolecules. Additionally, ICP-MS revealed that all metals in the ivy nanoparticle fraction were < 37 ppm, confirming that the ivy nanoparticles are organic.

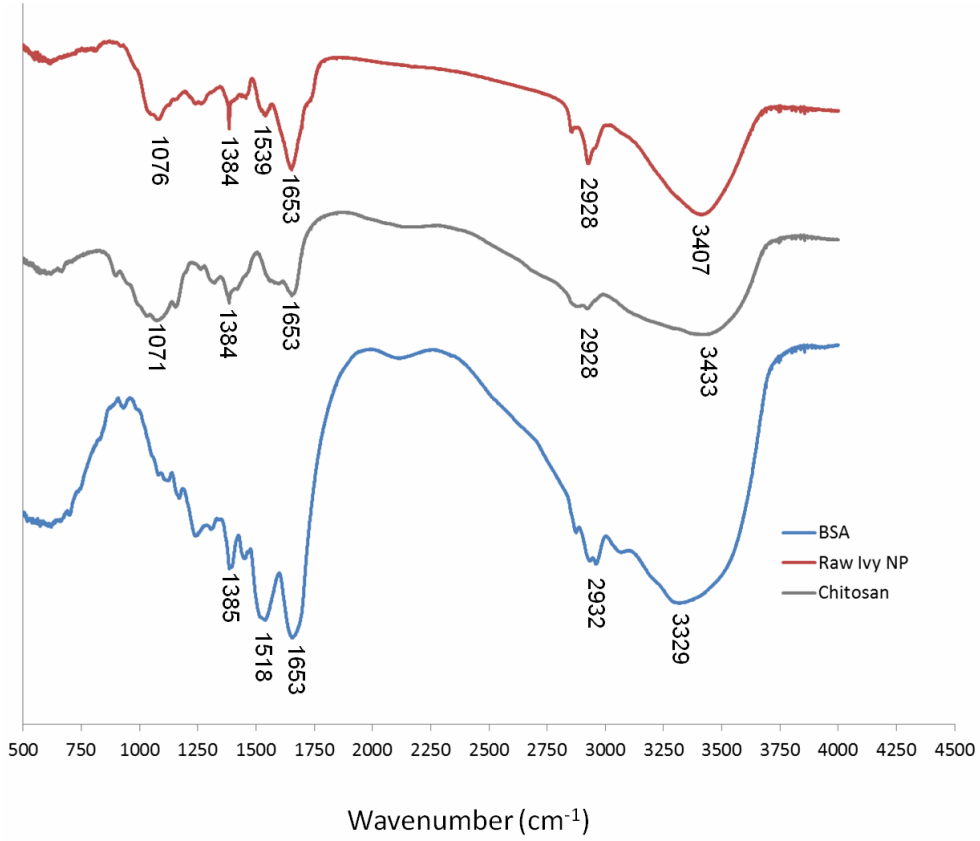


**Figure 4-6.** FTIR spectra of the ivy nanoparticles. The FTIR spectra for the ivy nanoparticles was compared with reference spectra for chitosan (a representative polysaccharide), and BSA (representative proteins). All three samples had a band at 1653 $cm^{-1}$, indicating vibration around the CO-NH bond, and around 2928-2932 $cm^{-1}$ indicating C-H vibration. In addition, the ivy sample shared a peak at 1071-1076 $cm^{-1}$ with the chitosan sample, indicating vibration of a CO-C bond, typical of sugars. This band was not present in the BSA sample. Similarly, the BSA sample had a strong peak at 1518 $cm^{-1}$, representing the amide II band, while the ivy nanoparticles had a weak band at 1539 $cm^{-1}$, indicating a weak amide II band, and the chitosan sample had no peak in this region. The FTIR spectra from top to bottom are: raw ivy nanoparticles, chitosan, and BSA (indicated by color in the online version).

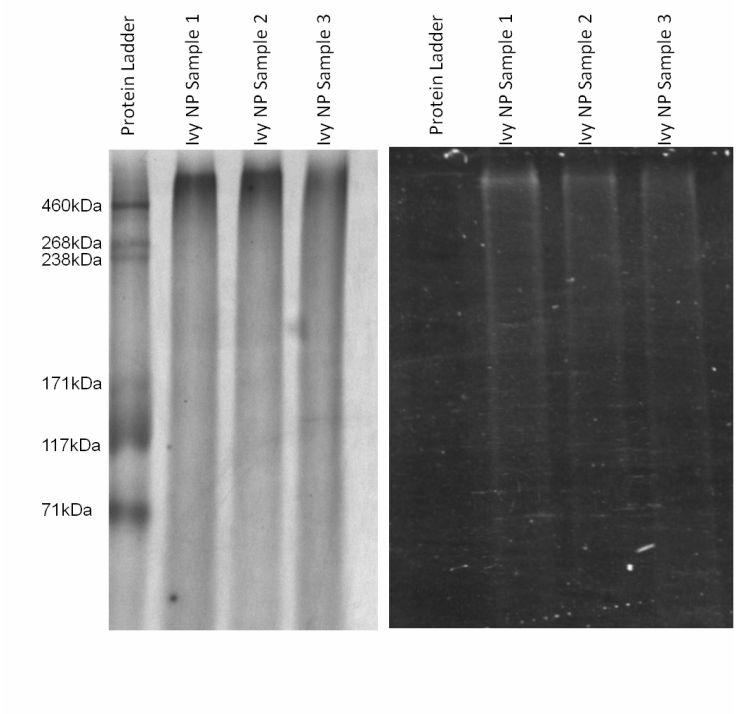


**Figure 4-7.** Results from SDS-PAGE of ivy nanoparticles. Left, results of the silver stain demonstrating the staining of the protein ladder, and all ivy nanoparticle samples. Right, results from glycoprotein stain showing positive staining for the high molecular weight nanoparticle band. Samples 1, 2, and 3 represent nanoparticles isolated from three separate trials. Note the lack of staining of the non-glycosylated proteins from the standard ladder.

## Supplemental

### Isolate and fractionate proteins involved in nanoparticle formation from adventitious roots of English ivy

In order to narrow down the pool of potential proteins contributing to nanoparticle formation in the adventitious roots of English ivy, several fractionation approaches were used. Initially, adventitious roots, ground roots and leaves/stems from English ivy were collected, extracted, dialyzed and processed as previously described [26]. Since ground roots and leaves/stems of English ivy did not yield nanoparticles, we aimed to profile the protein banding patterns of nanoparticle presence and absence. Total protein extracts were subjected to SDS-PAGE to identify common and/or different protein banding patterns among the various tissues of English ivy (**Figure 4-8**).

In order to fractionate those proteins involved in nanoparticle formation from adventitious roots of English ivy, proteins from processed roots were first examined for their ability to be separated based on charge using fast protein liquid chromatography (FPLC; ÄKTAFPLC™, GE Healthcare, Piscataway, NJ). For ion exchange chromatography, protein extracts were adjusted to pH 10 using 20 mM Tris (pH 10) buffer, were then filtered through a 0.2-µm-pore-size filter (Corning) and were loaded onto a HiTrap Q HP Sepharose™ anion-exchange column (GE Healthcare, Piscataway, NJ) that was previously equilibrated with 20mM Tris buffer (pH 10), and samples were collected using a fraction collector attached to the FPLC system. Under these conditions compounds with a negative charge bound to the resin with affinity dependent on the net charge of the compound. Protein fractions were eluted from the column with varying salt concentrations in 20mM Tris (pH 10) (**Figure 4-9A-B**). Most proteins were observed to be

eluted from the column at 100% salt, indicating a strong anionic charge, and were lost from collection to waste. Therefore, an identical sample was subjected to the same FPLC conditions and fractions of A1-B12 were collected as they eluted from the column, stored at 4 °C and subjected to SDS-PAGE (**Figure 4-9C-D**). A single high molecular band, >460 kDa, was observed beginning in the A11 fraction (**Figure 4-9C**), located at approximately the start of the FPLC protein peak (**Figure 4-**9B). As a means to further isolate the proteins contributing to the nanoparticle formation, we eluted using several alternative and subsequent salt gradients and verified the nanoparticle presence using UV/Vis spectroscopy (**Figures 4-10 to 4-14**). Fractions A1-A4, A5-A11, A12-B4 (eluted from 62-70% salt gradient) and B5-B10 (eluted from 100% salt gradient) (**Figure 4-10A**) were combined and subjected to UV/Vis spectroscopy (**Figure 4-3B**). Fraction A5-A11 yielded spectra similar to those previously observed for the nanoparticle [6, 7]. Fractions A1-A7, A8-A11, A12-B5 (eluted from 68-74% salt gradient) and B6-B9 (eluted from 100% salt gradient) (**Figure 4-11A**) were combined and subjected to UV/Vis spectroscopy (**Figure 4-11B**). Fractions A8-A11 and A12-B5 were similar in pattern, but none of the fractions yielded spectra similar to those previously observed for the ivy nanoparticle [6, 7]. Fractions A1-A4, A5-A11, A12-B5 (eluted from 48-55% salt gradient) and B6-B9 (eluted from 100% salt gradient) (**Figure 4-12A**) were combined and subjected to UV/Vis spectroscopy (**Figure 4-12B**). Fraction A5-A11 yielded spectra similar to those previously observed for the nanoparticle [6, 7]. Fractions A1-A6, A7-A12, B1-C2 (eluted from 75-80% salt gradient) and C3-D3 (eluted from 100% salt gradient) (**Figure 4-13A**) were combined and subjected to UV/Vis spectroscopy (**Figure 4-13B**). Fraction A7-A12 yielded spectra similar to those previously observed for the nanoparticle [6, 7]. Fractions A1-A6, A7-B2, B3-B12 (eluted from 85-95% salt gradient) and C1-D4 (eluted from 100% salt gradient) (**Figure 4-14A**) were combined and subjected to

UV/Vis spectroscopy (**Figure 4-14B**). Fraction A7-B2 yielded spectra similar to those previously observed for the nanoparticle [6, 7].

In addition to separating proteins from the adventitious roots of English ivy based on charge, we subsequently separated those proteins by using FPLC size exclusion chromatography (**Figure 4-15)**. Fractions under peak A11-B1 (**Figure 4-9**B-D) were combined and further fractionated on a size exclusion column (HiLoad 16/60 Superdex 200 prep grade, GE Life Sciences, GE Health Care, Piscataway, NJ) (**Figure 4-15A**). Fractions under peak A1-C7 from the size exclusion column were collected as they eluted from the column, stored at 4 °C and subjected to Laemmli SDS-PAGE containing beta-mercaptoethanol or 86 mM dithiothreitol (**Figure 4-15B**) or beta-mercaptoethanol plus either 6 M urea or 8 M urea plus 2 M thiourea plus 3% SDS (**Figure 4-15C-D**). Protein was observed in fractions B10, B11 and B12 no matter what reducing agent was used (**Figure 4-15**). However, with the addition of 6 M urea or 2 M thiourea plus 3% SDS to the beta-mercaptoethanol Laemmli buffer, an additional band below the >460 kDa band was observed in the fraction under peak B11 (**Figure 4-15D**). An identical sample was subjected to the same FPLC conditions and fractions of B8-C8 under the peak were collected as they eluted from the column, stored at 4 °C and subjected to UV/Vis spectroscopy (**Figure 4-16B-C**). Spectra of the fractions B11 and B12 under the peak had similar UV/Vis properties to that of the nanoparticles and therefore, were sent to MS Bioworks for LC-MS/MS analysis. Proteins identified by LC-MS/MS analysis using the ivy transcriptome are shown in **Table 4-1**. Fraction E5 under the peak was used as a background control as no protein bands were observed when ran on SDS-PAGE (data not shown). However, those proteins identified by LC-MS/MS yielded little information as to the composition of the nanoparticle (**Supplemental Table 4-1**).

Since anion and size exclusion fractionation did not provide adequate separation of the proteins, we examined the differences in anionic fractions eluted from 40%, 70% and 100% salt gradient between water extracted, 20 mM Tris pH 7 with 10 mM DTT and 10 mM DTT extracted nanoparticles from English ivy adventitious roots (**Figure 4-17A, 4-18A, and 4-19A**). We then wanted to determine if changing the buffer had an effect on the proteins that we could elute from the column so we did 3 different extractions: (1) the normal water extraction, a buffered system using 20 mM Tris pH 7 and the same buffered system with 10 mM DTT added. The majority of protein was eluted from water extracted, 20 mM Tris pH 7 with 10 mM DTT and 10 mM DTT extracted nanoparticle from 100% (**Figure 4-17A**), 70% (**Figure 4-18A**) or 40% salt gradient (**Figure 4-19A**) respectively. Therefore, we concluded that extraction buffer was an important factor in protein separation and subsequently focused research efforts on extraction methods and reducing agents for further resolution of the proteins contributing to nanoparticle formation. When examining samples that were extracted in water, 20 mM Tris buffer pH 7 or 20 mM Tris buffer pH 7 plus 10 mM DTT before and after dialysis (**Figure 4-20**), it was observed that spectra were similar for all extraction buffers following dialysis (**Figure 4-20B).** When compared to a known plant phenolic compound, chlorogenic acid, a peak around 325 nm was not observed in nanoparticles samples or diluted nanoparticle samples (**Figure 4-21**).

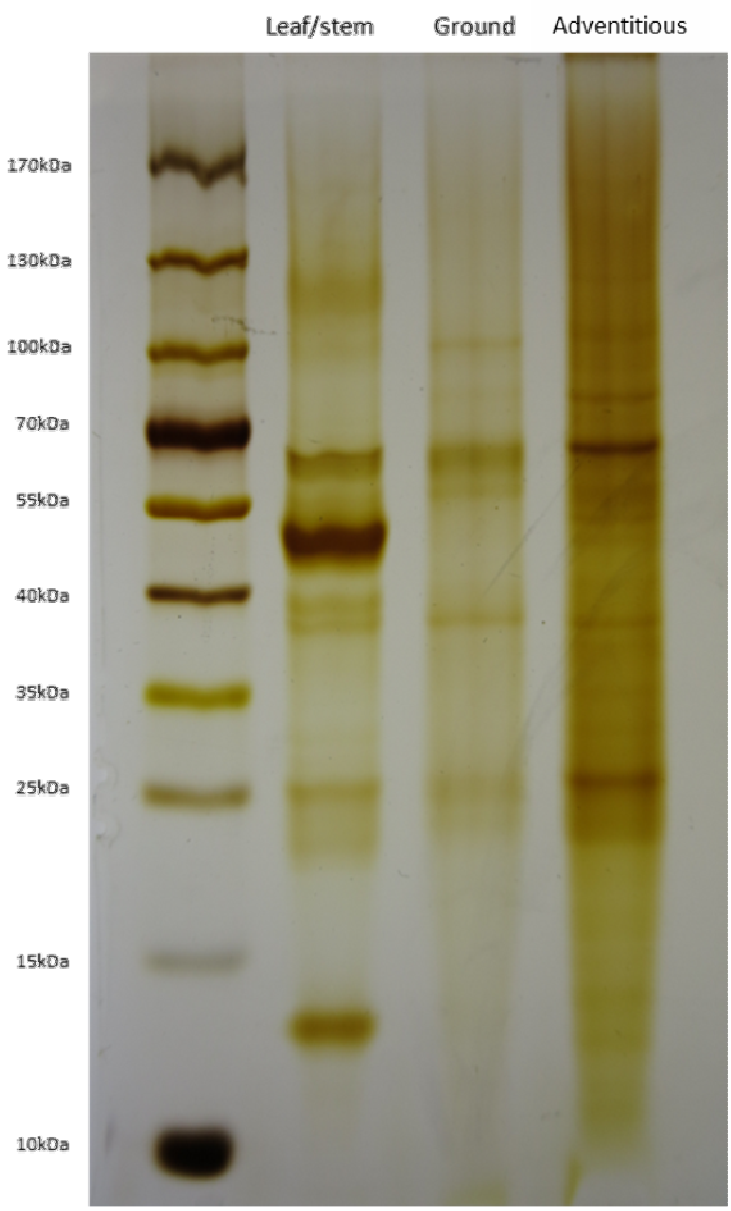


**Figure 4-8.** Silver stained SDS-PAGE of total protein extracted from leaf/stem, ground roots, and adventitious roots.

**Figure 4-9.** Fast Performance Liquid Chromatography (FPLC) chromatogram from ion exchange column. 10 ml of sample was loaded onto a HiTrap Q HP Sepharose™ anion-exchange column (GE Healthcare, Piscataway, NJ) that was previously equilibrated with 20 mM buffer (pH 10) and was connected to an FPLC (GE Healthcare, Piscataway, NJ). Fractions A1-B12 were collected under the peak. Solid blue line represents the proteins eluting from the column. Solid green line represents the salt gradient. (A) Sample was initially ran on anion exchange column, but most of the proteins under the last peak were discarded in the waste collector. Therefore, an identical sample was ran on anion exchange column and fractions A1-B12 were collected under the peak . (C) Results of the silver stain demonstrate the staining of the protein ladder and all ivy nanoparticle samples. Lanes show samples A1 thru B12.

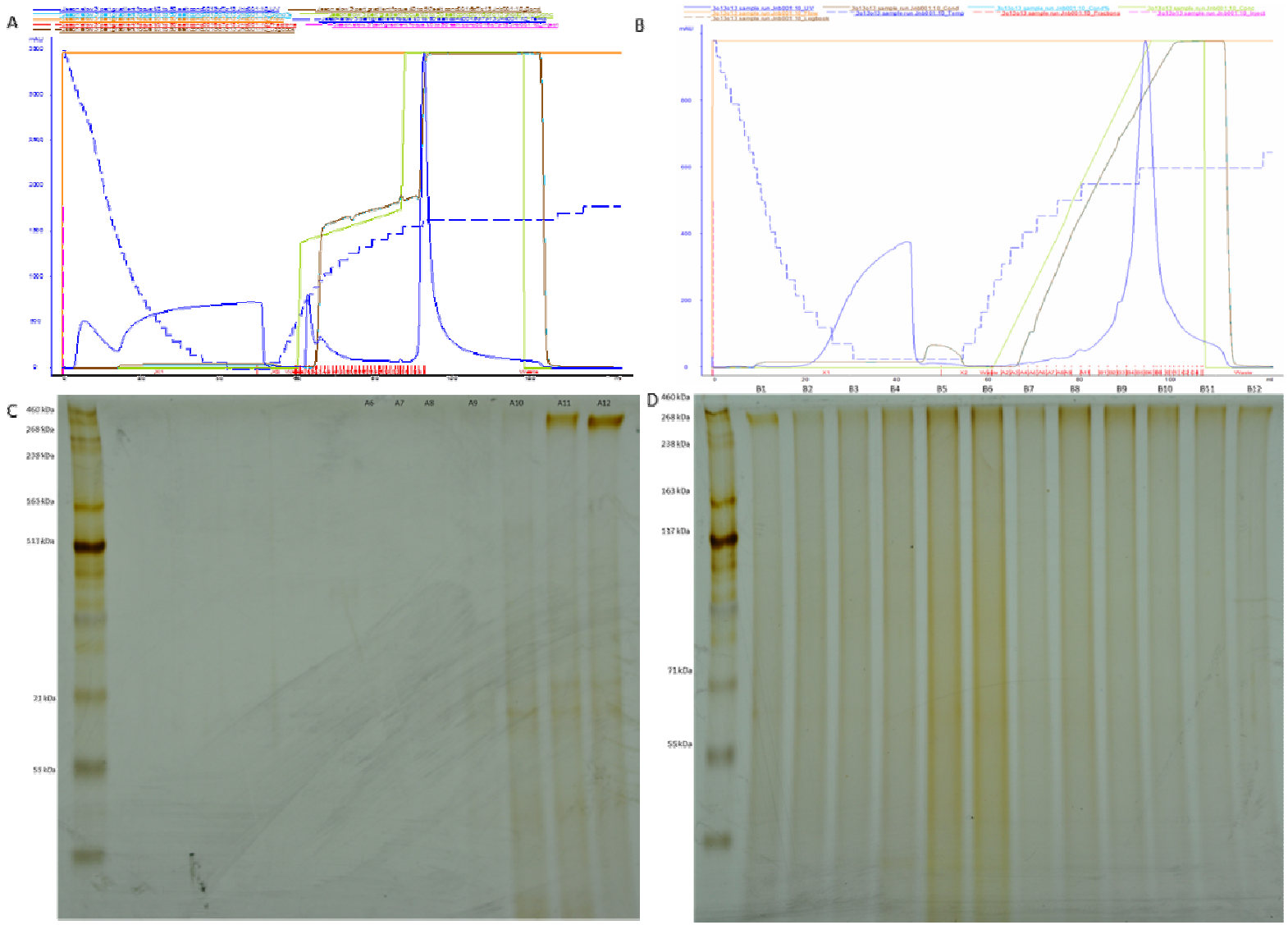


**Figure 4-9**. Continued

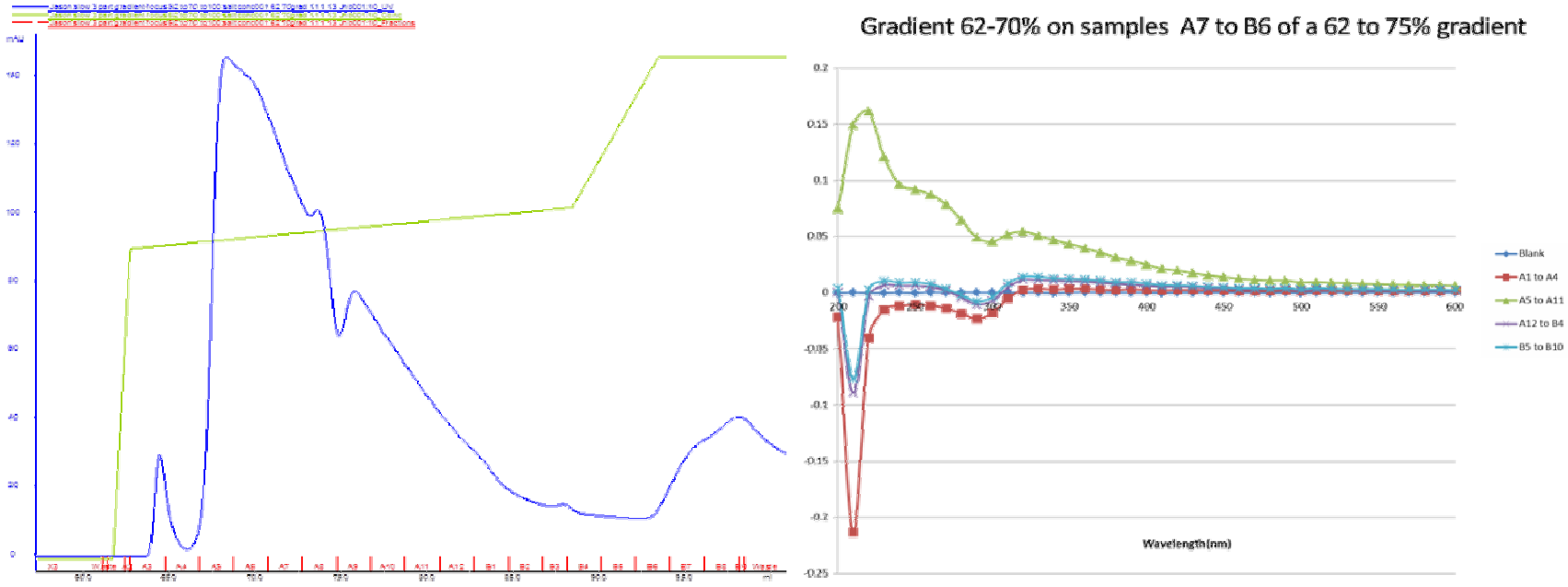


**Figure 4-10.** Fast Performance Liquid Chromatography chromatogram and physiochemical properties of nanoparticles extracted from English ivy adventitious roots fractionated using an anion-exchange column. (A) 10 ml of sample was loaded onto a HiTrap Q HP Sepharose™ anion-exchange column (GE Healthcare, Piscataway, NJ) that was previously equilibrated with 20mM Tris buffer (pH 10) and was connected to an FPLC (GE Healthcare, Piscataway, NJ). Solid blue line represents the proteins eluting from the column. Solid green line represents the salt gradient from 62-70% and 70-100%. (B) Fractions A1-A4, A5-A11, A12-B4, and B5-B10 were combined individually and subjected to UV/Vis spectroscopy.

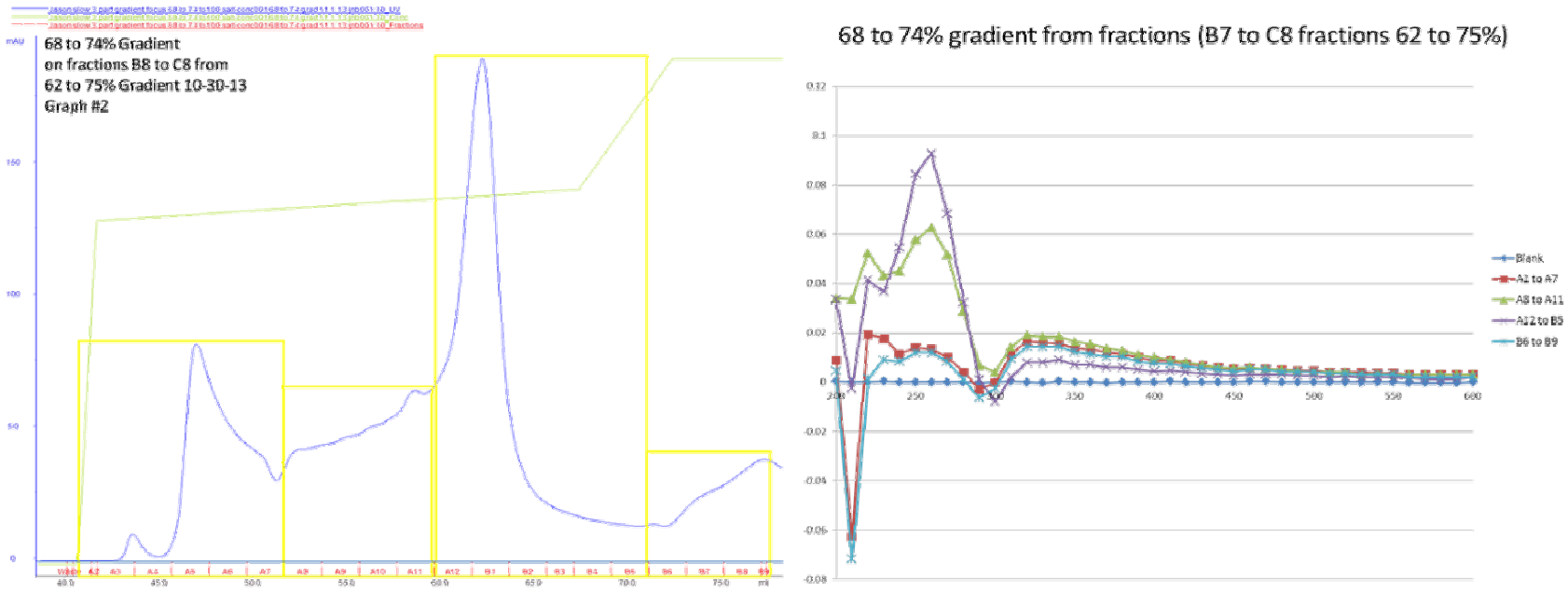


**Figure 4-11.** Fast Performance Liquid Chromatography chromatogram and physiochemical properties of nanoparticles extracted from English ivy adventitious roots fractionated using an anion-exchange column. (A) 10 ml of sample was loaded onto a HiTrap Q HP Sepharose™ anion-exchange column (GE Healthcare, Piscataway, NJ) that was previously equilibrated with 20mM Tris buffer (pH 10) and was connected to an FPLC (GE Healthcare, Piscataway, NJ). Solid blue line represents the proteins eluting from the column. Solid green line represents the salt gradient from 68-74% and 74-100%. (B) Fractions A1-A4, A5-A11, A12-B4, and B5-B10 were combined individually and subjected to UV/Vis

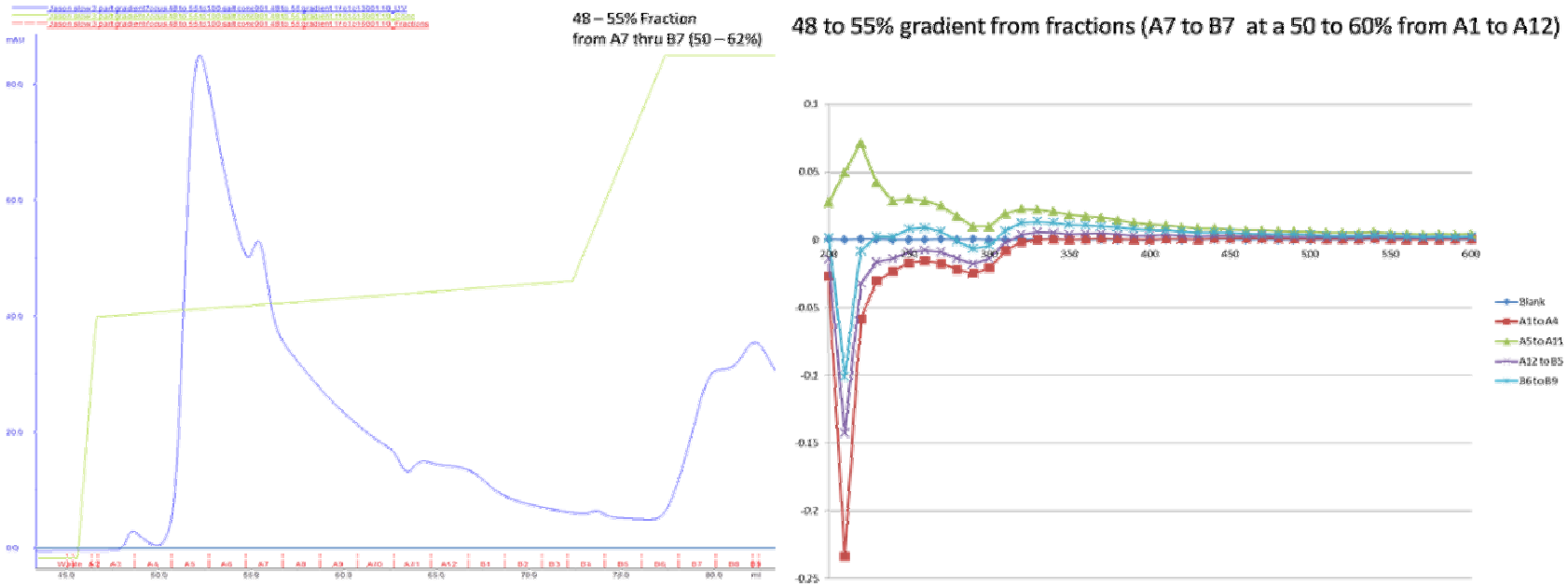


**Figure 4-12.** Fast Performance Liquid Chromatography chromatogram and physiochemical properties of nanoparticles extracted from English ivy adventitious roots fractionated using an anion-exchange column. Fractions A7 to B7 from 50-62% gradient were combined and loaded onto a HiTrap Q HP Sepharose™ anion-exchange column (GE Healthcare, Piscataway, NJ) that was previously equilibrated with 20mM Tris buffer (pH 10) and was connected to an FPLC (GE Healthcare, Piscataway, NJ). Solid blue line represents the proteins eluting from the column. Solid green line represents the salt gradient from 48-55% and 55-100%. (B) Fractions A1-A4, A5-A11, A12-B5, and B6-B9 were combined individually and subjected to UV/Vis spectroscopy.

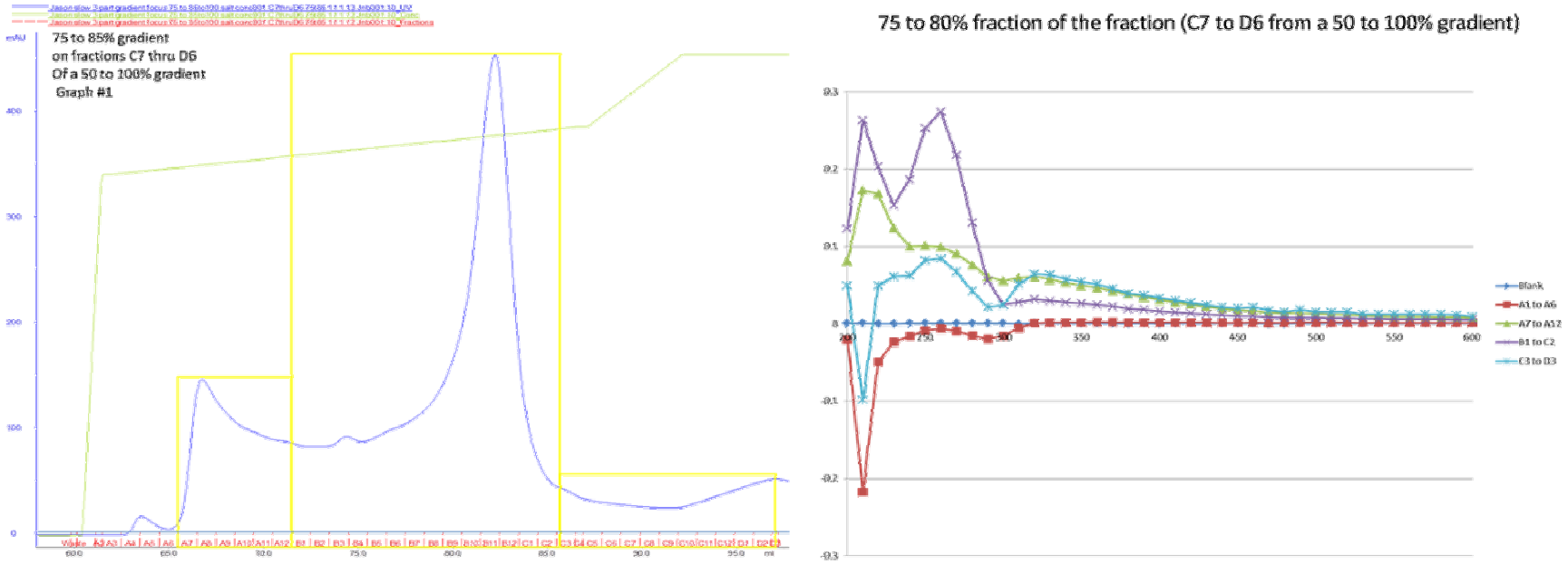


**Figure 4-13.** Fast Performance Liquid Chromatography chromatogram and physiochemical properties of nanoparticles extracted from English ivy adventitious roots fractionated using an anion-exchange column. Fractions C7 to D6 from 50-100% gradient were combined and loaded onto a HiTrap Q HP Sepharose™ anion-exchange column (GE Healthcare, Piscataway, NJ) that was previously equilibrated with 20mM Tris buffer (pH 10) and was connected to an FPLC (GE Healthcare, Piscataway, NJ). Solid blue line represents the proteins eluting from the column. Solid green line represents the salt gradient from 75-85% and 85-100%. (B) Fractions A1-A6, A7-A12, B1-C2, and C3-D3 were combined individually and subjected to UV/Vis spectroscopy.

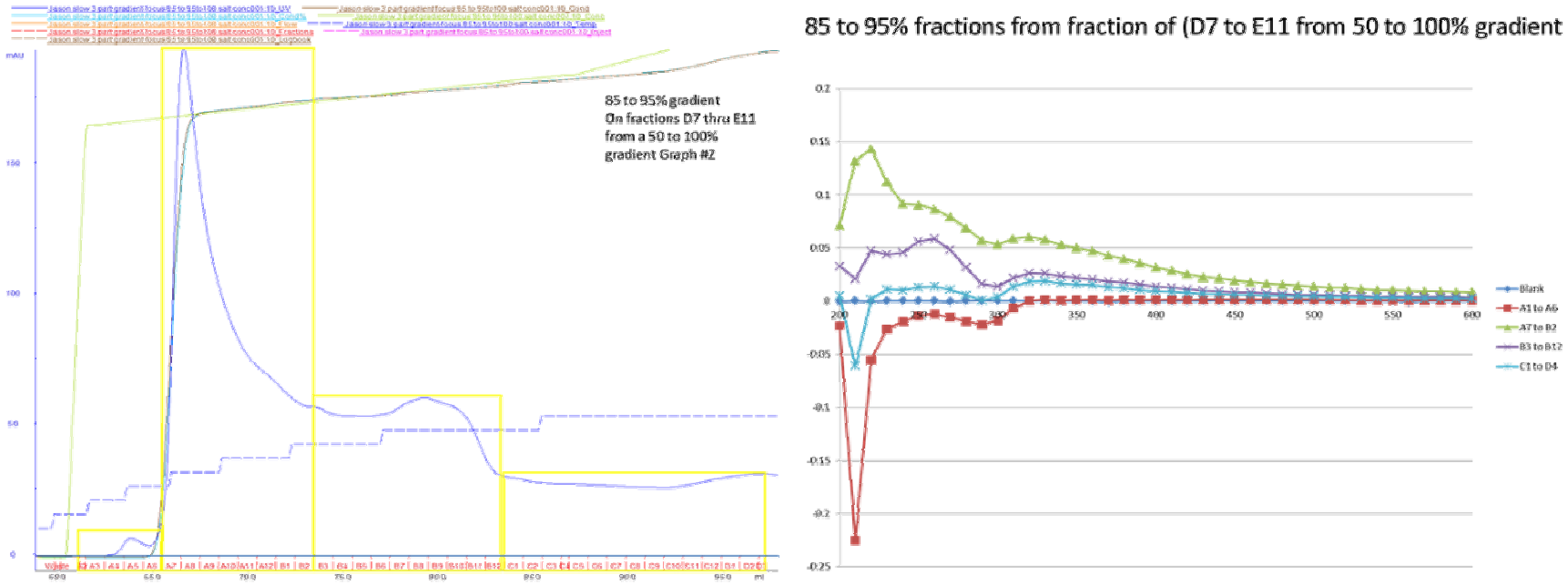


**Figure 4-14.** Fast Performance Liquid Chromatography chromatogram and physiochemical properties of nanoparticles extracted from English ivy adventitious roots fractionated using an anion-exchange column. Fractions D7 to E11 from 50-100% gradient were loaded onto a HiTrap Q HP Sepharose™ anion-exchange column (GE Healthcare, Piscataway, NJ) that was previously equilibrated with 20mM Tris buffer (pH 10) and was connected to an FPLC (GE Healthcare, Piscataway, NJ). Fractions A1-D3 were collected and subjected to UV/Vis spectroscopy. Solid blue line represents the proteins eluting from the column. Solid green line represents the salt gradient from 85-95% and 95-100%. (B) Fractions A1-A6, A7-B2, B3-B12, and C1-D4 were combined individually and subjected to UV/Vis spectroscopy.

**Figure 4-15.** Fast Performance Liquid Chromatography (FPLC) chromatogram from size exclusion column. Fractions under peak A11 through B1 from anion exchange column (Figure 2) were combined and further fractionated on a size exclusion column. (A) 2 ml of sample was loaded onto the size exclusion column and fractions A1-C7 were collected and (B, C, D) fractions under the peak A7-B12 were subjected to SDS-PAGE. Solid blue line represents the proteins eluting from the column. Results of the silver stain demonstrate the staining of the protein ladder and all ivy nanoparticle samples using (B) beta-mercaptoethanol (B1) or 86 mM dithiothreitol (DTT) (B2), (C) beta-mercaptoethanol for all samples, and (D) using beta-mercaptoethanol in all samples plus either 6 M urea or 2 M thiourea plus 3% SDS Laemmli buffer.

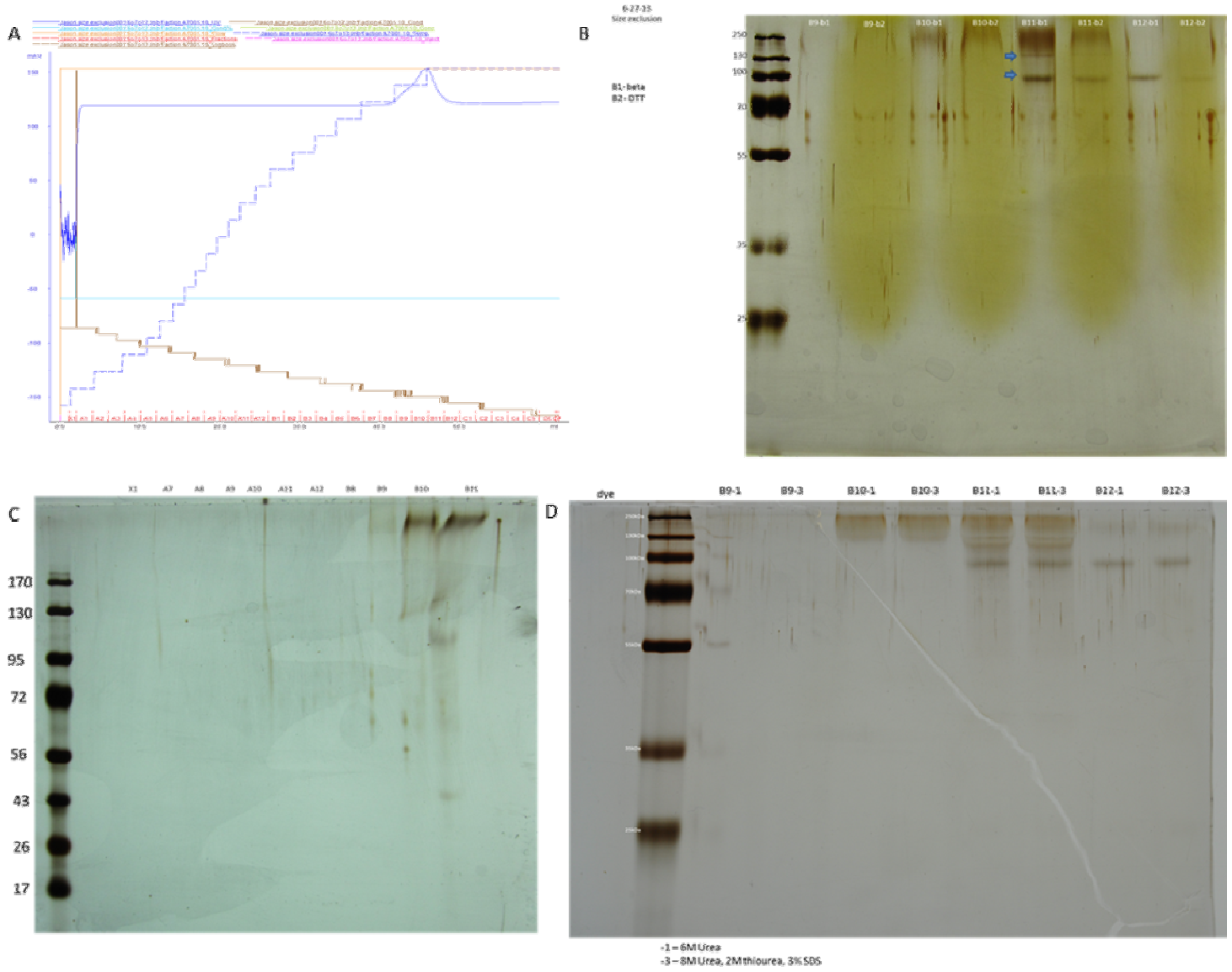


**Figure 4-15**. Continued

**Figure 4-16.** Fast Performance Liquid Chromatography (FPLC) chromatogram and physiochemical properties of nanoparticles extracted from English ivy adventitious roots fractionated using size exclusion column. (A) FPLC chromatogram when 2 ml of sample was loaded onto the size exclusion column. Solid blue line represents the proteins eluting from the column. (B) UV/Vis spectroscopy of nanoparticles extracted in 20 mM Tris-HCl at pH from English ivy adventitious roots and fractionated using size exclusion FPLC.Fractions B8-C6 under the peak were collected and subjected to UV/Vis spectroscopy.

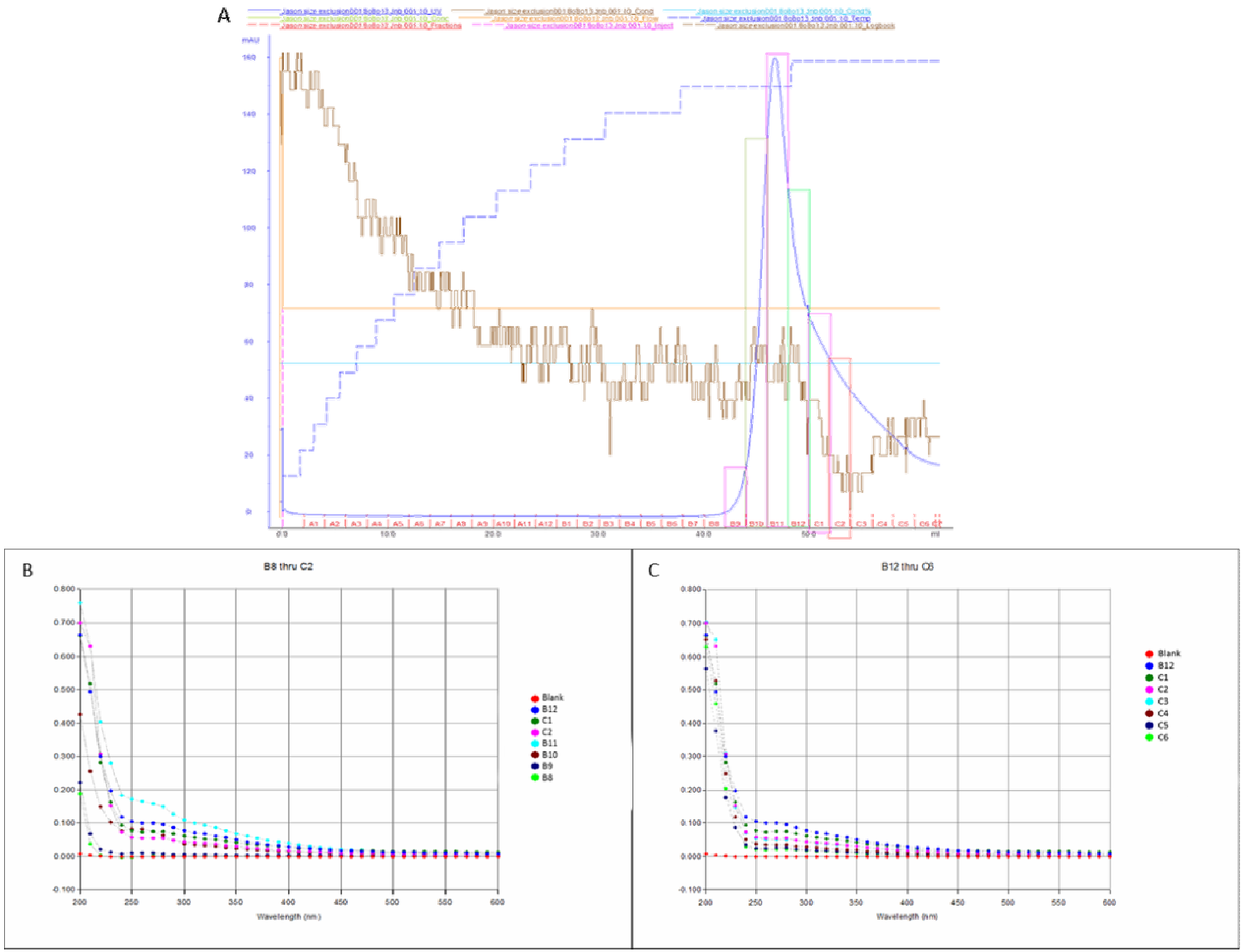


**Figure 4-16**. Continued.

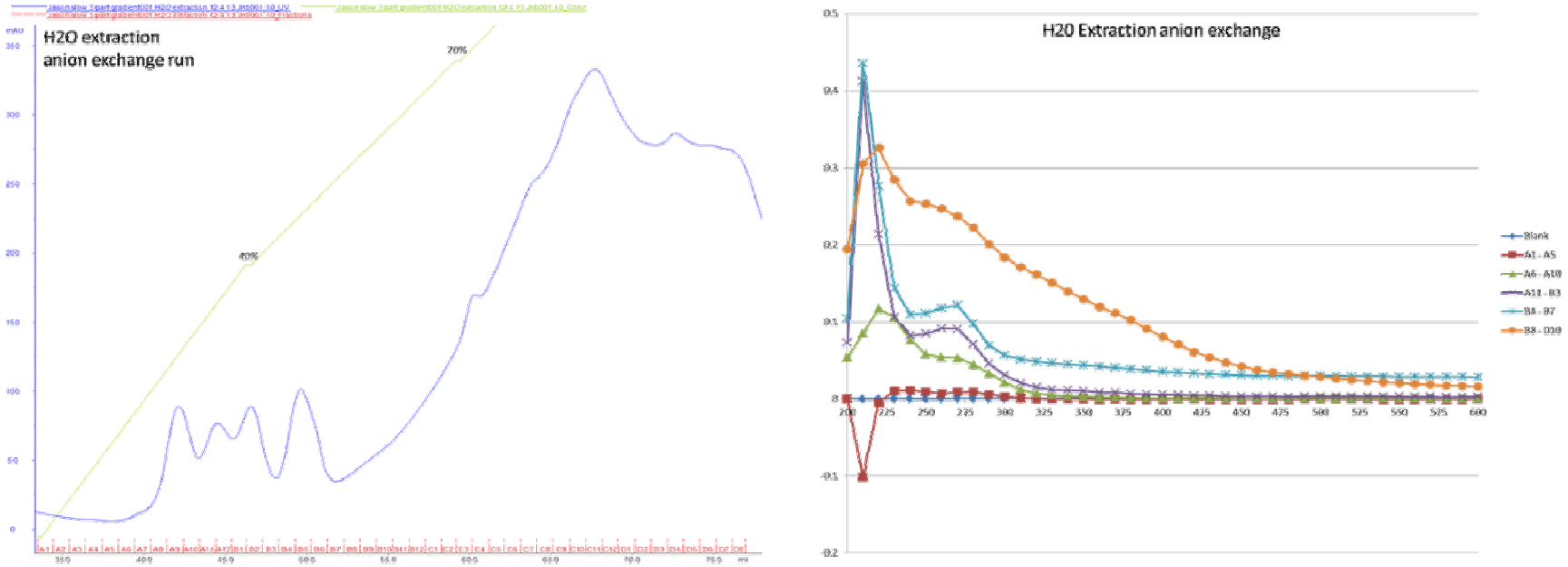


**Figure 4-17**. Fast Performance Liquid Chromatography (FPLC) chromatogram and physiochemical properties of nanoparticles extracted from English ivy adventitious roots fractionated from a HiTrap Q HP Sepharose™ anion-exchange column (GE Healthcare, Piscataway, NJ) that was previously equilibrated with 20mM Tris buffer (pH 10). (A) 10 ml of sample extracted in water was loaded onto a HiTrap Q HP Sepharose™ anion-exchange column (GE Healthcare, Piscataway, NJ) that was previously equilibrated with 20mM Tris buffer (pH 10) and was connected to an FPLC (GE Healthcare, Piscataway, NJ). Solid blue line represents the proteins eluting from the column. Solid green line represents the salt gradient. (B) Fractions A1-A5, A6-A10, A11-B3, B4-B7 and B8-D10 were combined individually and subjected to UV/Vis spectroscopy. In an effort to isolate the nanoparticle into its components, multiple runs of FPLC were performed and the UV/Vis was used to determining if the spectra matched those of the nanoparticle.

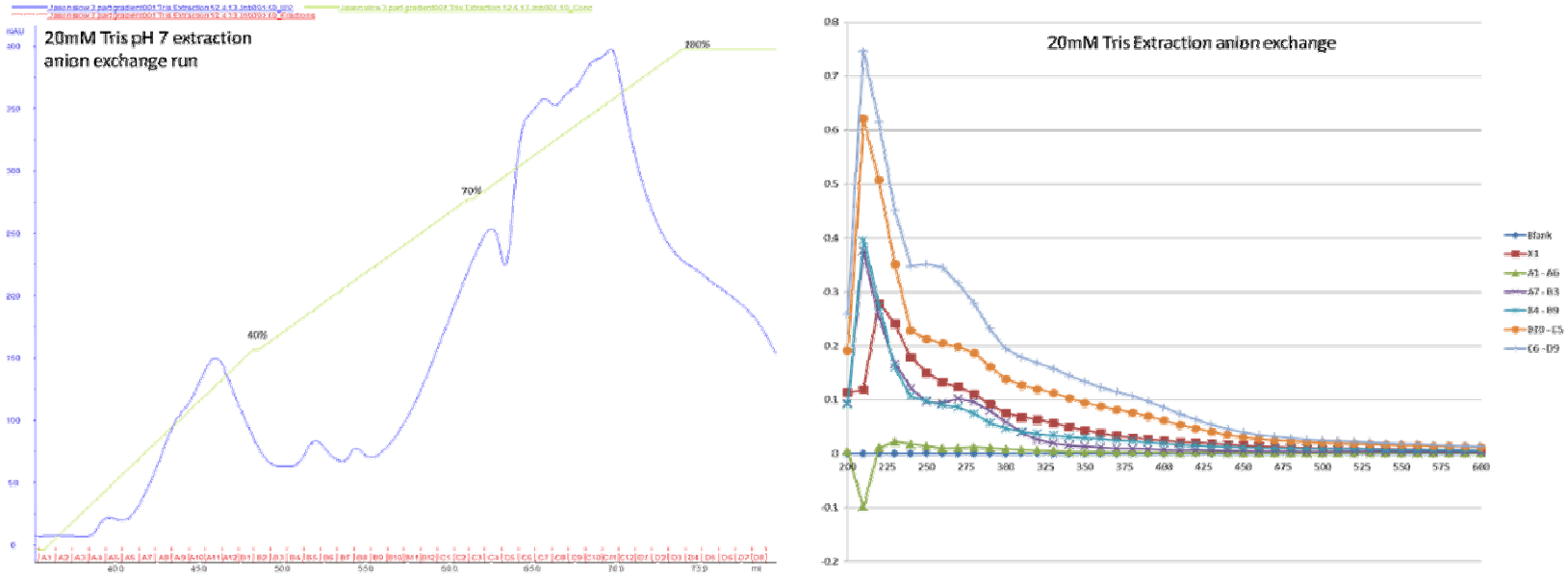


**Figure 4-18.** Fast Performance Liquid Chromatography (FPLC) chromatogram from ion exchange column and physiochemical properties of nanoparticles extracted from English ivy adventitious roots fractionated from a HiTrap Q HP Sepharose™ anion-exchange column (GE Healthcare, Piscataway, NJ) that was previously equilibrated with 20mM Tris buffer (pH 10). (A) 10 ml of sample extracted in 20mM Tris buffer was loaded onto a HiTrap Q HP Sepharose™ anion-exchange column (GE Healthcare, Piscataway, NJ) that was previously equilibrated with 20 mM Tris buffer (pH 10) and was connected to an FPLC (GE Healthcare, Piscataway, NJ). Solid blue line represents the proteins eluting from the column. Solid green line represents the salt gradient. (B) Fractions X1, A1-A6, A7-B3, B4-B9, B10-C5 and C6-D9 were combined individually and subjected to UV/Vis spectroscopy.

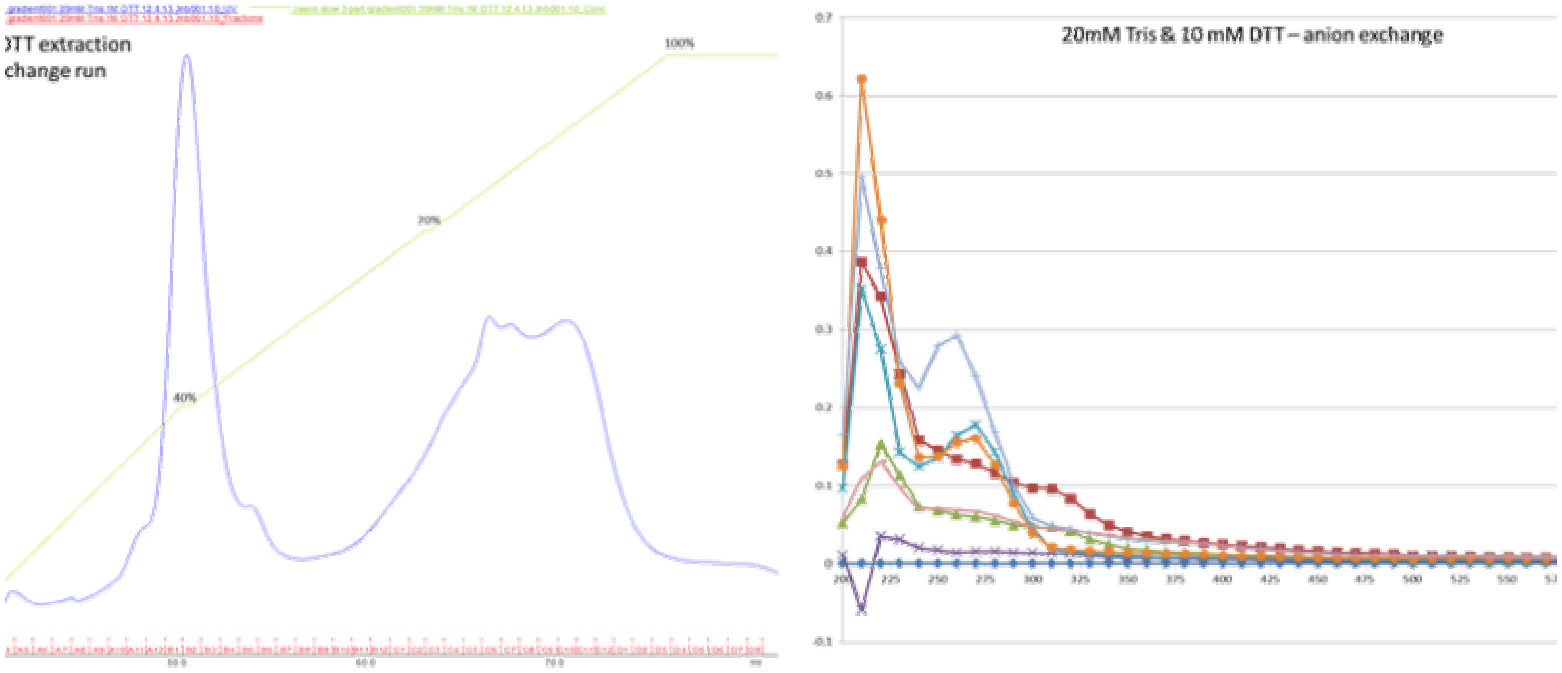


**Figure 4-19.** Fast Performance Liquid Chromatography (FPLC) chromatogram and physiochemical properties of nanoparticles extracted from English ivy adventitious roots fractionated from a HiTrap Q HP Sepharose™ anion-exchange column (GE Healthcare, Piscataway, NJ) that was previously equilibrated with 20mM Tris buffer (pH 10). (A) 10 ml of sample extracted in 20mM Tris buffer plus 10mM dithiothreitol was loaded onto a HiTrap Q HP Sepharose™ anion-exchange column (GE Healthcare, Piscataway, NJ) that was previously equilibrated with 20mM trisbuffer (pH10) and was connected to an FPLC (GE Healthcare, Piscataway, NJ). Solid blue line represents the proteins eluting from the column. Solid green line represents the salt gradient. (B) ractions X1, A1-A3, A4-A8, A9-B4, B5-B7, B8-D3 and D4-D8 were combined individually and subjected to UV/Vis spectroscopy.

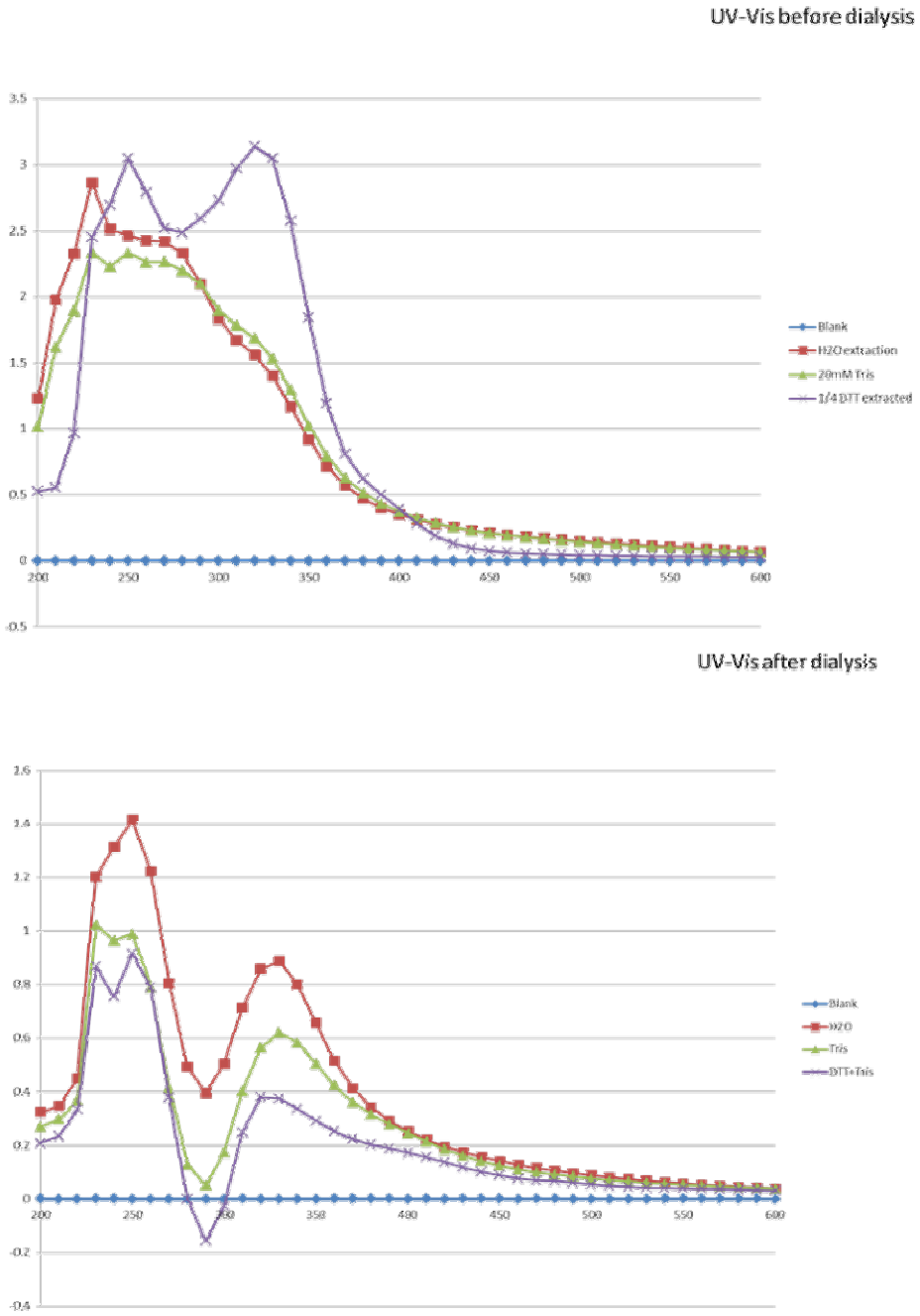


**Figure 4-20.** Physiochemical properties of nanoparticles extracted from English ivy adventitious roots. Samples were either extracted in water, 20 mM Tris buffer or 20 mM Tris buffer and 20 mM Tris buffer plus 10mM dithiothreitol (DTT). UV/Vis spectroscopy was performed before and after dialysis.

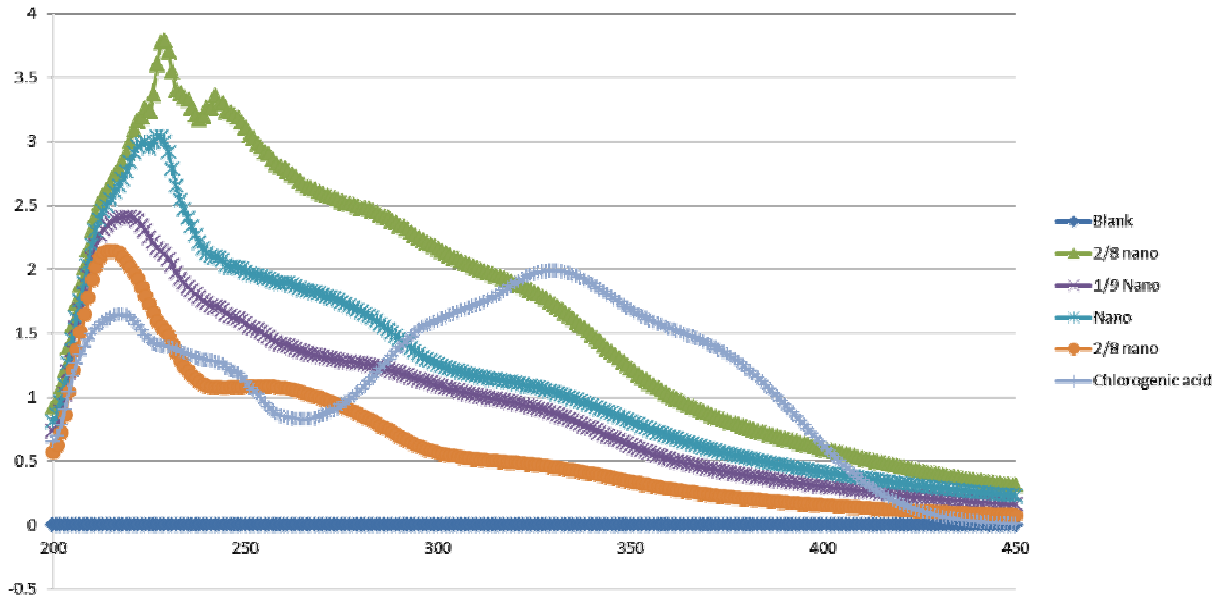


**Figure 4-21.** Physiochemical properties of nanoparticles extracted from English ivy adventitious roots were compared to a known plant phenolic compound, chlorogenic acid, to observe any similar properties to the ivy nanoparticle.

**Table 4-1.** Proteins present in ivy nanoparticles as identified using ivy transcriptome. Fractions B11, B12 and E5 under the peak obtained from FPLC size exclusion were sent to MS Bioworks for LC-MS/MS analysis. E5 was included as a sample to eliminate random proteins. No protein bands were observed when the E5 fraction using SDS-PAGE. No single protein appeared as the only protein reponsable for the formation of the nanoparticle.

| Proteins | Size | E5 | B11 | B12 | Band | Gene Length | Hit Description | Expression (Adventitious) | Expression (Ground) | Fold Change |
|---|---|---|---|---|---|---|---|---|---|---|
| 73 | 114,693 | 23 | 88 | 72 | 31 | 3128 | Uncharacterized protein | 30 | 25 | 1 |
| 11143 | 65,853 | 21 | 43 | 37 | 24 | 1796 | Uncharacterized FAD-binding protein | 335 | 117 | 2.8 |
| 20608 | 33,477 | 29 | 42 | 33 | 3 | 913 | putative acid phosphatase, partial [Aralia elata] | 57 | 1 | 48.9 |
| 46181 | 83,710 | 10 | 40 | 33 | 18 | 2283 | beta-glucosidase 24-like | 1756 | 95 | 18 |
| 116 | 93,207 | 7 | 36 | 24 | 9 | 2542 | Arabidopsis thaliana translation initiation factor 3B1 | 106 | 71 | 1 |
| 1487 | 89,320 | 0 | 32 | 36 | | 2436 | Probable ATP-citrate synthase subunit 1 | 239 | 15 | 15 |
| 43813 | 105,233 | 5 | 32 | 36 | | 2870 | Coatomer, alpha subunit | 53 | 25 | 2 |
| 66528 | 13,017 | 8 | 29 | 18 | | 355 | Histone H4 | 447 | 28 | 15 |
| 145 | 103,987 | 0 | 29 | 23 | | 2836 | 26S proteasome non-ATPase regulatory subunit 2 | 52 | 33 | 1.5 |
| 11026 | 74,873 | 0 | 28 | 26 | | 2042 | Phosphofructokinase | 97 | 16 | 5.9 |

# Chapter 5. Identification of the proteins involved in the formation of English ivy nanoparticles through an -omics based strategy

Adapted from:

Jason N. Burris, Scott C. Lenaghan, Y. Peng, Mingjun Zhang, Eric J. Carpenter, Zhijian Tian, Gane Ka-Shu Wong, and C. Neal Stewart, Jr. Identification of the proteins involved in the formation of English ivy nanoparticles through an -omics based strategy.

To be submitted to Journal of the Royal Interface.

I designed, executed and analyzed the experiments and wrote the manuscript.

## 5.1 Abstract

English ivy (*Hedera helix* L.) secretes a high strength nanocomposite adhesive from adventitious roots, which allows the plant to climb on vertical surfaces. Previous studies have determined that the ivy nanocomposite adhesive is primarily composed of proteinaceous nanoparticles and a polysaccharide matrix. Further study of isolated nanoparticles has revealed that these nanoparticles have ultraviolet (UV) protective capabilities and the potential for use as nanocarriers for delivery of therapeutic compounds. Considering the importance of the ivy nanoparticles in a variety of applications, the goal of this work was to identify the proteins involved in the formation of the ivy nanoparticles using an -omics approach. First, individual proteins were separated from purified ivy nanoparticles by adjusting the reducing conditions prior to SDS-PAGE. Using this strategy, it was possible to separate the ivy nanoparticles into 9 distinct protein bands ranging in molecular weight from 25 kDa to 130 kDa. After gel extraction, each band was sequenced using LC/MS/MS, and the sequence was queried against the UniProt

database to identify candidate proteins that comprise the nanoparticles. In addition to comparison with UniProt, a transcriptome for the ground and adventitious roots of English ivy was created in order to compare the isolated proteins with the reference material. The results of the -omics analysis indicated that the protein bands had high homology with 11 candidate proteins from the English ivy adventitious root transcriptome and 9 proteins from the UniProt database for a combined total of 11 unique protein candidates. Of special interest was a chaperonin protein, which has been known to participate in nanoparticle formation in other species. Based on these results, it was hypothesized that the pool of proteins isolated constitutes the essential building blocks of ivy nanoparticles, which lays the foundation for subsequent bioproduction.

## 5.2 Introduction

Previous studies have demonstrated that English ivy (*Hedera helix*) secretes a nanocomposite adhesive, from the root hairs of the adventitious roots, that allows it to climb and permanently adhere to vertical surfaces [1-2]. English ivy produces two different types of roots, adventitious roots and ground roots [6]. Adventitious roots are characterized by being short, non-branching and covered with root hairs normally forming on the stems in pathes and are primarily used to adhere the ivy on surfaces as it grows upward. Ground roots are lignified, branching and lack root hairs. The nanocomposite adhesive consists of uniform nanoparticles, 50-80 nm in size, surrounded by a polysaccharide matrix [1, 3]. Further analysis confirmed that the ivy nanocomposite adhesive has superior strength to known bioadhesives from algae, while exhibiting similar curing profiles [4]. In order to identify the mechanism generating this high strength adhesion, a contact fracture mechanics model was developed and concluded that van der Waals forces between the nanoparticles alone were not strong enough to generate the adhesive

strength observed experimentally [5]. Based on these results, it was hypothesized that the ivy nanoparticles were involved in cross-linking between the polysaccharide and the nanoparticles themselves, resulting in an epoxy-like system [4]. In order to test this hypothesis a tissue culture method was developed to generate bulk adventitious roots, and this system was used to harvest and purify ivy nanoparticles for chemical analysis [6-7]. Using inductively coupled plasma mass spectrometry (ICP-MS), it was proven that the ivy nanoparticles did not incorporate metals, such as $Ca^{++}$, into their three-dimensional structure to aid in cross-linking [7]. Further studies, including elemental analysis and SDS-PAGE, revealed that the ivy nanoparticles were formed from a complex of either single or multiple proteins/glycoproteins [7]. A recent study has further hypothesized that the ivy nanoparticles were composed of arabinogalactan proteins (AGPs) [8]. As a side-product of chemical analysis of the ivy nanoparticles, it was discovered that the nanoparticles exhibited unique optical properties, including UV absorbance over the range necessary for UV protection, i.e., a sunscreen [9]. In fact, the ivy nanoparticles were proven to have greater UV absorbance and lower cytotoxicity than $TiO_2$ and ZnO nanoparticles typically used as sunscreen protective agents [3]. Additional studies demonstrated that the ivy nanoparticles have good thermal and pH stability, which further indicates potential for use in sunscreen and cosmetic products [10]. In addition to cosmetics applications, ivy nanoparticles have been demonstrated as effective nanocarriers for drugs, indicating their potential for use in nanomedicine [8].

The objective of the study described herein was to use -omics approaches to identify candidate proteins and their genes responsible for nanoparticle composition. While recent research identified a single high molecular weight band from SDS-PAGE (>460 kD) as the major

component of the nanoparticle structure, it was hypothesized that the denaturation conditions were ineffective, which resulted in the protein complex retaining its native conformation [7]. Our strategy consisted of optimization of nanoparticle extraction and protein denaturation and separation to facilitate targeted proteomics analysis to identify individual candidate proteins that comprise the nanoparticles. In order to infer which candidate English ivy genes were responsible for encoding these proteins a comparative transcriptomic analysis was undertaken using ground roots and the nanoparticle-producing adventitious roots. Tandem implementation of proteomic and transcriptomic approaches were powerful tools for identification of candidate proteins and genes, which allow hypotheses to be generated about nanoparticle form and function.

## 5.3 Materials and methods

### 5.3.1 Adventitious root production

English ivy shoots were provided by Swan Valley Farms, Mount Vernon, Washington, USA. Production of adventitious roots was carried out as previously described with slight modifications [6]. Briefly, stems were segmented to 12.5 cm linear sections and all leaves except the most anterior were removed. Each stem was then soaked in indole butyric acid potassium salt (IBA) (Sigma, St. Louis, Missouri, USA) at 50 mg/L for 24 h. Post-treatment, stem segments were placed in modified Magenta GA7 boxes (Fisher, Waltham, Massachusetts, USA), 4 to a box, with 50 ml of water, and incubated with continuous light (83 $\mu mol/m^2s^1$) for 2 weeks.

### 5.3.2 Nanoparticle extraction and analysis

Adventitious roots were harvested from cultured stems, flash frozen in liquid nitrogen, and nanoparticles were extracted as described previously with slight modifications [9]. Briefly, 25 ml of 20 mM Tris-HCl was added to 8 g of frozen roots and blended for 2 min until completely homogenized. Homogenates were then passed through Whatman No. 1 filter paper contained in a Buchner funnel to remove large debris prior to centrifugation at 3,000× g for 30 min. The supernatant was then collected and dialyzed in Spectra cellulose ester dialysis membranes (300 kDa molecular weight cut-off [MWCO]; Spectrum Laboratories, Rancho Dominguez, California, USA) against 20 mM Tris-HCl for 48 h with 3 buffer changes, and the solution remaining in the tubing was removed and stored at 4 °C.

In order to assess the impact of storage conditions on the stability of the ivy nanoparticles, nanoparticles were either prepared fresh, frozen at -20 °C or -80 °C, or frozen at -80 °C and then lyophilized using a Labconco FreeZone 12 Liter Freeze Dry System (Labconco, Kansas City, Missouri, USA) and stored at -80 °C. After storage for 1 week, the nanoparticles were either reconstituted, in the case of the lyophilized nanoparticles, or thawed, in the case of frozen nanoparticles, and the size distribution and Zeta potential of the isolated nanoparticles was analyzed using a Malvern Zetasizer Nano ZS (Worcestershire, United Kingdom).

In addition to examining the effect of storage conditions on the ivy nanoparticles, the effect of oxidizing enzymes present in the adventitious root extract on nanoparticle formation was analyzed by using dithiothreitol (DTT) to inhibit oxidation. In these experiments, roots were macerated in 20 mM Tris-HCl at varying pH (4, 7 or 10), containing varying concentrations of

DTT (0, 2, 4, 6, 8 or 10 mM). The extent to which DTT inhibited oxidative enzymes present in the extract was determined by qualitatively comparing the color of the extract, with the darker color indicating a higher degree of oxidation. After addition of the DTT to the extract, nanoparticle isolation was carried out as described previously [6, 7]. To ensure that the structure of the ivy nanoparticles was not a result of oxidative reactions, the size distribution of the nanoparticle was analyzed as described previously [3-4, 6-10], and compared to controls. It was also important to ensure that DTT did not result in alteration of the nanoparticles leading to a loss of the characteristic UV/vis absorbance. As such, UV/vis spectroscopy was conducted on the DTT treated nanoparticles and controls, and analyzed using a Biotek Synergy HT Microplate Reader (Biotek, Winsooki, Vermont, USA).

### 5.3.3 Sample preparation for LC/MS/MS and protein identification

Once collected, ivy nanoparticles were subjected to various denaturing and/or reducing conditions in order to obtain the best resolved bands. Samples were added to a sample buffer containing differing amounts of urea (2 M to 8 M), thiourea (1 M to 2 M), 3% sodium dodecyl sulfate (SDS) and DTT with 0.03% bromophenol blue [11] and run on SDS-PAGE gels to optimize band resolution and separation. Ivy nanoparticles collected from the extraction were mixed 1:1 with Laemmli buffer containing 2 M thiourea, 8 M urea, 3% SDS and 10% 2-mercaptoethanol and boiled for 10 min. After denaturation, samples were electrophoresed on Tris-glycine gels (5% stacking, 12% resolving) (Jule, Inc., Milford, Connecticut) at 1 W for 24 h in SDS-Tris-glycine running buffer re-circulated at 4 °C. Gels were stained with ProtoBlue safe Colloidal Coomassie G-250 stain (National Diagnostic, Atlanta, Georgia). The nine most distinct bands from the gels stained with ProtoBlue were excised, transferred to individual microfuge

tubes, and shipped on ice to MS Bioworks (Ann Arbor, Michigan, USA) for sequencing and analysis (**Figure 5-1**). MS Bioworks conducted the sequencing by first washing the gel slices with 25 mM ammonium bicarbonate and acetonitrile and then further reducing the samples with 10 mM DTT at 60 °C. Next, samples were alkylated with 50 mM iodoacetamide and trypsin digested at 37 °C for 4 h prior to quenching with formic acid. Following quenching, the supernatant was analyzed by nano LC/MS/MS using a Waters NanoAcquity HPLC system equipped with a trapping column and eluted over a 75 µm analytical column at 350 nL/min; both columns were packed with Jupiter Proteo resin (Phenomenex, Torrance, California, USA). Following HPLC, the peptides were analyzed in a ThermoFisher Orbitrap Velos Pro (Waltham, Massachusetts, USA) mass spectrometer operating in data-dependent mode, with 60,000 full width at half maximum (FWHM) resolution and MS/MS performed in the linear trap quadrupole (LTQ). The 15 most abundant peptide ions were selected for MS/MS. Data was processed using the Mascot software (Matrix Science Inc, Boston, Massachusetts) with the following parameters: enzyme: trypsin, database: UniProt virdiplantea, fixed modification: carbamidomethyl (C), variable modification : oxidation (M), acetyl (Protein N-term), pyro-Glu (N-term Q, deamidaton (NQ), mass values: monoisotopic, peptide mass tolerance:10 ppm, fragment mass tolerance: 0.6 Da, max missed cleavages: 2. Mascot data files were parsed into the Scaffold software (Proteome software Inc., Portland, Oregon, USA) for validation, filtering, and to create a non redundant list per sample. Data were filtered using a protein threshold of 99.0%, a minimum number of peptides as 5, a peptide threshold of 95%, and an exclusive spectrum count. Peptide identifications were accepted if they could be established with > 20% probability as specified by the peptide prophet algorithm [12]. Protein identifications were accepted if they could be established at greater than 99% probability and contained at least 1 identified peptide. Protein

probabilities were assigned by the protein prophet algorithm [13]. Proteins that contained similar peptides and could not be differentiated based on MS/MS analysis alone were grouped to satisfy the principles of parsimony.

### 5.3.4 Sequencing of the reference English ivy root transcriptome

An English ivy reference transcriptome from roots was produced by cDNA library construction of RNA extracted from adventitious and ground roots of English ivy. Both root types (adventitious and ground) were collected, and frozen with liquid nitrogen into 2 separate tubes. RNA was extracted from each tube using Trizol and purified using an RNeasy mini kit (Qiagen, Valencia, California, USA). Each RNA sample was then incorporated into a GenTegra (GenTegra Pleasanton, California, USA) water soluble chemical matrix, air dried and shipped to BGI-Shenzhen (BGI) (BGI Shenzhen, Yantian District, Shenzhen, China) for cDNA construction and sequencing, as described previously [14]. Sequencing was performed using an Illumina GA IIx platform on both the adventitious and ground roots cDNA and raw sequence reads were trimmed prior to scaffold assembly [15]. Only high quality reads were used in subsequent assemblies, with a consensus library created using all the assemblies. The reference transcriptome constituted the combined data of two Illumina libraries, one each from adventitious and ground roots, which allowed subsequent for comparison of the expression levels between the 2 samples.

### 5.3.5 *De novo* assembly and assessment of transcriptome quality

The *de novo* transcriptome assembly was conducted as described previously [15]. The original reads used for assembly of the ivy transcriptome and the assembled scaffolds are publically available on the 1000 Plants (1kp) website (http://mirrors.iplantcollaborative.org/browse/iplant /home/shared/onekp_pilot). The reference transcriptome was further annotated by comparison against the UniProt database using BLASTX (with e-value cutoff of 10-3). Expression profiles analysis was performed by using the RNAseq module in the CLC genomic workbench (Qiagen, Valencia, California, USA).

### 5.3.6 RNA extraction and reverse transcriptase polymerase chain reaction (RT-PCR)

In order to validate the sequence data obtained from the English ivy transcriptome and obtain longer ivy-specific sequence, 10 primer sets were designed based on the sequences identified from comparison of the 9 isolated protein bands and the ivy transcriptome. Primers were created using SnapGene (GSL Biotech LLC, Chicago, Illinois, USA) with the following parameters: 18-22 nt long and a minimum melting temperature of 55 °C. The sequences of primers (synthesized by Integrated DNA Technologies, Coralville, Iowa, USA) are shown in **Table 5-1**. After design of the primers, tissue from adventitious roots, ground roots and leaves from English ivy were snap frozen and macerated into a powder in liquid nitrogen. Macerated tissue was then added to Tri reagent (Molecular Research Center, Cincinnati, Ohio, USA) at 100 mg tissue to 1 ml of Tri reagent. Samples were allowed to sit for 5 min at room temperature and subsequently centrifuged at 6,000 × g. The supernatant was transferred to a new tube. Tri reagent was the added directly to a Direct-zol™ RNA Kit column (Zymo Research Irvine, California, USA) and RNA was

extracted based on manufacturer's instructions. RNA was quantified and analyzed for quality using Nanodrop ND-1000 (Thermo Fisher Scientific, Wilmington, Delaware, USA). First-strand cDNA was synthesized using the Superscript III first strand synthesis system (Thermo Fisher Scientific Wilmington, Delaware, USA). cDNA was concentrated and cleaned using a DNA Clean & Concentrator column (Zymo Research Irvine, California, USA) according to manufacturer's instructions. Synthesized cDNA was checked for quality and quantified on the Nanodrop ND-1000. Ten different PCR using GoTaq polymerase (Promega, Madison, Wisconsin, USA) were performed for each tissue type using the specified primers. One primer set was made from each gene. PCR was carried out for 30 cycles at 52 °C using an Eppendorf Mastercycler® (Eppendorf, Hamburg, Germany). Ten microliters of all PCR products were then run on a 1% agarose gel at 105 V for 45 min and analyzed by direct visualization after ethidium bromide staining.

## 5.4 Results and discussion

### 5.4.1 Isolation of proteins from ivy nanoparticles

In recent studies on isolation of ivy nanoparticles, the nanoparticles were frozen and lyophilized prior to chemical analysis [7]. While this procedure is suitable for chemical analysis, lyophilization and subsequent reconstitution often affects the solubility of proteins [16] , and thus may inhibit downstream analysis using standard molecular approaches (i.e. gel electrophoresis). In order to test the hypothesis that the high molecular weight band observed in previous ivy nanoparticle studies was the result of incomplete solubilization of the nanoparticles [7], reconstitution of the nanoparticles using various storage methods was examined. From these

experiments it was determined that the lyophilized nanoparticles were not completely soluble in water or a 20 mM Tris buffer, pH 7, even in excess of solution. Increasing the pH of the Tris buffer to 8 led to a further decrease in solubility, with the formation of a larger insoluble pellet after centrifugation. Similar results were observed when samples were frozen at either -20 C or -80 C and then slowly thawed at room temperature. Despite the lack of an insoluble pellet after centrifugation prior to freezing, the thawed samples all contained a substantial pellet. Based on these data, it was concluded that the ivy nanoparticles cannot be completely solubilized after freeze-thaw cycles or lyophilization. These results may explain the presence of only a single high molecular weight band in previous SDS-PAGE analysis, as the insoluble fraction may have been unable to run through the gel, even in the event of complete denaturation.

While the incomplete solubilization of the nanoparticles after freeze-thawing and lyophilization may provide some insight into why we only observed the single high molecular weight band, it cannot fully explain why the high molecular weight band could not be observed in freshly extracted nanoparticles using DTT. One hypothesis is that the nanoparticles were actually the result of agglomeration of proteins created by oxidizing enzymes present in the extract. During nanoparticle isolation, it was observed that the extract rapidly turned from a dull yellow to a dark brown/black after the extract came in contact with oxidation. Previous studies from plant extracts and tea have noted that nanoparticles can form as the result of complexation of plant polyphenolics with other chemicals, such as caffeine [17-20]. The formation of these tea-extract nanoparticles has been shown to be catalyzed by polyphenol oxidases (PPOs) present in the solution [17-19]. To test the hypothesis that the ivy nanoparticles were formed as a result of a similar mechanism, DTT was added to the extraction solution at varying concentrations (0-10

mM) to prevent oxidation and inactivate the polyphenol oxidases. It has been previously shown that enzymatic 'browning' can be inhibited by thiol compounds, and that phenolic compounds, such as those found in the roots of English ivy, can be oxidized by polyphenol oxidases (PPO) causing 'browning' [21-25]. Qualitative analysis revealed that at 10 mM DTT the ivy nanoparticle extract did not undergo any enzymatic 'browning', indicating inhibition of the PPOs. At concentrations below 10 mM DTT, varying levels of 'browning' occurred, thus extraction with 10 mM DTT at varying pH (4, 7, and 10) was chosen for analysis of nanoparticle formation. To determine if the nanoparticles formed with inhibition of the PPOs, the presence and size distribution of the nanoparticles in 10 mM DTT extracted samples was analyzed using dynamic light scattering (DLS), zeta potential analysis, and UV/vis spectroscopy (**Figure 5-2**). DLS conducted on 10 mM DTT extracted nanoparticles obtained from three different extraction buffers (pH 4, pH 7 or pH 10) confirmed the presence of ivy nanoparticles at all three pHs tested (**Figure 5-2A**). The average Z diameter of ivy nanoparticles in the DTT extracted samples was 141.3 nm +/- 4 for pH 7, 148.6 nm +/- for pH 10 and 333.6 nm +/- 13.52 for pH 4, which was similar to previously published results (**Figure 5-2A**) [10]. In addition, zeta potential analysis indicated that the ivy nanoparticles had a negative surface charge that changed in magnitude according to pH (pH 7 (-23.9 mV), pH 10 (-34.5 mV), and pH 4 (-11.2 mV)) (**Figure 5-2B**). Further the polydispersity index (PDI) of the nanoparticles changed from 0.240 and 0.257 to 0.508 as the pH decreased, indicating a uniform dispersion at neutral and basic pH, with agglomeration at acidic pH. These results were consistent with previous research that observed that at neutral and alkaline conditions ivy nanoparticles were more stably dispersed than in acidic conditions [10]. A previous study in which the zeta potential of ivy nanoparticles in ultrapure water was observed to be -35.3 mV [7], was comparable to zeta potential values of the

ivy nanoparticles in buffer at pH 10 (-34.5 mV) (**Figure 5-2B**). In addition to the zeta potential and DLS analysis, previous studies have indicated that water-extracted ivy nanoparticles absorb UV light over the range of 200-400 nm [3]. Similar spectral properties were observed when the nanoparticles were extracted in buffer with the addition of 10 mM DTT at pH 7 (**Figure 5-2C**). DTT extracted nanoparticles were observed to have similar absorbance from 250 nm to 400 nm compared to water extracted nanoparticles, indicating that these properties were maintained despite the modification to the extraction procedure (**Figure 5-2C**). Based on these results, it was clear that the addition of DTT was able to inhibit oxidative reactions, as indicated by a lack of enzymatic 'browning', and that the inhibition of this process did not affect the formation or properties of the ivy nanoparticles. From these data it was possible to reject the hypothesis that the ivy nanoparticles were formed from the reaction of PPOs with other phenolic components of the root extract, demonstrating a novel mechanism for nanoparticle formation.

In addition to inhibiting oxidative enzymes, DTT has been shown to increase the solubility of numerous proteins prior to separation using SDS-PAGE [26]. For this reason, it was anticipated that the ivy nanoparticles extracted using 10 mM DTT would be more amenable to separation, indicating if the ivy nanoparticles were composed of a single high molecular weight protein or a complex of smaller proteins. The results from analysis of SDS-PAGE with DTT extracted nanoparticles revealed the presence of nine distinct protein bands, which ranged from 25 kDa to 130 kDa (**Figure 5-2**). The high molecular weight band observed in previous studies was no longer present in the DTT extracted nanoparticles, indicating that the proteins had increased solubility, which allowed for better separation. Alternatively, the inhibition of PPOs may have prevented complexation of other proteins onto the surface of the ivy nanoparticles, interfering

with denaturation. Despite the mechanism, the addition of 10 mM DTT to the ivy nanoparticle extraction and isolation procedure did not affect the physiochemical properties of the nanoparticles, but did allow the identification of 9 protein bands for subsequent analysis using LC/MS/MS peptide sequencing.

## 5.4.2 Identification of proteins involved in nanoparticle formation

### 5.4.2.1 Comparison of the sequence data to UniProt

Initial results from peptide sequencing of the 9 ivy nanoparticle protein bands led to identification of 231 proteins when compared to the UniProt database (**Figure 5-1**). Using the scaffold software program (Proteome software Inc., Portland, Oregon, USA), these proteins were confidently narrowed down to the top 9 candidate proteins (one per top candidate for each band) based upon a protein threshold of 99.0%, a minimum number of peptides as 5, a peptide threshold of 95%, and an exclusive spectrum count. These proteins (**Figure 5-1**, **Table 5-2**) were identified as clathrin heavy chain, aconitate hydratase, sucrose synthase isoform, luminal-binding protein 5, chaperonin CPN60-2, adenoslhomocyteinase, 6-phospogluconate dehydrogenase, glyceraldehydes-3-phosphate dehydrogenase, and proteasome subunit alpha type-6.

### 5.4.2.2 English ivy adventitious root and ground root transcriptome

cDNA extracted from nanoparticle-producing adventitious roots and non-producing ground roots was used to generate an ivy root transcriptome. The average quality score of the RNAseq raw reads was 35.5 and 35.6 for adventitious and ground roots, respectively (**Figure 5-3A, 5-3C**). A quality score between 35 and 40 indicates good quality, as indicated in the frequency of quality

scores (**Figure 5-3B, 5-3D**). Sequencing on the Illumina GA IIx platform produced approximately 2.1 Gb of high-quality bases from approximately 25 M 90 bp paired-end sequence reads from both adventitious and ground root samples (**Table 5-3**). Assembly from adventitious root and ground root reads returned approximately 205,180 or 233,335 scaffolds, respectively (**Table 5-3**). A total of 32,331 sequences were annotated with an average length of 996 bp, yielding a total of approximately 32.21 Mb of data (**Table 5-3**). The number of assembled transcripts with an average length greater than 600 bp, 1000 bp and 1500 bp was 32,522, 16,972 and 7,610, respectively (**Figure 5-4**). Expression profiles of genes found in adventitious and ground roots were determined (**Figure 5-5**). A scatter plot visually shows expression values in ground roots versus expression values in adventitious roots, allowing for the identification of highly expressed and specific genes for adventitious roots (**Figure 5-5**). Additionally, there were 2,529 genes uniquely expressed in adventitious roots compared with 6,719 in ground roots (**Figure 5-6**). A total of 36,118 expressed genes were common to both adventitious and ground roots. By comparing the two transcriptomes a total of 18,111 genes were shown to be higher expressing in adventitious roots while 15,744 genes were found to be higher expressing in ground roots (**Figure 5-6**).

The sequence of the 9 protein bands isolated from the nanoparticles was compared with the ivy transcriptome to determine if different proteins were identified using this reference library. In total, 633 candidate proteins were identified from all 9 bands that corresponded to annotated transcripts from the adventitious root transcriptome (**5-2**). Using the same criteria as the comparison with the UniProt database, the top 11 protein candidates were identified from 9 bands (**Table 5-2**). Two of the bands produced 2 protein identities per band. Multiple protein hits

from a single band could be due to the short 8 amino acid long reads from the LC/MS/MS data. These proteins (**Table 5-2**) were identified as tripeptidyl-peptidase 2, putative aconitate hydratase, glycine dehydrogenase, phospholipase D alpha 1, phenylalanine ammonia-lyase G2B (PAL), chaperonin CPN60-2, adenosylhomocysteinase, catalase isozyme 2, beta-glucosidase 12, glyceraldehyde-3-phosphate dehydrogenase, and proteasome subunit alpha type-6.

#### 5.4.2.3 Comparison between results from UniProt and ivy transcriptome

Without an English ivy reference genome, estimating the number of genes sequenced, their % coverage, and whether they have been assembled correctly can be a challenge [27-28]. Therefore, the English ivy transcriptome assembly was validated by a search of contigs/transcripts against UniProt. Overall, 9 bands had similar protein candidates between the ivy transcriptome and UniProt. However, some of the potential nanoparticle proteins identified by the ivy transcriptome were not identified by the UniProt analysis, such as tripeptidyl-peptidase, glycine dehydrogenase, phospholipase D alpha, PAL, catalase isozyme 2, and beta-glucosidase. It is most likely that those proteins identified from the ivy transcriptome are more significant hits than from the UniProt database due to the greater normalized total spectra (**Table 5-3**). Four proteins were identified from both the English ivy transcriptome and UniProt databases— aconetitate hydratase, adenoslhomocyteinase, glyceraldehydes-3-phosphate dehydrogenase, and proteasome subunit alpha type-6. These proteins are commonly shown to be involved in various growth and metabolic processes.

#### 5.4.2.4 Comparative expression of nanoparticle proteins between ground and adventitious roots

As anticipated, the results from comparison of the adventitious root library with the ground root library indicated that 9 of the 11 protein candidates were more highly expressed in the adventitious roots than ground roots. The 2 genes with the highest fold expression in adventitious roots compared with ground roots were phenylalanine ammonia-lyase (14-fold increase), and beta-glucosidase (18-fold increase) (**Table 5-4**). This high expression is expected since the PAL enzyme is known to be a precursor of lignin, which contributes to mechanical strength of plant tissues, especially of importance in growing roots [29], while beta-glucosidase 12 has been shown to be involved in carbohydrate metabolism and growth [30-32]. Other genes up-regulated in adventitious roots were; chaperonin, adenoslhmocysteinase, glyceraldehyde-3-phosphate dehydrogenase, and the proteasome subunit alpha type, >3-fold; and glycine dehydrogenase, >4-fold (**Table 5-4**). Tripeptidyl-peptidase 2, a serine protease of the proteasome pathway, may function with the 20S proteasome to degrade oxidized proteins generated by environmental stress in *Arabidopsis* [30, 32], while aconitate hydratase was shown to be involved in carbohydrate metabolism [30-32] Glyceraldehyde-3-phophate dehydrogenase mediates plant responses to abscisic acid and water deficiency by activating PLD and producing phosphatidic acid [33-34]. Considering that the harsh and relatively unstable conditions encountered by adventitious roots and the fact that we induced adventitious root production from ivy stems using a high-titer of IBA treatment, it is not surprising that this tissue would have a high abundance of proteins associated with environmental stress.

Of the 11 genes found from the transcriptome, only phospholipase D alpha (PLDA) and catalase isozyme were more highly expressed, 2 to 24 fold higher transcripts levels, in the ground roots than the adventitious roots (**Table 5-4**). PLDA, in response to stress, acidifies the cell by hydrolyzing glycerol-phospholipids at terminal phosphodiesteric bonds to generate phosphatidic acids [21] and mediates wound induction of jasmonic acid [24] and wound-induced metabolism of polyunsaturated fatty acids [25]. In addition, it plays a key role in cold [23], drought [22, 35] and salt tolerance to the plant [36]. Catalase isozyme 2 has been identified in all organisms that respire aerobically and provides protection from the toxic effects of hydrogen peroxide [37].

Primers were designed for each of the genes identified from LC/MS/MS (**Table 5-1**) and were used for RT-PCR analysis (**Figure 5-7**). RT-PCR analysis demonstrated the presence of the genes found from the ivy transcriptome to be transcriptionally active in both adventitious roots and leaves of English ivy (**Figure 5-7**), further validating our proteomic analysis. Once PCR products were amplified, products were verified using sequencing (UT Genomics Core, University of Tennessee, Knoxville, TN, USA).

### 5.4.3 Hypothetical role of proteins in the formation of ivy nanoparticles

While the nanoparticle was shown to be putatively composed of at least 11 proteins including one protein previously shown to produce nanostructures[42], based on previous reports we hypothesize that the chaperonin proteins encase the other protein constituents to form the nanoparticle structure. It was previously shown that doxorubicin (DOX) a cationic anticancer drug was able to complex with the ivy nanoparticle [8], indicating that the ivy nanoparticle is anionic. This anionic characteristic provides some explanation to the co-extraction of other

proteins identified from LC/MS/MS. Type I chaperonins are large oligomeric proteins involved in the folding and assembly of other proteins [38]. Chaperonin CPN60-2 and chaperonin CPN60-1, have been shown to play a vital role in protein folding and translocation in both eukaryotic and prokaryotic cells [39]. There are two subtypes of CPN60, alpha and beta, which can combine to form hetero-oligomeric chaperonin species [38]. These subtypes demonstrate 50% homology to each other and have been found to be present in two or more paralogous forms in higher plants [40]. Chaperonins form labile oligomers that can quickly dissociate into monomeric forms when diluted and in the presence of ATP [41-44]. Previous studies have demonstrated that chaperone proteins are capable of self-assembling into nanoparticle structures, approximately 25 nm in diameter [42]. It is possible that a similar mechanism is occurring with the ivy nanoparticles, where the chaperone proteins are forming a multi-subunit protein cage that results in the formation of a nanoparticle.

Plants have been shown to utilize the coat protein clathrin as an endocytic mechanism to internalize exogenous material and regulate signaling at the cell surface [45-46]. Clathrin is the major protein of the polyhedral coat of coated pits and vesicles and is a trimer of 190 kDa heavy chains each associated with an approximate 25 kDa light chain [47-48]. It has been shown that clathrin-dependent internalization machinery is the primary endocytic mechanism in plant cells and is hypothesized to play a role in nutrient transport, communication, cell signaling and immunity [46]. Thus, clathrins may provide a means of transport of the nanoparticles from within the cell to the extracellular environment. In addition to the potential role of clathrins in transport of the nanoparticle to the extracellular environment, luminal-binding protein 5 is found in plant tissues with a high proportion of rapidly dividing cells and in organs of secretory tissues.

Additionally this protein is required in the folding process of *de novo* synthesized secretory proteins in unstressed cells , and thus, may contribute to the secretion of nanoparticles from adventitious roots [49-50].

In addition, the PAL enzyme has been reported to be involved in the flavonoid pathway, which confers UV resistance to plant tissue [51]. It is possible that the presence of the PAL protein in the ivy nanoparticles is what contributes to the ivy nanoparticle's unique UV/Vis spectra, and may indicate the possibility of using these nanoparticles as a UV protective agent.

## 5.5 Conclusions

In this study, a modified protein extraction method was developed for the isolation of ivy nanoparticles and subsequent identification of the proteins involved in their formation. The addition of DTT to the extraction buffer was able to prevent oxidation of the extract, inhibiting PPOs, but did not alter the physiochemical properties of the ivy nanoparticles. Further, the increased solubility imparted by the addition of DTT allowed for separation of the single >460 kDa band from the ivy nanoparticles into its 9 principle components. This increased separation allowed for the 9 bands to be sequenced and compared to both an ivy root transcriptome, created in this work, and the UniProt database. From these comparisons, 11 and 9 protein candidates were identified respectively. Of these proteins, the PAL enzyme was hypothesized to be responsible for the UV protective effects associated with the ivy nanoparticles. Further, the identification of a chaperonin, known to form nanoparticles in other systems, provides a potential protein involved in forming the base structure of the nanoparticles. Associated with the base structure, identification of a clathrin may indicate a potential route of transport of the

nanoparticles from within the cell to the extracellular environment, as the ivy nanoparticles are known to be secreted from root hairs present on the adventitious roots. While further studies are necessary to identify how the proteins identified are interacting to form the 3D structure of the ivy nanoparticles, these studies provide a reasonable launching point. Additionally, future work to create knockdowns to observe loss of function and recombinant expression in a bacterial or yeast system would verify the role of each of the genes in nanoparticle formation identified from our LC/MS/MS analysis. It is anticipated that through further study of these proteins, it will be possible to gain insight into the mechanism of nanoparticle formation in plants, and to increase the potential for these nature nanomaterials in commercial applications, including sunscreens, paint additives, and nanocarriers for drug delivery.

## Acknowledgments

We thank the National Science Foundation CBET #0965877, the University of Tennessee, and the Ivan Racheff Chair of Excellence Endowment for funding. We also thank financial supporters of the 1KP consortium as well as the members of the 1000 Transcriptomes Project (1KP) for collecting and making available the data that made this project possible.

## References

1. Lenaghan S.C., Zhang M. 2012 Real-time observation of the secretion of a nanocomposite adhesive from English ivy *(Hedera helix*). Plant Science **183**, 206-211.

2. Zhang M., Liu M., Prest H., Fischer S. 2008 Nanoparticles secreted from ivy rootlets for surface climbing. Nano Letters **8**(5), 1277-1280.

3. Xia L., Lenaghan S.C., Zhang M., Zhang Z., Li Q. 2010 Naturally occurring nanoparticles from English ivy: an alternative to metal-based nanoparticles for UV protection. Journal of Nanobiotechnology **8**(1), 12.

4. Xia L., Lenaghan S., Zhang M., Wu Y., Zhao X., Burris J., Neal Stewart C., Jr. 2011 Characterization of English ivy (*Hedera helix*) adhesion force and imaging using atomic force microscopy. Journal of Nanoparticle Research **13**(3), 1029-1037.

5. Wu Y., Zhao X., Zhang M. 2010 Adhesion mechanics of ivy nanoparticles. Journal of Colloid and Interface Science **344**(2), 533-540.

6. Burris J.N., Lenaghan S.C., Zhang M., Stewart C.N. 2012 Nanoparticle biofabrication using English ivy (*Hedera helix*). Journal of Nanobiotechnology **10**, 41.

7. Lenaghan S.C., Burris J.N., Chourey K., Huang Y., Xia L., Lady B., Sharma R., Pan C., LeJeune Z., Foister S. 2013 Isolation and chemical analysis of nanoparticles from English ivy

(*Hedera helix* L.). Journal of The Royal Society Interface **10**(87), 20130392.

8. Huang Y., Wang Y.-J., Wang Y., Yi S., Fan Z., Sun L., Lin D., Anreddy N., Zhu H., Schmidt M., et al. 2015 Exploring naturally occurring ivy nanoparticles as an alternative biomaterial. Acta Biomaterialia **25**, 268-283.

9. Li Q., Xia L., Zhang Z., Zhang M. 2010 Ultraviolet extinction and visible transparency by ivy nanoparticles. Nanoscale Research Letters **5**(9), 1487-1491.

10. Huang Y., Lenaghan S.C., Xia L., Burris J.N., Stewart Jr C.N., Zhang M. 2013 Characterization of physicochemical properties of ivy nanoparticles for cosmetic application. Journal of Nanobiotechnology **11**(1).

11. Warren C.M., Krzesinski P.R., Greaser M.L. 2003 Vertical agarose gel electrophoresis and electroblotting of high molecular weight proteins. Electrophoresis **24**(11), 1695-1702.

12. Keller A., Nesvizhskii A.I., Kolker E., Aebersold R. 2002 Empirical statistical model to estimate the accuracy of peptide identifications made by MS/MS and database search. Analytical Chemistry **74**(20), 5383-5392.

13. Nesvizhskii A.I., Keller A., Kolker E., Aebersold R. 2003 A statistical model for identifying proteins by tandem mass spectrometry. Analytical Chemistry **75**(17), 4646-4658.

14. Johnson M.T.J., Carpenter E.J., Tian Z., Bruskiewich R., Burris J.N., Carrigan C.T., Chase M.W., Clarke N.D., Covshoff S., dePamphilis C.W., et al. 2012 Evaluating methods for isolating total RNA and predicting the success of sequencing phylogenetically diverse plant transcriptomes. PLoS ONE **7**(11), e50226.

15. Peng Y., Abercrombie L.L., Yuan J.S., Riggins C.W., Sammons R.D., Tranel P.J., Stewart C.N. 2010 Characterization of the horseweed (Conyza canadensis) transcriptome using GSFLX 454 pyrosequencing and its application for expression analysis of candidate non-target herbicide resistance genes. Pest Management Science **66**(10), 1053-1062.

16. Arakawa T., Prestrelski S.J., Kenney W.C., Carpenter J.F. 2001 Factors affecting short-term and long-term stabilities of proteins. Advanced Drug Delivery Reviews **46**(1–3), 307-326.

17. Gröning R., Breitkreutz J., Baroth V., Müller R. 2001 Nanoparticles in plant extracts--factors which influence the formation of nanoparticles in black tea infusions. Die Pharmazie **56**(10), 790-792.

18. Gröning R., Breitkreutz J., Baroth V., Müller R.S. 2002 Nanoparticles in plant extracts: influence of drugs on the formation of nanoparticles and precipitates in black tea infusions. European Journal of Pharmaceutical Sciences **15**(2), 149-155.

19. Roberts E. 1963 The phenolic substances of manufactured tea. X.—The creaming down of tea liquors. Journal of the Science of Food and Agriculture **14**(10), 700-705.

20. Yi S., Wang Y., Huang Y., Xia L., Sun L., Lenaghan S.C., Zhang M. 2014 Tea nanoparticles for immunostimulation and chemo-drug delivery in cancer treatment. Journal of Biomedical Nanotechnology **10**(6), 1016-1029.

21. Fan L., Zheng S., Wang X. 1997 Antisense suppression of phospholipase D alpha retards abscisic acid-and ethylene-promoted senescence of postharvest Arabidopsis leaves. The Plant Cell **9**(12), 2183-2196.

22. Mane S.P., Vasquez-Robinet C., Sioson A.A., Heath L.S., Grene R. 2007 Early PLDα-mediated events in response to progressive drought stress in Arabidopsis: a transcriptome analysis. Journal of Experimental Botany **58**(2), 241-252.

23. Rajashekar C., Zhou H.-E., Zhang Y., Li W., Wang X. 2006 Suppression of phospholipase Dα1 induces freezing tolerance in Arabidopsis: response of cold-responsive genes and osmolyte accumulation. Journal of Plant Physiology **163**(9), 916-926.

24. Wang C., Zien C.A., Afitlhile M., Welti R., Hildebrand D.F., Wang X. 2000 Involvement of phospholipase D in wound-induced accumulation of jasmonic acid in Arabidopsis. The Plant Cell **12**(11), 2237-2246.

25. Zien C.A., Wang C., Wang X., Welti R. 2001 In vivo substrates and the contribution of the common phospholipase D, PLDα, to wound-induced metabolism of lipids in Arabidopsis. Biochimica et Biophysica Acta (BBA)-Molecular and Cell Biology of Lipids **1530**(2), 236-248.

26. Rabilloud T. 1996 Solubilization of proteins for electrophoretic analyses. Electrophoresis **17**(5), 813-829.

27. Parchman T.L., Geist K.S., Grahnen J.A., Benkman C.W., Buerkle C.A. 2010 Transcriptome sequencing in an ecologically important tree species: assembly, annotation, and marker discovery. BMC genomics **11**(1), 1.

28. Wheat C.W. 2010 Rapidly developing functional genomics in ecological model systems via 454 transcriptome sequencing. Genetica **138**(4), 433-451.

29. Vanholme R., Demedts B., Morreel K., Ralph J., Boerjan W. 2010 Lignin biosynthesis and structure. Plant Physiology **153**(3), 895-905.

30. Book A.J., Yang P., Scalf M., Smith L.M., Vierstra R.D. 2005 Tripeptidyl peptidase II. an oligomeric protease complex from Arabidopsis. Plant Physiology **138**(2), 1046-1057.

31. Opassiri R., Pomthong B., Onkoksoong T., Akiyama T., Esen A., Cairns J.K. 2006 Analysis of rice glycosyl hydrolase family 1 and expression of Os4bglu12 β-glucosidase. BMC Plant Biology **6**(1), 1.

32. Polge C., Jaquinod M., Holzer F., Bourguignon J., Walling L., Brouquisse R. 2009 Evidence for the existence in Arabidopsis thaliana of the proteasome proteolytic pathway activation in response to cadmium. Journal of Biological Chemistry **284**(51), 35412-35424.

33. Guo L., Devaiah S.P., Narasimhan R., Pan X., Zhang Y., Zhang W., Wang X. 2012 Cytosolic glyceraldehyde-3-phosphate dehydrogenases interact with phospholipase Dδ to transduce hydrogen peroxide signals in the Arabidopsis response to stress. The Plant Cell **24**(5), 2200-2212.

34. Rius S.P., Casati P., Iglesias A.A., Gomez-Casati D.F. 2008 Characterization of Arabidopsis lines deficient in GAPC-1, a cytosolic NAD-dependent glyceraldehyde-3-phosphate dehydrogenase. Plant Physiology **148**(3), 1655-1667.

35. Uraji M., Katagiri T., Okuma E., Ye W., Hossain M.A., Masuda C., Miura A., Nakamura Y., Mori I.C., Shinozaki K. 2012 Cooperative function of PLDδ and PLDα1 in abscisic acid-induced stomatal closure in Arabidopsis. Plant Physiology **159**(1), 450-460.

36. Zhang Q., Lin F., Mao T., Nie J., Yan M., Yuan M., Zhang W. 2012 Phosphatidic acid regulates microtubule organization by interacting with MAP65-1 in response to salt stress in Arabidopsis. The Plant Cell **24**(11), 4555-4576.

37. Elstner E.F. 1982 Oxygen activation and oxygen toxicity. Annual Review of Plant Physiology **33**(1), 73-96.

38. Vitlin Gruber A., Nisemblat S., Azem A., Weiss C. 2013 The complexity of chloroplast chaperonins. Trends in Plant Science **18**(12), 688-694.

39. Zhang X., Beuron F., Freemont P.S. 2002 Machinery of protein folding and unfolding. Current Opinion in Structural Biology **12**(2), 231-238.

40. Martel R., Cloney L.P., Pelcher L.E., Hemmingsen S.M. 1990 Unique composition of plastid chaperonin-60: α and β polypeptide-encoding genes are highly divergent. Gene **94**(2), 181-187.

41. Bonshtien A.L., Parnas A., Sharkia R., Niv A., Mizrahi I., Azem A., Weiss C. 2009 Differential effects of co-chaperonin homologs on cpn60 oligomers. Cell Stress and Chaperones **14**(5), 509-519.

42. Dickson R., Weiss C., Howard R.J., Alldrick S.P., Ellis R.J., Lorimer G., Azem A., Viitanen P.V. 2000 Reconstitution of higher plant chloroplast chaperonin 60 tetradecamers active in protein folding. Journal of Biological Chemistry **275**(16), 11829-11835.

43. Lissin N.M. 1995 In vitro dissociation and self-assembly of three chaperonin 60s: the role of ATP. FEBS letters **361**(1), 55-60.

44. Musgrove J.E., Johnson R.A., Ellis R.J. 1987 Dissociation of the ribulosebisphosphate carboxylase large subunit binding protein into dissimilar subunits. European Journal of Biochemistry **163**(3), 529-534.

45. Alberts B., Johnson A., Lewis J., Walter P., Raff M., Roberts K. 2002 Molecular biology

of the cell 4th edition: international student edition. New York: Garland Science. Available from: http://www.ncbi.nlm.nih.gov/books/NBK21054/.

46. Dhonukshe P., Aniento F., Hwang I., Robinson D.G., Mravec J., Stierhof Y.-D., Friml J. 2007 Clathrin-mediated constitutive endocytosis of PIN auxin efflux carriers in Arabidopsis. Current Biology **17**(6), 520-527.

47. Kirchhausen T., Harrison S.C. 1981 Protein organization in clathrin trimers. Cell **23**(3), 755-761.

48. Ungewickell E., Branton D. 1981 Assembly units of clathrin coats. Nature **289**(5796), 420-422.

49. Denecke J., Goldman M., Demolder J., Seurinck J., Botterman J. 1991 The tobacco luminal binding protein is encoded by a multigene family. The Plant Cell **3**(9), 1025-1035.

50. Gething M.-J., McCammon K., Sambrook J. 1986 Expression of wild-type and mutant forms of influenza hemagglutinin: the role of folding in intracellular transport. Cell **46**(6), 939-950.

51. Tarchevsky I., Yakovleva V., Egorova A. 2008 Proteomic analysis of changes in pea roots caused by the apoptosis-inducing concentration of salicylic acid. Doklady Biochemistry and Biophysics **422**, 274-278.

# Appendix

## Figures and Tables

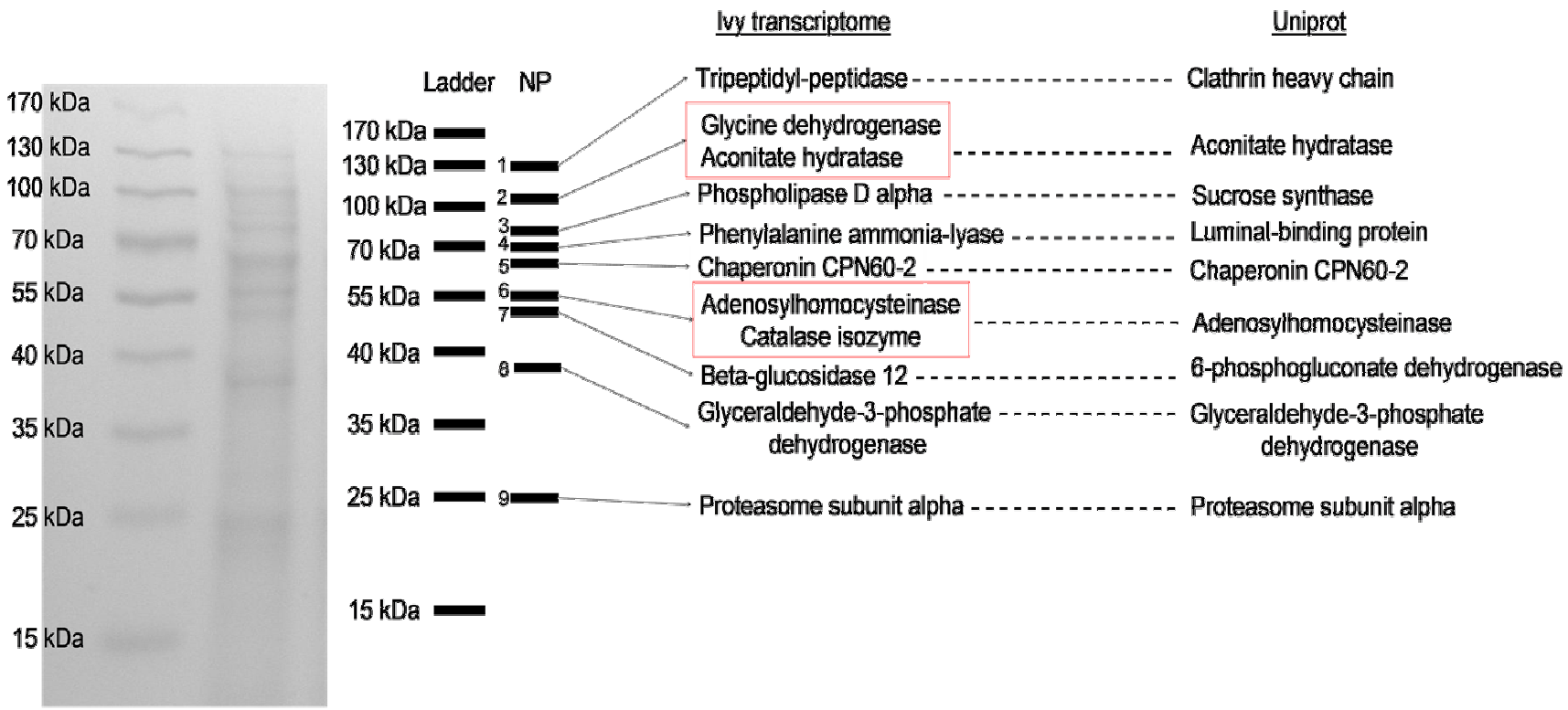


**Figure 5-1.** Results from SDS-PAGE of ivy nanoparticles extracted with 20 mM Tris-HCl pH 7 containing 10 mM dithiothreiol (DTT). 9 distinct bands were excised using a razor and sent off to MC Bioworks for sequencing. The artificial gel shows the bands and their corresponding identification from the mass spec data.

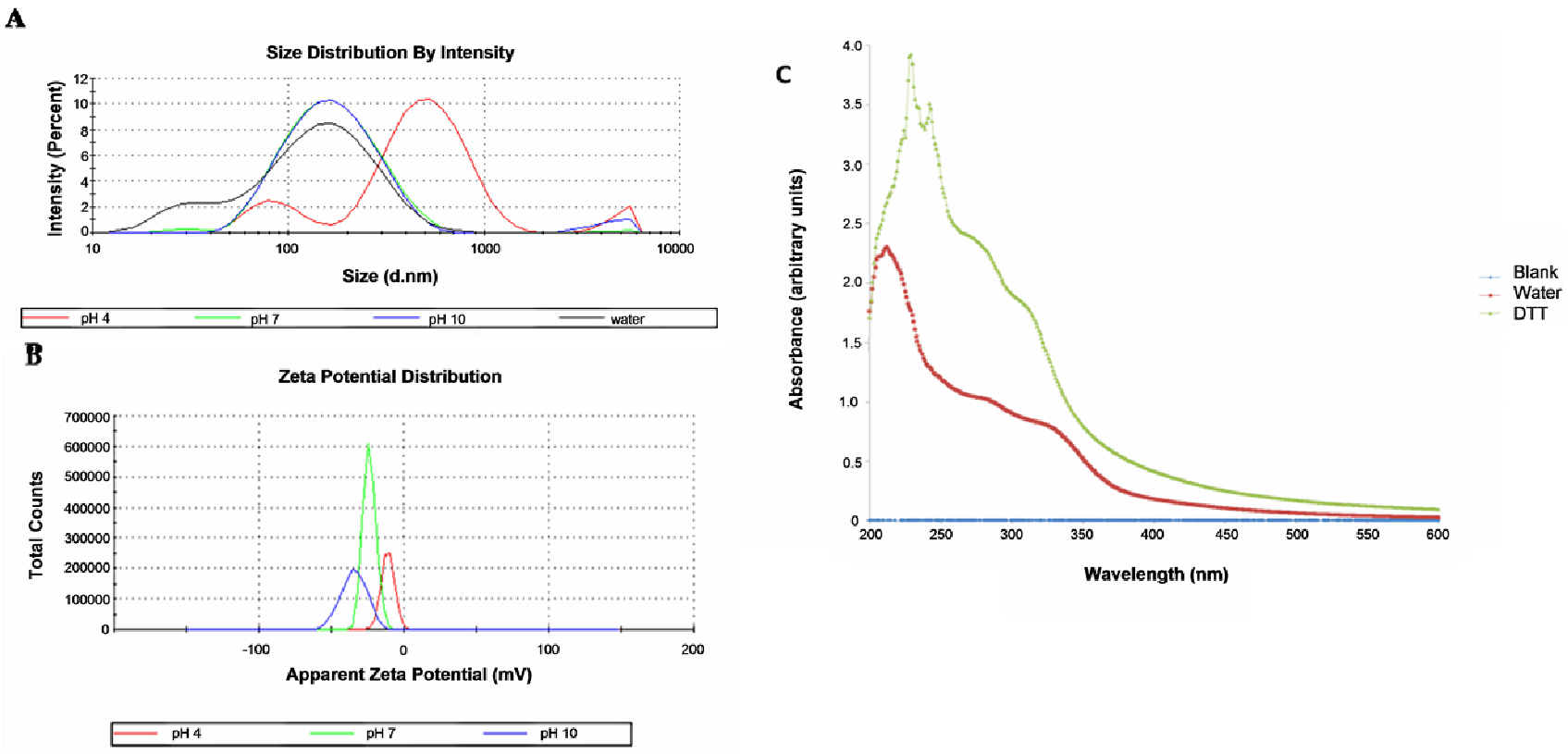


**Figure 5-2.** Physicochemical properties of nanoparticles extracted from English ivy adventitious roots. (A) Dynamic light scattering (DLS) analysis of ivy nanoparticles extracted in 20 mM Tris-HCl containing 10 mM dithiothreiol (DTT) at pH 4, pH 7 and pH 10. (B) Zeta Potential analysis of ivy nanoparticles extracted in 20 mM Tris-HCl containing 10 mM dithiothreiol (DTT) at pH 4, pH 7 and pH 10. (C) UV/vis spectra of ivy nanoparticles extracted in water or 20 mM Tris-HCl containing 10 mM dithiothreiol (DTT) at pH 7.

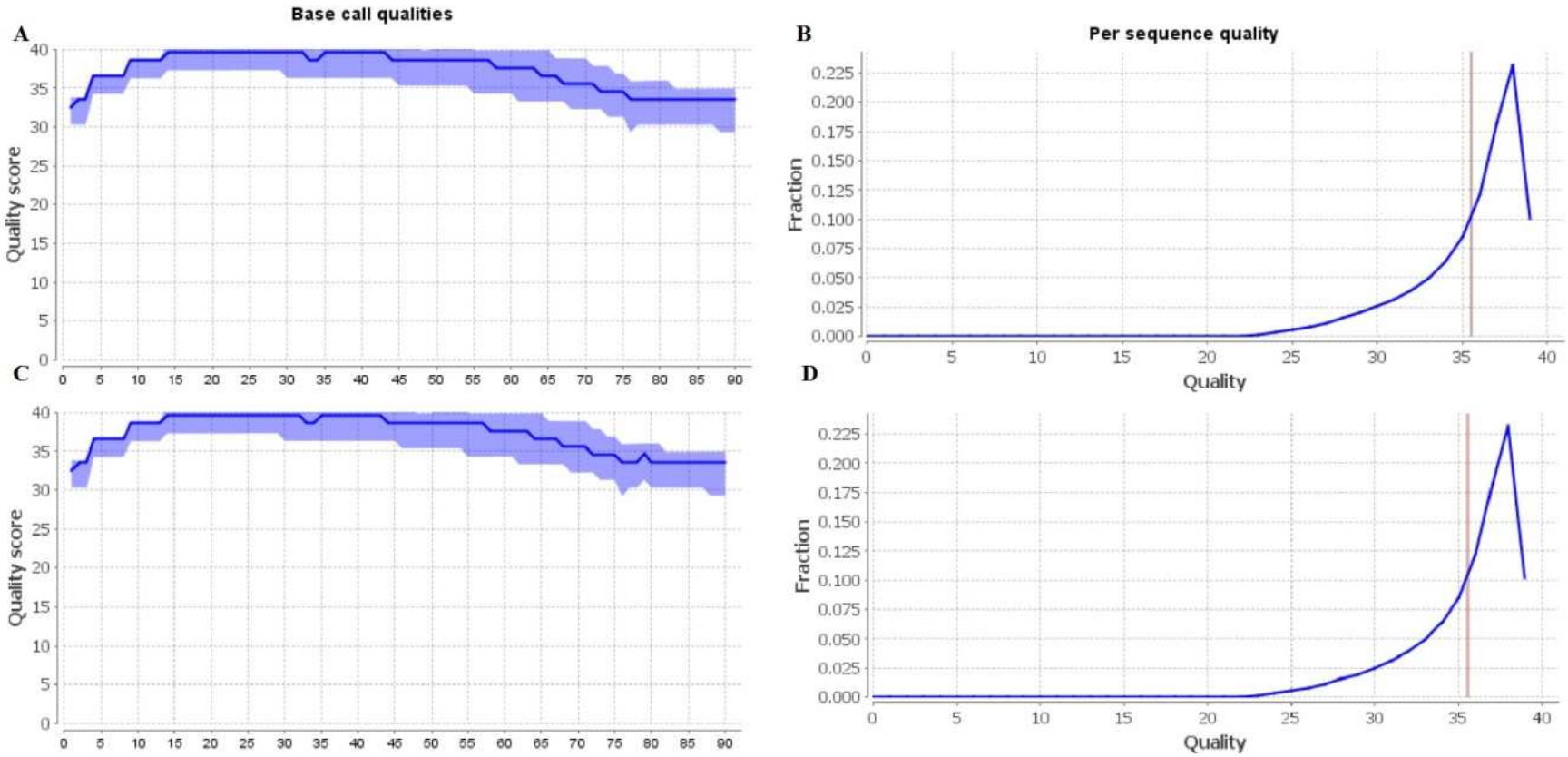


**Figure 5-3.** Average quality scores of the RNAseq raw reads of adventitious (A, B; average quality score 35.5) and ground root (C, D; average quality score 35.6) samples from English ivy.

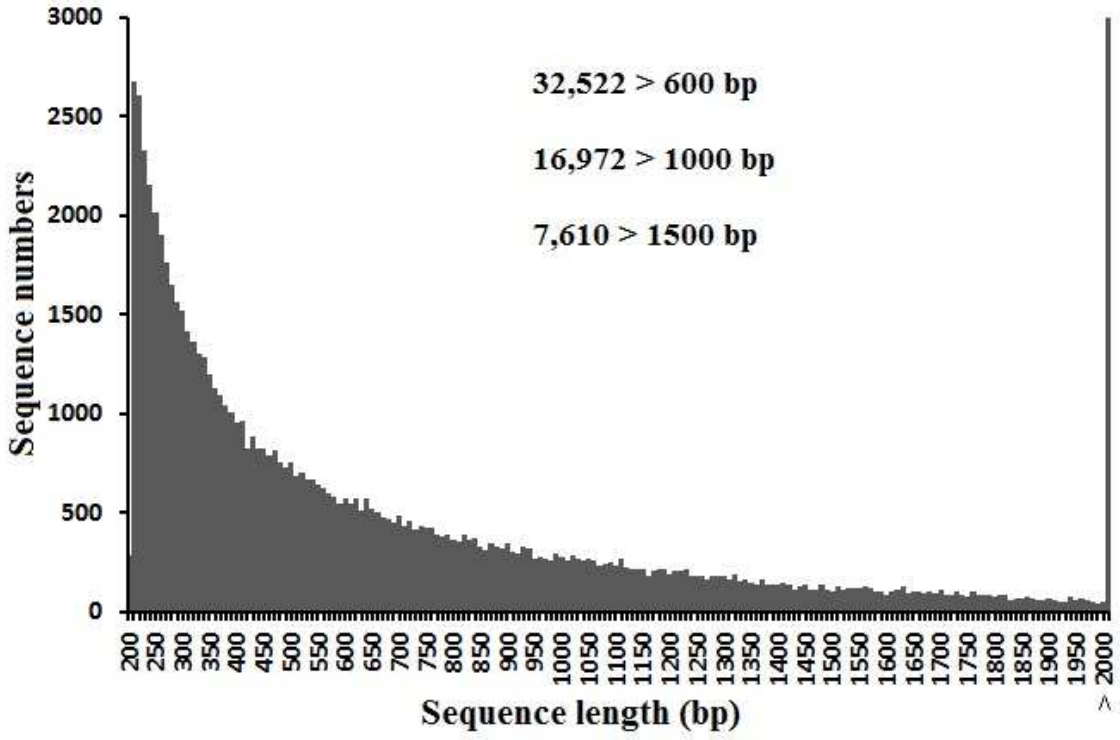


**Figure 5-4.** *De novo* transcriptome consensus assembly of English ivy. Length distributions of *de novo*-assembled contigs. The majority of assembled contigs were >600 bp.

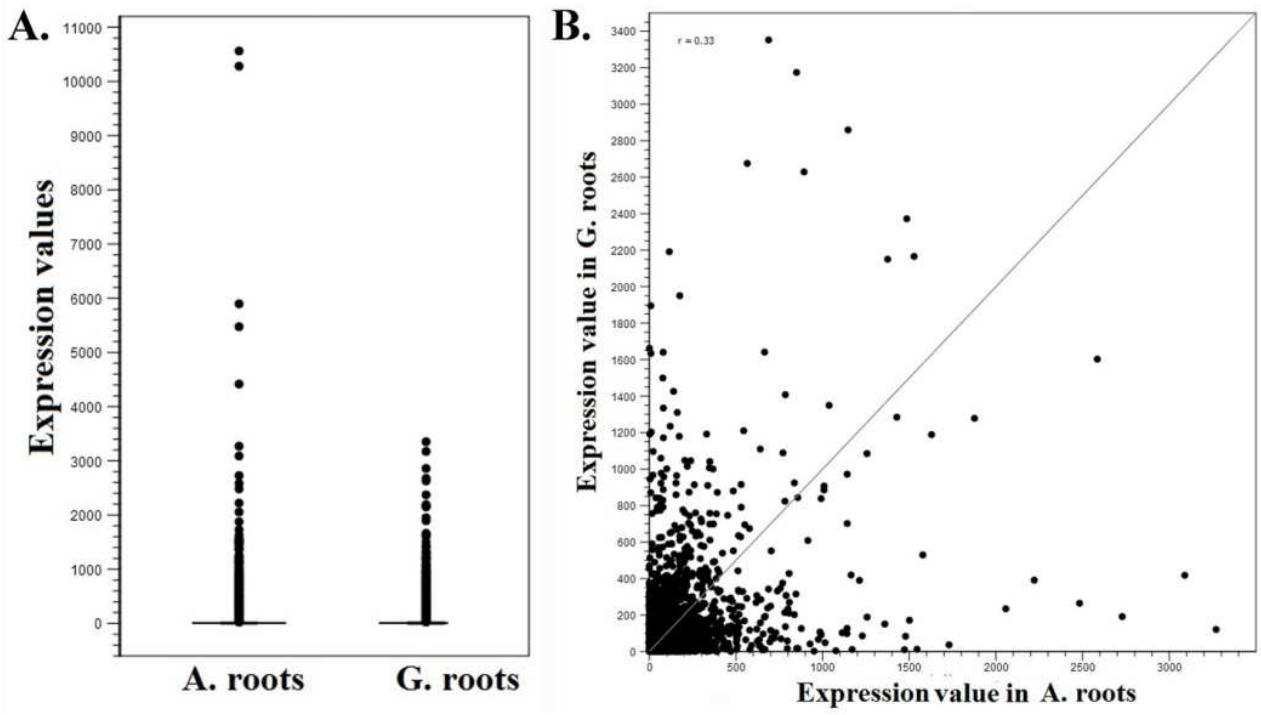


**Figure 5-5.** Expression profiles of genes in adventitious roots (A. roots) and ground roots (G. roots). (A) Box plot shown the expression of genes in adventitious and ground roots. (B) Scatter plot shows the expression profiles of individual genes in both adventitious and ground roots.

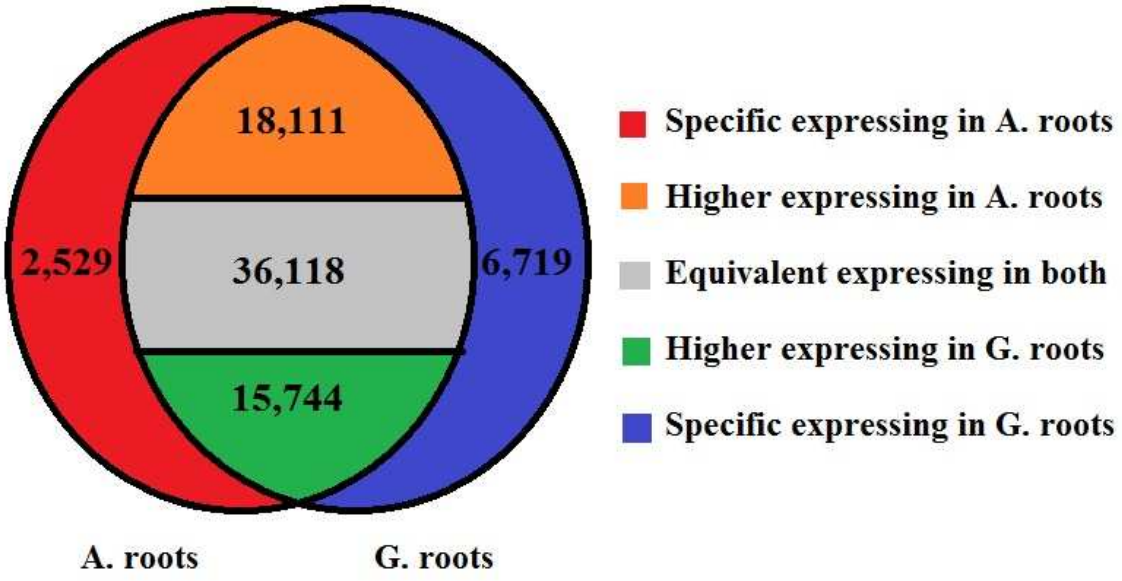


**Figure 5-6**. Pictograph representing the variation in gene expression (exclusively expressed in adventitious roots (genes found to be only expressed in adventitious roots; red), higher expression in adventitious roots (orange), equivalent expression in adventitious and ground roots (grey), higher expression in ground roots (green) and exclusively expressed in ground roots (genes found to be only expressed in ground roots; blue) in adventitious (A. roots) and ground roots (G. roots) of English ivy.

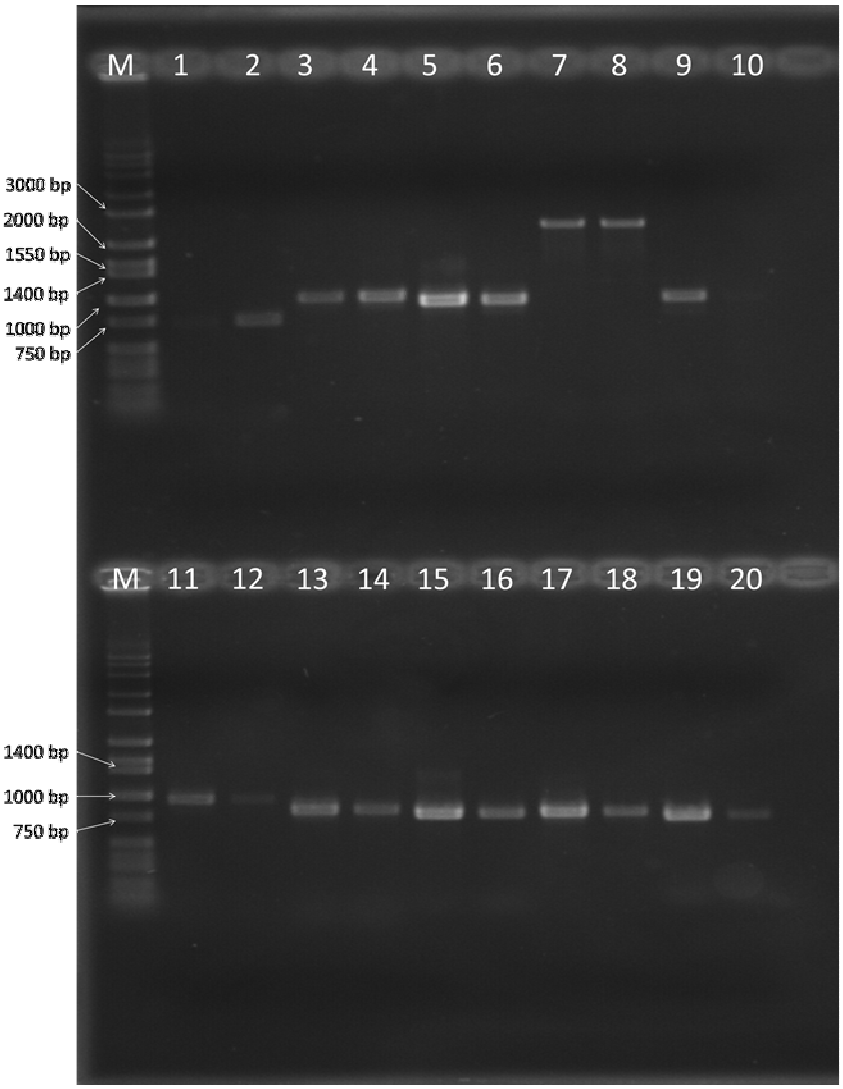


**Figure 5-7.** RT-PCR analysis on total RNAs extracted from adventitious roots and leaves of English ivy. Expression of tripeptidyl-peptidase (lanes 1 and 2), glycine dehydrogenase (lanes 3 and 4), aconitate hydratase (lanes 5 and 6), phospholipase D alpha (lanes 7 and 8), phenylalanine ammonia-lyase (lanes 9 and 10), chaperonin (lanes 11 and 12), adenosylhomocysteinase (lanes 13 and 14), beta-glucosidase (lanes 15 and 16), glyceraldehyde-3-phosphate dehydrogenase (lanes 17 and 18), and proteasome subunit alpha type (lanes 19 and 20) in adventitious roots (odd lanes) and leaves (even lanes) of English ivy. M: high molecular weight marker (Hi-Low DNA ladder, Minnesota Molecular, Minneapolis, Minnesota).

**Table 5-1.** Primer sequences used for RT-PCR confirmation of the expression of proteins identified from LC/MS/MS analysis in adventitious roots of English ivy.

| Hit Description | Primer name | Sequence |
|---|---|---|
| Tripeptidyl-peptidase | 10541F | TAGGCCTTTGCAACGGAGAG |
| | 10541R | AGGGCATTCTTGTGAGTCCG |
| Phospholipase D alpha | 10691F | CTGCGCAGTGGAGGTGGT |
| | 10691R | CTCCATGCCGGGAAGCTC |
| Chaperonin CPN60-2 | 12229F | TCCCTCAACTCCAGCATTGG |
| | 12229R | GCGCAGGTTGGCACAATATC |
| Phenylalanine ammonia-lyase | 13095F | AACGATTGGTCAGGTGGCAG |
| | 13095R | CCATATGCGGGCCTAGCCAT |
| Glycine dehydrogenase | 545F | GTGATACTTTTCCCCGCCGA |
| | 545R | CTTGTAGCCTTGTCCCTCCG |
| Putative aconitate hydratase | 45254F | ACCTCCGTATCAAACCGTGC |
| | 45254R | AGGAGCCCATTGGTACAGGA |
| Adenosylhomocysteinase | 46923F | CAAAGCTGGGGTGACCAG |
| | 46923R | CGGACCCGACCTGATTG |
| Beta-glucosidase | 46181F | CGGAAGTGTGTCATCTCGCT |
| | 46181R | TTGCCAGCACTCCAAGA |
| Glyceraldehyde-3-phosphate dehydrogenase | 13414F | CCGGCTCCACTAATCCAT |
| | 13414R | GAGATCCCTTGGGCCAGC |
| Proteasome subunit alpha type | 9802F | TCCATAACTGGTCGCAAGCAC |
| | 9802R | AGGCAATGATTCGGTCTGTGT |

**Table 5-2.** Proteins present in ivy nanoparticles as identified using ivy transcriptome or UniProt database.

| | Ivy transcriptome | | | UniProt database | |
|---|---|---|---|---|---|
| **Hit Description** | **Molecular weight** | **Normalized total spectra** | **Hit Description** | **Molecular weight** | **Normalized total spectra** |
| Tripeptidyl-peptidase | 353 kDa | 121 | Clathrin heavy chain | 190 kDa | 103 |
| Putative aconitate hydratase | 251 kDa | 168 | Aconitate hydratase | 109 kDa | 56 |
| Glycine dehydrogenase | 313 kDa | 130 | | | |
| Phospholipase D alpha | 225 kDa | 102 | Sucrose synthase isoform 1 | 92 kDa | 71 |
| Phenylalanine ammonia-lyase | 193 kDa | 106 | Luminal-binding protein 5 | 73 kDa | 59 |
| Chaperonin CPN60-2 | 145 kDa | 188 | Chaperonin CPN60-2 | 61 kDa | 80 |
| Adenosylhomocysteinase | 86 kDa | 141 | Adenosylhomocysteinase | 53 kDa | 130 |
| Catalase isozyme 2 | 143 kDa | 120 | | | |
| Beta-glucosidase 12 | 191 kDa | 131 | 6-phosphogluconate dehydrogenase | 54 kDa | 56 |
| Glyceraldehyde-3-phosphate dehydrogenase | 130 kDa | 130 | Glyceraldehyde-3-phosphate dehydrogenase | 32 kDa | 91 |
| Proteasome subunit alpha type-6 | 92 kDa | 86 | Proteasome subunit alpha type-6 | 32 kDa | 42 |

**Table 5-3.** Summary of RNAseq, assembly and annotation results on adventitious and ground root samples in English ivy.

| Sample ID | Number of sequences | Average length | Total size | G/C content (%) |
|---|---|---|---|---|
| Adventitious roots | 25,030,290 | 90 bp | 2.10 Gb | 44.0 |
| Ground roots | 25,141,182 | 90 bp | 2.11 Gb | 43.3 |
| Adventitious root assembly | 205,180 | 249 bp | 51.19 Mb | 40.7 |
| Ground root assembly | 233,335 | 237 bp | 55.25 Mb | 40.2 |
| Total consensus assembly | 79,221 | 705 bp | 55.86 Mb | 41.5 |
| Annotated sequences | 32,331 | 996 bp | 32.21 Mb | 41.6 |
| Unknown sequences | 46,890 | 504 bp | 23.65 Mb | 41.2 |

**Table 5-4.** Comparison of fold expression changes of genes identified from our analysis in adventitious versus ground roots in English ivy transcriptome.

| Gene Name | Gene Length | Hit Accession | Hit Description | Expression (Adventitious) | Expression (Ground) | Fold Change |
|---|---|---|---|---|---|---|
| 10541 | 4153 | Q64560 | Tripeptidyl-peptidase | 56.23903756 | 47.07208984 | 1.194 |
| 45254 | 2969 | Q6YZX6 | Putative aconitate hydratase | 30.90267883 | 22.87008781 | 1.351 |
| 545 | 3736 | P49362 | Glycine dehydrogenase | 165.3798894 | 37.20849158 | 4.444 |
| 10691 | 2732 | O04865 | Phospholipase D alpha | 317.4201711 | 734.9895868 | -2.315 |
| 13095 | 2339 | Q43052 | Phenylalanine ammonia-lyase | 286.501722 | 20.53709187 | 13.95 |
| 12229 | 1690 | Q05046 | Chaperonin CPN60-2 | 97.3068862 | 25.63885626 | 3.795 |
| 46923 | 1027 | Q01781 | Adenosylhomocysteinase | 657.0366331 | 187.4003711 | 3.506 |
| 12514 | 1706 | P30567 | Catalase isozyme | 258.63792 | 6340.540004 | -24.515 |
| 46181 | 2283 | Q7XKV4 | Beta-glucosidase | 1756.648712 | 95.02794987 | 18.485 |
| 13414 | 1557 | P26520 | Glyceraldehyde-3-phosphate dehydrogenase | 218.4137693 | 64.29746706 | 3.396 |
| 9802 | 1073 | O48551 | Proteasome subunit alpha type | 118.4709884 | 34.32838307 | 3.451 |

# Chapter 6. Conclusions

In these studies, we developed an enhanced system for the production of English ivy adventitious roots and their nanoparticles by modifying GA7 Magenta boxes and identifying the optimal concentration of IBA for adventitious root growth. This system was the first such platform for growing and harvesting organic nanoparticles from plants, and represents an important step in the development of plant-based nanomanufacturing. It is a significant improvement on the utilization of plant systems for the formation of metallic nanoparticles, and provides an easy system for the generation of bulk ivy nanoparticles for translation into biomedical and cosmetic applications.

The development of this bulk extraction method was necessary for collecting enough nanoparticles for use in subsequent analyses and for any biomedical or cosmetic applications of economic significance. Through experiments conducted using ICP-MS, we were able to prove that the ivy nanoparticles were devoid of any metallic components, thus confirming that the ivy nanoparticles were indeed organic in composition. Elemental analysis revealed a high, ~10:1, C:N ratio, and FTIR confirmed the presence of peaks related to C-N bonding. FTIR spectra of ivy nanoparticles were compared with a polysaccharide standard, chitosan, and protein standard, BSA, and it was found that the ivy nanoparticles were similar in structure to both samples, indicating that these nanoparticles were most likely composed of glycoproteins. Using gel electrophoresis, the ivy nanoparticles formed a single high molecular weight band (>480 kDa), which stained positive for both proteins and glycoproteins through silver and glycoprotein specific stains.

Individual proteins were separated from a previously identified high molecular weight band by adjusting the reducing conditions prior to SDS-PAGE. Using the denaturing conditions of 2 M thiourea, 8 M urea and 3% SDS in conjunction with 10 mM DTT in the extraction buffer provided the greatest denaturation and best resolution, resolving nine additional bands and maintaining nanoparticle size and stability. Using this strategy, it was possible to separate the ivy nanoparticles into nine distinct protein bands ranging in molecular weight from 10-175 kDa. After gel extraction, each band was sequenced using LC/MS/MS, and blasted against the UniProt database and the ivy transcriptome. In this study we utilized a modified protein extraction method for the production and identification of ivy nanoparticles. Briefly, denaturing conditions of 2 M thiourea, 8 M urea and 3% SDS in conjunction with 10 mM DTT used in the extraction buffer provided the greatest denaturation and best resolution, resolving nine bands from the single >460 kDa original band, while maintaining nanoparticle size and stability. The results of the omics analysis identified 14 protein candidates from the English ivy transcriptome and 9 from the UniProt database for a combined total of 20 individual putative proteins with 2 (chaperonin 60-1, chaperonin 60-2) previously shown to form nanoparticles in other systems. Transcriptome analysis revealed that many of the protein candidates to be enzymes involved in abiotic and biotic stress response and growth regulators. Interestingly the PAL enzyme was identified as a top candidate, which is found in the flavanoid pathway and has shown to confer UV resistance in plants. Of the proteins identified, the chaperonins are the most probable candidates for nanoparticle formation observed in ivy root hairs. Chaperonins have been shown to be involved in protein folding and have the ability to form nanoparticle structures. While these structures have been reported in the literature as much smaller than our observed nanoparticles, it is possible that upon their disassembly and refolding larger nanoparticle structures can be created,

such as those observed in ivy.  Further studies are necessary  to confirm the fuctions of the proteins listed here, such as through production of knockouts to determine the true core of the nanoparticle. Additional methods such as high performance liquid chromoatography (HPLC) or fast performance liquid chromatography (FPLC) can be used to separate and eliminate nonessential proteins that may be bound to the nanoparticle complex and providing no functional component to its structure. Additionally, by overexpressing the defined proteins in another system, such as in yeast, bacteria or a model plant system, we may be able to identify how multiple proteins are interacting to form the 3D structure of the ivy nanoparticles. Based on these data, we have identified a pool of protein candidates that may be contributing to nanoparticle formation and secretion in ivy. Continued research into these proteins will likely assist in the development of new high strength adhesives. Further, it will now be possible to scale-up the procedure developed in this work to collect enough ivy nanoparticles for future applications in drug delivery and cosmetics.

# Vita

Jason Neil Burris was born on April 11, 1977 in Waxhaw, NC to Nelson and Patti Burris. He attended Union County Public Schools and graduated from Parkwood High School in 1995. Jason attended North Carolina State University and graduated with a Bachelor's of Science Degree in Horticulture Science in May 2005. While Jason was working as a research technician at the University of Tennessee, he graduated August 2010 with his Masters of Science degree in Plant Science. His Ph.D. research was focused on the bioproduction, nanoparticle isolation and molecular analysis of the nanocomposite adhesive of English ivy (*Hedera helix*) under the direction of Dr. C.N. Stewart, Jr. Jason graduated with his Ph.D. degree in Plant Molecular Biology in August 2016.